Cementation Processes and Sand Petrography of the Zia Formation, Albuquerque Basin, New Mexico

by

Joseph R. Beckner

Submitted in Partial Fulfillment
of the Requirements for the

Masters of Science in Geology

New Mexico Institute of Mining and Technology
Department of Earth and Environmental Science
Socorro, New Mexico

December 1996

ABSTRACT

The Zia Formation (Miocene) consists of gravels, sands and muds deposited in fluvial, eolian, and playa lake environments. Although much of the formation is poorly consolidated, resistant zones of calcite cementation are common. These zones range in size from isolated nodules to tabular cemented zones several meters thick that extend for over two kilometers laterally. This thesis has three parts, each examining separate but related topics: Part 1 addresses the environments of precipitation (i.e., pedogenic, vadose non-pedogenic, phreatic) of the principal types of cementation, part 2 addresses the provenance of the Zia Formation, and part 3 examines the relationship between oriented concretions and paleocurrents in the Zia Formation.

Using a combination of microscopic, macroscopic, and geochemical characteristics, I inferred the environments of precipitation of the principle types of cementation. Nodules and rhizocretions with micritic fabrics and alveolar structures are inferred to be vadose carbonates. Ovoid or elongate concretions, characterized by blocky spar cements, and preservation of primary sedimentary structures are inferred to be phreatic carbonates. Most cemented units in the Zia Formation reflect characteristics of both phreatic and vadose zone cementation (e.g., preservation of sedimentary structures plus rhizocretions and alveolar microtextures). $\delta^{13}C$ values for vadose cement tend to be 1 $^o/_{oo}$ heavier and $\delta^{18}O$ values tend to be similar or slightly lighter than phreatic cements. $\delta^{13}C$ and $\delta^{18}O$ values for units with mixed features tend to have intermediate values. Cementation types that exhibit a mixture of features may reflect past fluctuations of the water table, where vadose cements were moved into the phreatic zone. Vadose zone cementation occurred principally in association with soil development, whereas phreatic zone cementation occurred preferentially in zones of high primary permeability. In many cases early vadose cements provided nucleation sites for later phreatic cementation. Tabular units in the Zia Formation are frequently laterally extensive, decreasing potential reservoir/aquifer quality by forming significant barriers to vertical fluid flow. These barriers could result in compartmentalization of the reservoir/aquifer, and extensively reduce production if wells were screened on only one side of a cemented layer.

Zia Formation sands can be subdivided into two distinct groups on the basis of composition. The lower Zia Formation (Piedra Parada, Chamisa Mesa, and Canada Pillares Members) changes composition up section from felspathic litharenites to lithic arkoses. The upper Zia Formation (Unnamed Member) is mainly differentiated from the lower by greater amounts of feldspar. Compositional changes in the lower part of the Zia Formation are due to grainsize reduction without a change in provenance (e.g., reworking of polycrystalline quartz, volcanic, and chert rock fragments into smaller grains of quartz and feldspar). A change in provenance is suggested for the transition from lower to upper Zia Formation because of changes in the amount and type of feldspar (e.g., more total feldspar; increase in microcline), an increase in mafic volcanic rock fragments, and a decrease in chert. This change may be the result of additional detrital input from the Santa Fe block, Nacimiento block, or northern volcaniclastic sources. The primary diagenetic process that affected the Zia Formation was calcite cementation. Micritic calcite with alveolar textures and circumgranular cracking are interpreted to result from vadose cementation, whereas those exhibiting drusy to poikilotopic spar cements are interpreted as resulting from phreatic cementation. Most cemented units in the Zia Formation show the influence of both environments. Clay matrix and pore cements are only significant in units that are not cemented with calcite. Intergranular porosity is the dominant porosity type in cemented and uncemented units. The main porosity type in phreatic units results from incomplete cementation. In vadose units, porosity typically results from grain and cement dissolution, and circumgranular cracking.

Both the fluvial and eolian deposits in the Miocene Zia Formation contain numerous oriented concretions which are interpreted to reflect paleo-groundwater flow orientation in the phreatic (saturated) zone. Paleocurrent directions from the eolian sediments in the Zia Formation indicate prevailing westerly winds, and paleocurrent data for fluvial facies in the Canada Pillares and Unnamed Members indicates an east to southeasterly transport direction. Concretion orientations for the eolian sediments in the Zia Formation are dominantly NE-SW, with azimuths ranging from 16-19°. Concretion orientations for fluvial sediments in the Zia Formation are

dominantly southeasterly, with azimuths ranging from 161-169°. For fluvial sediments, concretion orientations are subparallel to paleocurrent directions (< 35° difference in mean vectors). For eolian sediments concretion orientations are consistently 60-90° from paleocurrent directions. Assuming that cementation is controlled by transport, this difference in orientation implies that the direction and scale of permeability anisotropy in fluvial and eolian depositional systems are fundamentally different. Elongate concretions show much less scatter in orientation than paleocurrent data in all systems, Because of consistency of orientation and ease of measurement, concretion orientations in both fluvial and eolian sediments can provide a rapid means of estimating paleo-groundwater flow directions.

ACKNOWLEDGMENTS

TABLE OF CONTENTS

LIST OF FIGURES

LIST OF TABLES

INTRODUCTION

A fundamental problem in any study of early terrestrial diagenesis is identifying vadose versus phreatic alterations. Early diagenetic alterations in terrestrial sediments occur in both vadose (unsaturated) and phreatic zones. Although many studies have investigated vadose carbonate formation (primarily pedogenic), few studies have focused on terrestrial phreatic cementation. Fewer yet have addressed the problem of differentiating between different environments of precipitation. The Zia Formation provides an excellent opportunity to study a variety of terrestrial cementation variations in both eolian and fluvial environments. In the Zia Formation I have been able to infer the environments of cement formation and the relationships between these environments and the subsequent spatial distribution of cementation.

During the course of the study, two other studies of a related nature were also undertaken. This thesis contains three manuscripts intended for separate publication in professional journals. Because the manuscripts were written as separate papers, they contain their own reference sections.

Part 1 is a discussion of the origin and spatial distribution of early vadose and phreatic cementation in the Zia Formation. In this study I investigated the relationships between depositional environment, lithology, and geochemistry on macroscopic and microscopic characteristics of calcite cementation.

Part 2 is a discussion of the sand petrography of the Zia Formation, with emphasis on provenance and diagenesis. This study determines composition of host lithology and provenance, and the effects of diagenesis on porosity.

Part 3 is a discussion of the relationships between oriented concretions and paleogroundwater flow for fluvial and eolian sediments. Oriented concretions in fluvial and eolian environments exhibit different characteristics. This section explores possible reasons for this difference and their implication for paleogroundwater flow.

Appendix A contains information about methods used to develop and define the facies associations used in the above studies. Appendix B contains the tabulated

1

petrographic data used in Part 2. Appendix C contains the tabulated orientation and

paleocurrent data used in Part 3. Appendix D contains definitions of certain terms used in

text.

Part 1

Origin and Spatial Distribution of Early Vadose and Phreatic Calcite Cements in the Zia Formation, Albuquerque Basin, New Mexico

ABSTRACT

The Miocene Zia Formation consists of gravels, sands and muds deposited in fluvial, eolian, and playa lake environments. Although much of the formation is poorly consolidated, resistant zones of calcite cementation are common. These zones range in size from isolated nodules to tabular cemented zones several meters thick that extend laterally over two kilometers. The calcite cemented zones are highly complex, exhibiting a wide range of macroscopic and microscopic textures and geometries. After considering a combination of microscopic, macroscopic, and geochemical characteristics, we have inferred the environment of precipitation (i.e., pedogenic, vadose non-pedogenic, phreatic) of the principal types of cementation. Nodules and rhizocretions with micritic fabrics and alveolar structures are inferred to be vadose carbonates. Ovoid or elongate concretions, characterized by blocky spar cements, and preservation of primary sedimentary structures are inferred to be phreatic carbonates. Most cemented units in the Zia Formation reflect characteristics of both phreatic and vadose zone cementation (e.g., preservation of sedimentary structures plus rhizocretions and alveolar microtextures). $\delta^{13}C$ values for vadose cement tend to be 1 $^o/_{oo}$ heavier, and $\delta^{18}O$ values tend to be similar or slightly lighter than phreatic cements. $\delta^{13}C$ and $\delta^{18}O$ values for units with mixed features tend to have intermediate values. Most cementation types that exhibit a mixture of features may reflect past fluctuations of the water table, where vadose cements were moved into the phreatic zone. Vadose zone cementation occurred principally in association with soil development, whereas phreatic zone cementation occurred preferentially in zones of high primary permeability. In many cases early vadose cements provided nucleation sites for later phreatic cementation. Tabular units in the Zia Formation are generally laterally extensive, decreasing potential reservoir/aquifer quality by forming significant barriers to vertical fluid flow. These barriers could result in compartmentalization of the reservoir/aquifer, and extensively reduce production if wells were screened on only one side of a cemented layer.

INTRODUCTION

Understanding fluid flow in aquifers and hydrocarbon reservoirs requires an understanding of heterogeneities in porosity and permeability in the material. A number of workers have examined the influence of primary depositional controls on aquifer heterogeneity (e.g., Weber, 1982; Anderson, 1989, 1990; Davis et al., 1993). To date, however, few studies have examined the influence of diagenetic alterations on porosity and permeability heterogeneities. To predict the subsurface distribution of diagenetic alterations that influence flow, it is necessary to understand the diagenetic processes involved and to determine the controls on the spatial distribution of diagenetic alterations. In this paper we examine controls on the origin and spatial distribution of early calcite cements in Miocene Zia Formation of New Mexico, in which calcite-cemented low permeability zones can extend for several kilometers laterally.

Unlike marine sediments, where early diagenesis typically occurs entirely within the phreatic (saturated) zone, early diagenetic alterations in terrestrial sediments occur in both vadose (unsaturated) and phreatic zones. Furthermore, in terrestrial sediments significant alterations can occur during pedogenesis. Thus, a fundamental problem in any study of early terrestrial diagenesis is identifying vadose versus phreatic alterations. Although many studies have investigated pedogenic carbonate formation, few studies have focused on non-pedogenic cementation. Fewer still have addressed the problem of differentiating among different types of cements. In the Zia Formation we have been able to infer the environments of cement formation and the relationships between these environments and the subsequent spatial distribution of cementation. Our principal conclusion is that cementation in the phreatic zone occurred preferentially in zones of high primary permeability, whereas vadose cementation occurred principally in association with soil development. Furthermore, pedogenic carbonates apparently served as nucleation sites for later phreatic cementation, leading to complex zones of mixed pedogenic and phreatic cements.

TERMINOLOGY

Because the terminology for early carbonate cements is complex and somewhat ambiguous, it is necessary to define the terms used in this study. These terms will also be defined in Appendix D. We subdivide carbonate cements into three principal types: (1) <u>Pedogenic carbonate</u> is carbonate that precipitated in an active soil (i.e., the precipitation was related to pedogenic processes such as: atmospheric fallout of carbonate, weathering, evapotranspiration, biological activity, etc.. Most detailed studies of early (i.e., before significant burial diagenesis) calcite cementation in semi-arid and arid settings have been on pedogenic carbonates (Gile et al., 1966; Reeves, 1976, Esteban and Klappa, 1983; Klappa, 1983; Rabinhorst et al., 1984; Machette, 1985; Wright, 1986; Monger et al., 1991; Mack et al., 1993). (2) <u>Vadose non-pedogenic carbonate</u> is carbonate that precipitated in the vadose zone, but is not related to pedogenesis. Vadose, non-pedogenic carbonates have been reported in the literature (e.g., Carlisle, 1983; Goudie, 1983; Semeniuk and Searle, 1985; Wright and Tucker, 1991), although few criteria were described to distinguish them from pedogenic cements. (3) <u>Phreatic carbonate</u> is carbonate that precipitated by non-pedogenic processes in the phreatic zone. Terrestrial phreatic carbonates have been described by many previous workers (Netterberg, 1969; Mann and Horwitz, 1979; Arakel and McConchie, 1982; Carlisle, 1983; Arakel et al., 1989; Wright and Tucker, 1991; Spötl and Wright, 1992; Burns and Matter, 1995; Mozley and Davis, 1996).

The terms *calcrete* and *caliche* are frequently used to describe some of the cement types mentioned above. They are also used to describe a variety of cryptocrystalline calcium carbonate deposits resulting from pedogenic processes, that eventually forms indurated masses (Gile et al., 1966; Read, 1974; Reeves, 1976; Semeniuk and Meager, 1981; Esteban and Klappa, 1983; Carlisle, 1983; Klappa, 1983; Netterberg and Caiger, 1983; Machette, 1985; Milnes, 1992). The term calcrete has also been used to describe a wide variety of calcium carbonate deposits resulting from groundwater processes (Netterberg, 1969; Mann and Horwitz, 1979; Semeniuk and Meager 1981; Arakel and McConchie, 1982; Semeniuk and Searle, 1985; Jacobson, et al., 1988; Arakel et al., 1989;

Wright and Tucker, 1991; Spötl and Wright, 1992). These terms will be avoided, as they have been used in a variety of ways by different authors.

GEOLOGIC SETTING

The Zia Formation is the basal rift filling unit of the Santa Fe Group in the Albuquerque Basin, part of the more than 1000-kilometer long Rio Grande Rift of Colorado and New Mexico (Lozinsky, 1994). The 10 to 21 Ma Zia Formation makes up the Lower Santa Fe Group in the northern part of the basin (Lozinsky, 1994), and is exposed in a 55 km long arc extending from the Rio Puerco in the west to 24 km north of Albuquerque, New Mexico (Gawne, 1981). The upper part of the Zia Formation (15 - 10 Ma) was deposited during the most active period of rifting (Chapin and Cather, 1994). The study site is on the western margin of the Albuquerque Basin, about 20 km from Albuquerque, on the King Ranch (Fig. 1.1). The Zia Formation in this area is typified by exposed, resistant, well-cemented horizons bounding poorly consolidated sediments. The Zia Formation can be divided into sand-dominated, eolian (Piedra Parada) and fluvial-eolian (Chamisa Mesa) members; a mud-dominated, fluvial member (Canada Pillares Member); and the sand-dominated, eolian/fluvial Unnamed Member (Gawne, 1981; Tedford, 1982; Fig. 1.2,1.3). The lower contact of the Zia Formation is unconformable with the Eocene Galisteo Formation and the Crevasse Canyon Formation of the Cretaceous Mesaverde Group (Gawne, 1981; Tedford, 1982). The upper contact is the Sand Hill Fault, a major normal fault that offsets the Zia Formation and units of the Upper Santa Fe Group by about 600 meters (Hawley and Haase, 1992).

Facies associations (Miall, 1990) were defined from a detailed analysis of lithofacies in the study area (Table 1.1; Fig. 1.4; Appendix A). Classification used for fluvial sediments is from Miall (1990) and Davis et al. (1993). The terms facies and facies/lithofacies association are also used to define eolian sediments and sedimentary

Table 1.1. Summary of lithologic information for facies associations. Terminology modified from Miall (1990), and Davis et al. (1993).

Facies Association	Lithofacies Present	Geometry	Grain Size/Sorting	Cementation Types
CH Channel + Levee	tough cross-bedded sand(St) planar laminated sand (Sp) low angle crossbedded sand (Sl) horizontally laminated sand (Sh) ripple cross-laminated sand (Sr) massive sand (Sm) massive, crudely bedded silts and muds (Fm) finely laminated to rippled silts and muds (Fl) laminated silt, sand, and clay (Fsc)	tabular to lenticular .2 to 3 m thick 10 m to >2 km in lateral extent	fine to coarse, moderately sorted sand/sandstone	type-1 and type-3 (phreatic) tabular units
SS Sand Sheet Deposits	trough cross-bedded sand(St) planar laminated sand (Sp) low angle crossbedded sand (Sl) horizontally laminated sand (Sh) ripple cross-laminated sand (Sr) massive sand (Sm)	tabular, massive, lenticular, to thin wedge-shaped sands, .2 to 4 m thick .5 m to .5km in lateral extent	poorly sorted sands and silty sands	thin sandstone sheets are commonly well cemented
OF Overbank Fines	massive, crudely bedded silts and muds (Fm) finely laminated to rippled silts and muds (Fl) laminated silt, sand, and clay (Fsc) silts and clays w/rhizocretions (Fr)	tabular to thin and lobate .1 to 3 m thick 5 to .2 km lateral extent	muds and silts	poorly cemented, isolated nodules, platy, and rod concretions
P Paleosol Horizons	paleosols on sand (Ps) paleosols on silts and clays (Psc) silts and clays w/rhizocretions (Fr) massive sand w/rhizocretions (Smr)	tabular to discontinuous and patchy .1 to 1 m thick .1 to > 1km lateral extent	muds, silts,very fine to medium silty and clayey sands/sandstones	nodular, platy, and rod concretions, and type-2 and type-3 (vadose) tabular units
EC Cross-stratified Eolian Dune bodies	trough cross-bedded sand(Ste) planar laminated sand (Spe) low angle crossbedded sand (Sle) horizontally laminated sand (She) ripple cross-laminated sand (Sre) massive sand (Sme)	tabular, lenticular and wedge-shaped 1-3 m thick > 1km lateral extent	fine to lower coarse moderately to well sorted sand/sandstone	scattered ovoid to elongate concretions and small type-1 and type-3(phreatic tabular units
ES Eolian Sandsheet Deposits	low angle crossbedded sand (Sle) horizontally laminated sand (She) ripple cross-laminated sand (Sre)	tabular 1- 2 m thick > 1km lateral extent	fine to medium moderately to poorly sorted sand/sandstone	coarser layers generally form well cemented type-1 and type-3 (phreatic)
ID Interdune Deposits	low angle crossbedded sand (Sle) horizontally laminated sand (She) rpple cross-laminated sand (Sre) massive Sand (SM)	tabular, lenticular and discontinuous .1 to .5 m thick 10 m to > 1km lateral extent	all sizes, generally poorly sorted or bimodal	small type-1 and type-3 (phreatic) tabular units
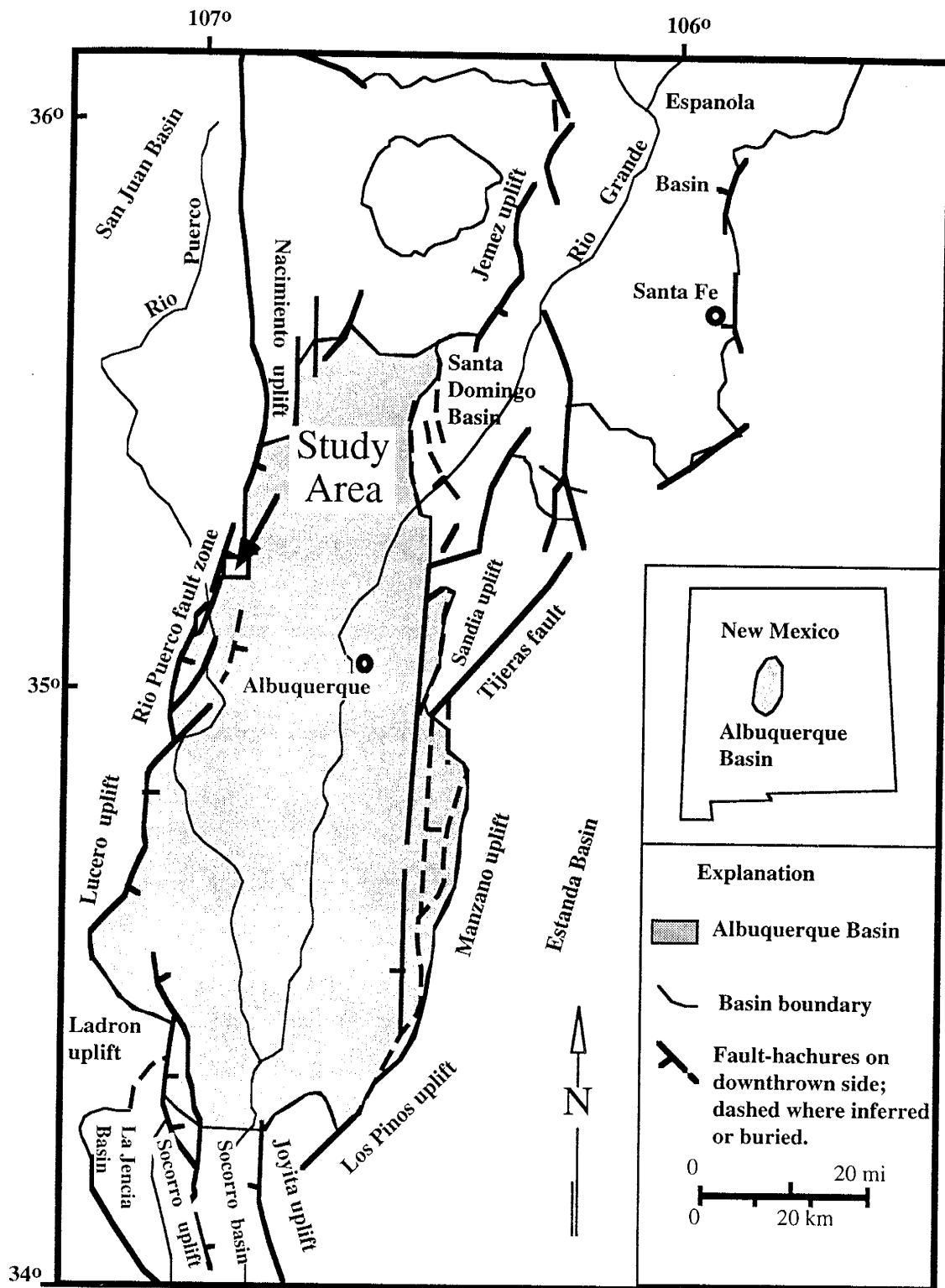
Figure 1.1. Map of the Albuquerque Basin showing the King brothers ranch study area. Modified from Lozinsky (1994).

AGE	Stratitgraphic Units	Depo. Env.	Meters	Lithology	Sample Locations

Sample Locations

72895-6 72895-2 72895-3
72895-4 72895-5 72896-6a
72895-6b 72895-7
6295-4
81995-20
81995-19
81994-18
81994-17
81994-16
8594-16
72194-3
8594-15
81994-15
81994-14 8594-14
8594-13 81994-9
81994-8
81994-7
81994-6
81994-5
81994-4
72195-2
81994-3 8594-12
81994-2
8594-11 81994-1
72195-1
122394-1
122394-2
122394-3
122394-4
122394-5
122394-6
122394-7
122394-8
122394-9 1395-1
122394-10 1395-2
1395-3
1395-4
1395-5
1395-6
1395-7
1395-8
1395-9
1395-10
1395-11 8594-10
81895-1
8594-9
81895-2
8594-8
8394-7 8594-7
81895-3
8594-6
8394-6
8594-5
8594-4A
8594-4
8394-5
8594-2
8394-4
8394-3
8594-1A
8594-1B
8594-1
8394-2
8394-1

EXPLANTION

Muds
Silty Sand
Sand
Unconformable Contact
Faulted Contact

AGE: 10 to 15 Ma Early Clarendonian to Late Barstovian; 15 to 21 Ma Hemingfordian to late Arikareean

LOWER SANTE FE GROUP — ZIA FORMATION

"UNNAMED" MEMBER: Sand Dominated Fluvial, Playa, Sand Dominated Fluvial, Eolian, Fluvial-Eolian, Eolian

CANADA PILLARES MEMBER: Mud Dominated Fluvial
CHAMISA MESA MEMBER: Fluvial Eolian
PIEDRA PARADA MEMBER: Eolian, Fluvial/Eolian

GALISTEO FM — MESAVERDE GROUP

Figure 1.2. Generalized stratigraphic column of the Zia Formation showing ages, lithologies, depositional environments, and locations of samples. This stratigraphic column was constructed from the four detailed columns whose locations are shown in Figure 3. Terminology and ages from Tedford (1982) and Lozinsky (1988).
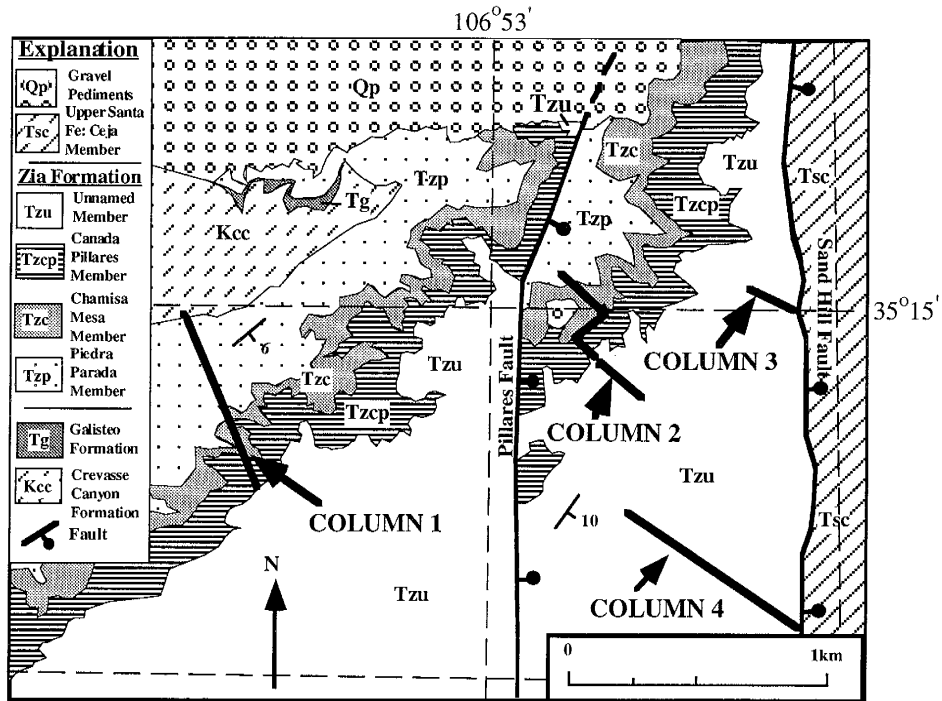
Figure 1.3. Geologic map of study area showing locations of stratigraphic columns. Geologic map modified from Gawne (1981).

**Sand Dominated Fluvial
Environment**

Explanation

Large and Small Channel Bodies (CH)

Sand Sheet Deposits (SS)

Overbank Fines (OF)

Paleosol Horizon (P)

Cross-stratified Eolian Dune
Deposits (EC)

Eolian Sheetsand Deposits (ES)

Interdune Deposits (ID)

**Mud Dominated Fluvial
Environment**

Eolian Environment
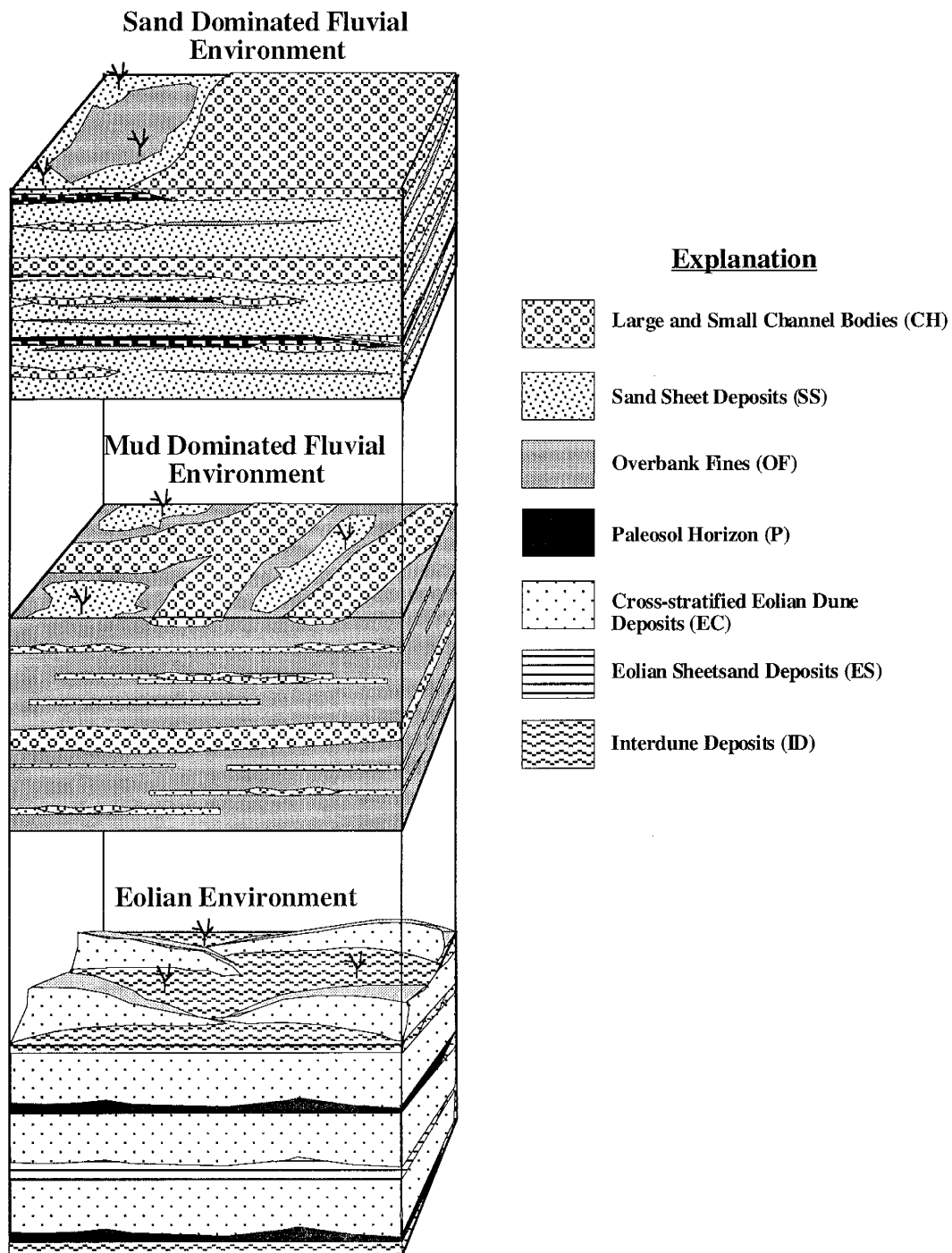
Figure 1.4. Schematic depositional geometry of the Zia Formation. Facies associations are described in Table 1.1 and Appendix A.

characteristics (Kocurek, 1981; Kocurek and Dott, 1981; Porter, 1987; Chan, 1989). Symbols used for fluvial and eolian facies associations (e.g., CH, OF, EC, ES; Table 1.1; Fig. 1.4; Appendix A) were developed for this study. Paleosol formation is a function of surface exposure time and landscape stability. Paleosols are important to understanding depositional environments and ancient flood basin accretion rates (Leeder, 1975; Allen, 1986; Atkinson, 1986; Kraus and Bown, 1986; Davis, et al., 1993). Because of this importance they will be considered separate from sheet sand and overbank deposits.

METHODS

Sections of the Zia Formation were measured along four transects to examine lateral and vertical variations in lithology and cementation (Fig. 1.3). Key beds were traced laterally throughout the study area to evaluate the continuity of cementation and variations in bedding thickness and cement morphologies. Cemented units were classified by outcrop morphology, surface textures, and sedimentary structures. Seventy-six samples were collected along the four measured sections for petrographic and geochemical analysis (Fig. 1.2). Laterally continuous units were sampled in more than one area to examine variations in petrographic and geochemical characteristics. Thin sections were made from most of the samples. Samples were impregnated with blue-dyed epoxy before thin section preparation to identify original porosity. These thin sections were analyzed for authigenic textures and mineralogy using a standard petrographic microscope, under plain light, crossed-polarized light, and cathodoluminesence. Mean grain size, sorting and roundness data were collected from outcrops and thin sections using visual comparators (grain size: Amstrat Inc.; sorting: Pettijohn, Potter, and Seiver, 1972; roundness: Powers, 1953). The cathodoluminesence was done on a microscope equipped with a MAAS/Nuclide model ELM-3 Luminoscope. A Chittick apparatus (modified from Dreimanis, 1962), was used to determine the total percentage calcite, and to test for the presence of other carbonates. The analytical precision based on 10 samples is better than 3 %. On selected samples, a JEOL-733 Superprobe, equipped with a high resolution back-scattered electron detector,

X-ray mapping features, and image analysis software was used to determine elemental composition and zoning in cements. Sample operating conditions were 20 nA sample current and 1-10 μm beam diameter. Carbonate standards were used and sample totals are 100 +/-2 % for all values. Finally, a Finnigan MAT Delta E isotope ratio mass spectrometer was used to analyze carbon and oxygen isotope values for each sample. Carbon and oxygen values were measured from CO_2 gas liberated from whole rock samples using 100% phosphoric acid. Data is reported in parts per mil ($^o/_{oo}$), relative to PDB for oxygen and carbon. The analytical precision, determined from 6 standards, is better than .1 $^o/_{oo}$ for both carbon and oxygen.

SAND PETROGRAPHY

Most of the Zia Formation in the King Ranch area can be classified as lithic arkoses (Fig. 1.5). The Zia Formation can be further subdivided into two distinct domains on the QFL diagram. One domain contains the lower Zia Formation (Piedra Parada, Chamisa Mesa, and Canada Pillares Members), the other domain contains the Unnamed Member. The lower Zia Formation changes from a felspathic litharenite (Piedra Parada Member) to lithic arkoses (Chamisa Mesa, Canada Pillares Members). The Unnamed Member exhibits scattered compositions, but is differentiated from the lower members by greater amounts of feldspar (Fig. 1.5).

Volcanic rock fragments of intermediate composition are generally the most abundant lithic fragments, averaging 70 to 90% of all rock fragments (Fig. 1.5). Chert is the most common sedimentary rock fragment, although some units contain abundant detrital carbonate (Fig. 1.5). These carbonate fragments resemble pedogenic carbonates and may be derived from erosion of underlying pedogenic units.

Most volcanic lithics are fresh and well rounded, however, chemical alteration has removed unstable phenocrysts such as hornblende from some volcanic grains, leaving euhedral voids. More irregular voids indicate dissolution of aphanitic/glassy groundmasses. Potassium feldspars vary from fresh to deeply altered to clays.
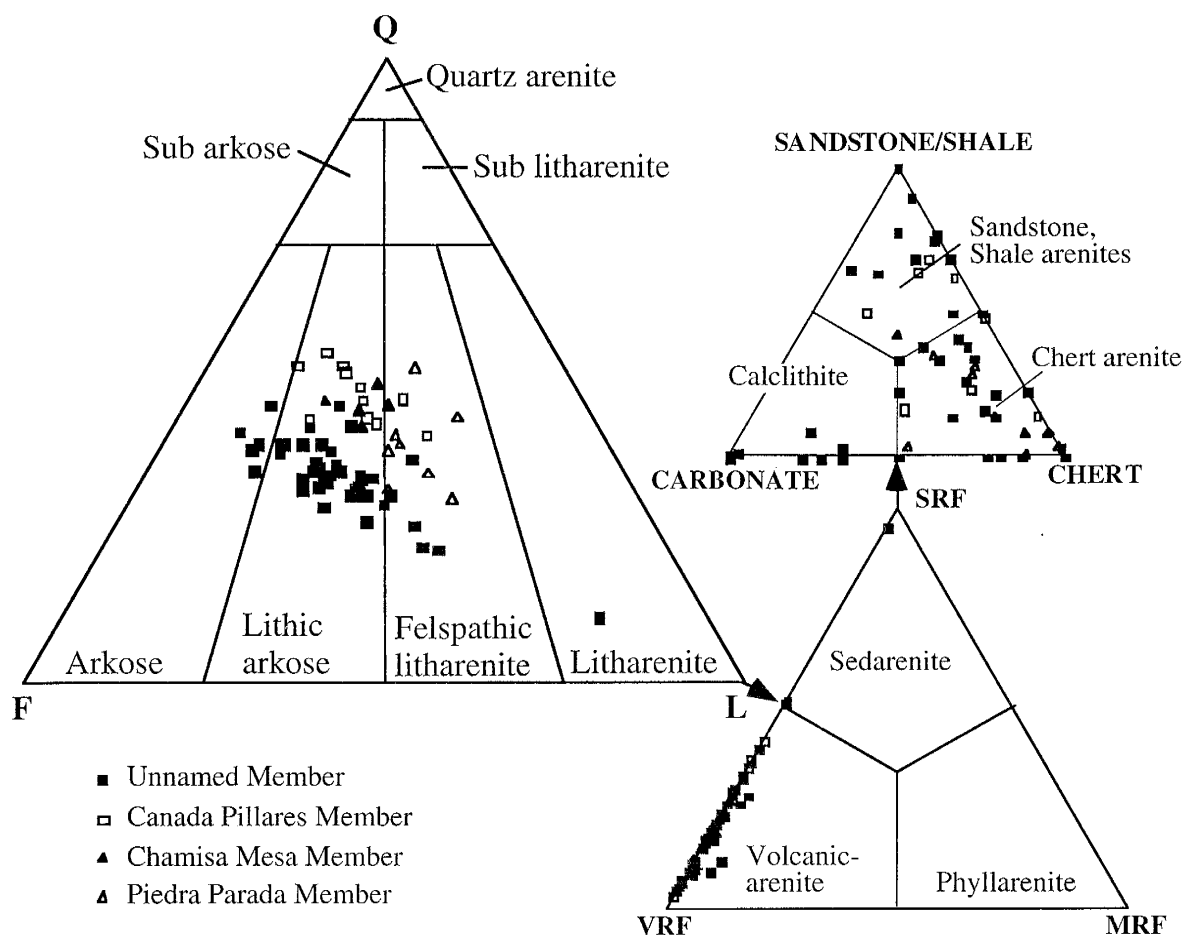
Figure 1.5. Ternary plot of sand composition by member of the Zia Formation. Sample that plots as a litharenite contains a large amount of detrital carbonate. Classification from Folk (1974).

TYPES OF CALCITE CEMENTATION

Calcite cementation in the Zia Formation is complex, exhibiting a wide range of macroscopic and microscopic morphologies. Four principal types of isolated concretions, and three principal types of laterally extensive tabular units were identified. A summary and description of facies associations, lithofacies types, lithologic data, and cementation types are shown in Table 1.1. Descriptive data and interpretations for each cementation type are provided in Table 1.2. Details of the stratigraphic spatial distribution and lithofacies/lithologic associations of these cementation types are shown in Figures 1.6-1.11.

EXPLANATION

LITHOLOGY

sand/sandstone

silty sand

shaly sand

sandy silt

silt/siltstone

silty shale

sandy shale

shale/mudstone

gravel/conglomerate

algal tufa

PHYSICAL STRUCTURES

trough cross-stratificaton

high angle planar bedding

low angle tabular bedding

planar cross stratification

wavy parallel bedding

current ripples

graded bedding

rip-up clasts

mudcracks

micritic nodules

teepee structures

DEGREE OF CEMENTATION

very well cemented

well cemented

moderately cemented

poorly cemented

trace to no cement

ICHNOFOSSILS

rhizocretions

burrows

Figure 1.6. Explanation of symbols and patterns used in stratigraphic columns in Figures 1.7 - 1.10.

Table 1.2. Summary of descriptive data and interpretations of cementation types in the Zia Formation.

Cementation Type	Host Lithology	Outcrop Morphology	Surface Textures	Microtextures	Environment of Precipitation
nodular concretions	clays, clay-rich silty sand	0.1-5 cm diameter ovoid to irregular shapes	smooth to pitted, tubed and grooved	micritic fabric, meniscus cements, circumgranular cracking, crystallaria, alveolar textures, grain dissolution	vadose
ovoid to elongate concretions	fine to coarse sand	1-4 cm diameter ovoid to > 10 m elongate shapes	smooth to warty	poikilotopic to blocky spar	phreatic
platy concretions	clays, clay-rich silty sand	5-50 cm across plates that seem to follow relict textures	smooth to pitted, tubed and grooved	micritic fabric, meniscus cements, circumgranular cracking, alveolar textures, grain dissolution	vadose
rod concretions	clays, silty sand, and sand	0.1-5 cm diameter, 3-50 cm long; single or branching, thin downwards	mostly smooth, but sometimes pitted, tubed and grooved	micritic fabric, circumgranular cracking, alveolar textures, grain dissolution	vadose
type-1 tabular cemented unit	fine to coarse sand	generally >10 m lateral extent, with preserved sedimentary structures; sharp lower, and generally sharp upper boundaries	smooth to warty surface	poikilotopic to blocky spar	phreatic
type-2 tabular cemented unit	very fine to medium grained clayey to silty sand	generally 10-200 m lateral extent; massive, mottled, wavy-platy, brecciated, teepee, laminar features; sharp upper and diffuse lower boundaries	smooth to pitted, tubed and grooved	micritic fabric, meniscus cements, circumgranular cracking, radial spar, alveolar and fenestral textures, grain dissolution	vadose
type-3 (phreatic) tabular cemented unit	fine to medium grained sand	generally >10 m lateral extent, with preserved sedimentary structures plus rod shapes	smooth to warty, sometimes very irregular with pits, tubes, and grooves	blocky spar and sparry floating grain textures	phreatic >> vadose
type-3 (vadose) tabular cemented unit	very fine to medium grained clayey to silty sand	massive, mottled, with nodules, rods, and plates; some sedimentary structures preserved	smooth to pitted, tubed and grooved	micritic fabric, meniscus cements, circumgranular cracking, alveolar and micrite-spar textures	vadose >> phreatic
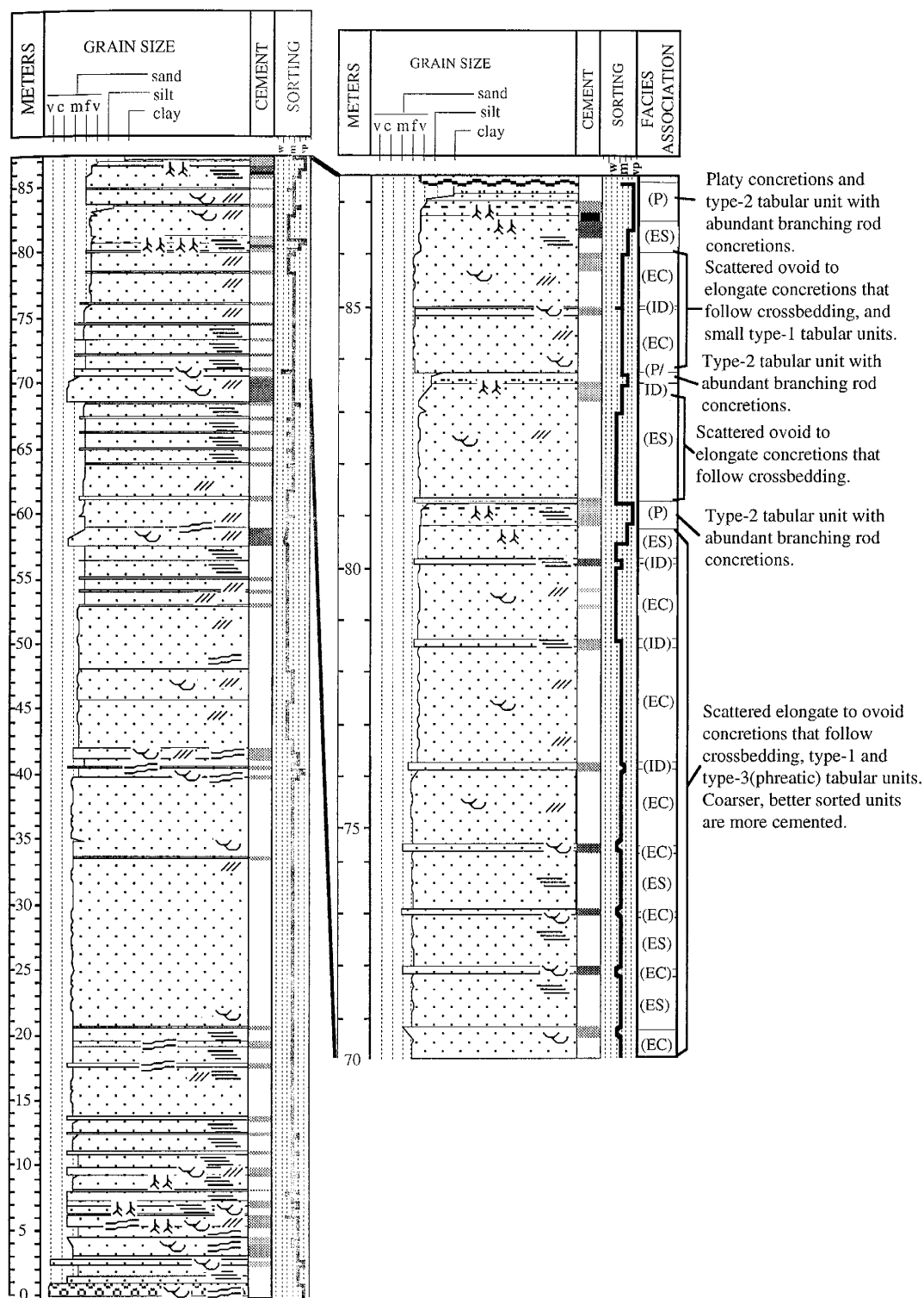
Figure 1.7. Stratigraphic column of fluvial-eolian and eolian sediments of the Piedra Parada Member. Nodular, platy, and rod-shaped concretions are associated with paleosol horizons (P), and interdune (ID) facies associations. Small type-1 tabular units and scattered ovoid to elongate concretions dominate in the cross-stratified eolian facies (EC). Note that coarser portions of eolian sandsheets (ES) and interdune deposits are preferentially cemented. For explanation of symbols and patterns used in columns, see Figure 1.6.
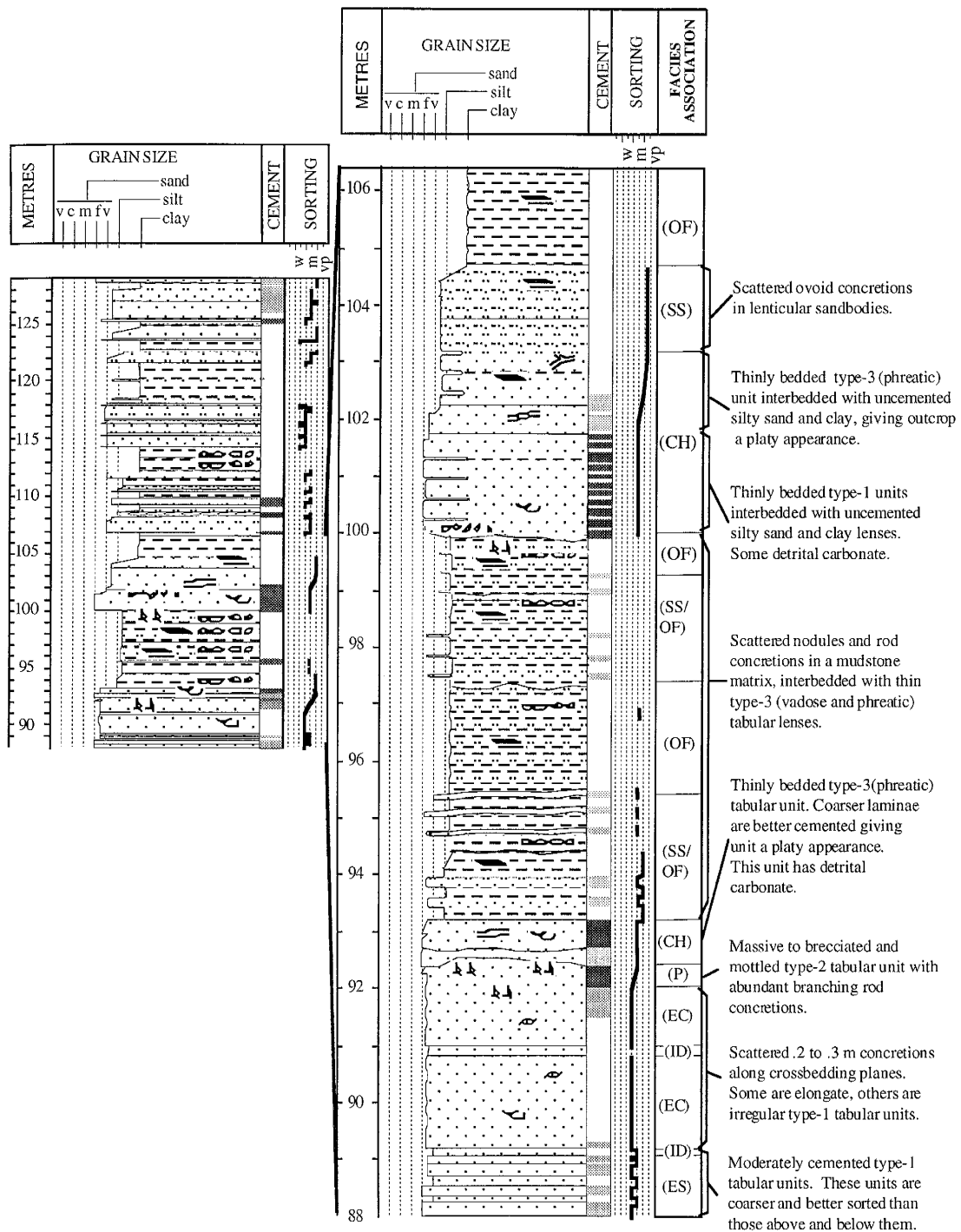
Figure 1.8. Stratigraphic column of fluvial, fluvial-eolian, and eolian sediments of the Chamisa Mesa and Canada Pillares Members. Note correlation between coarser better sorted channel (CH) associations and good cementation. Nodular, platy and rod-shaped concretions are associated with sheet sand (SS) and overbank fine (OF) sediments. Scattered ovoid and elongate concretions dominate in the cross-stratified eolian facies (ES). Note the coarser portions of eolian sand sheets (ES) are preferentially cemented. For explanation of symbols and patterns used in columns see Figure 1.6.

20
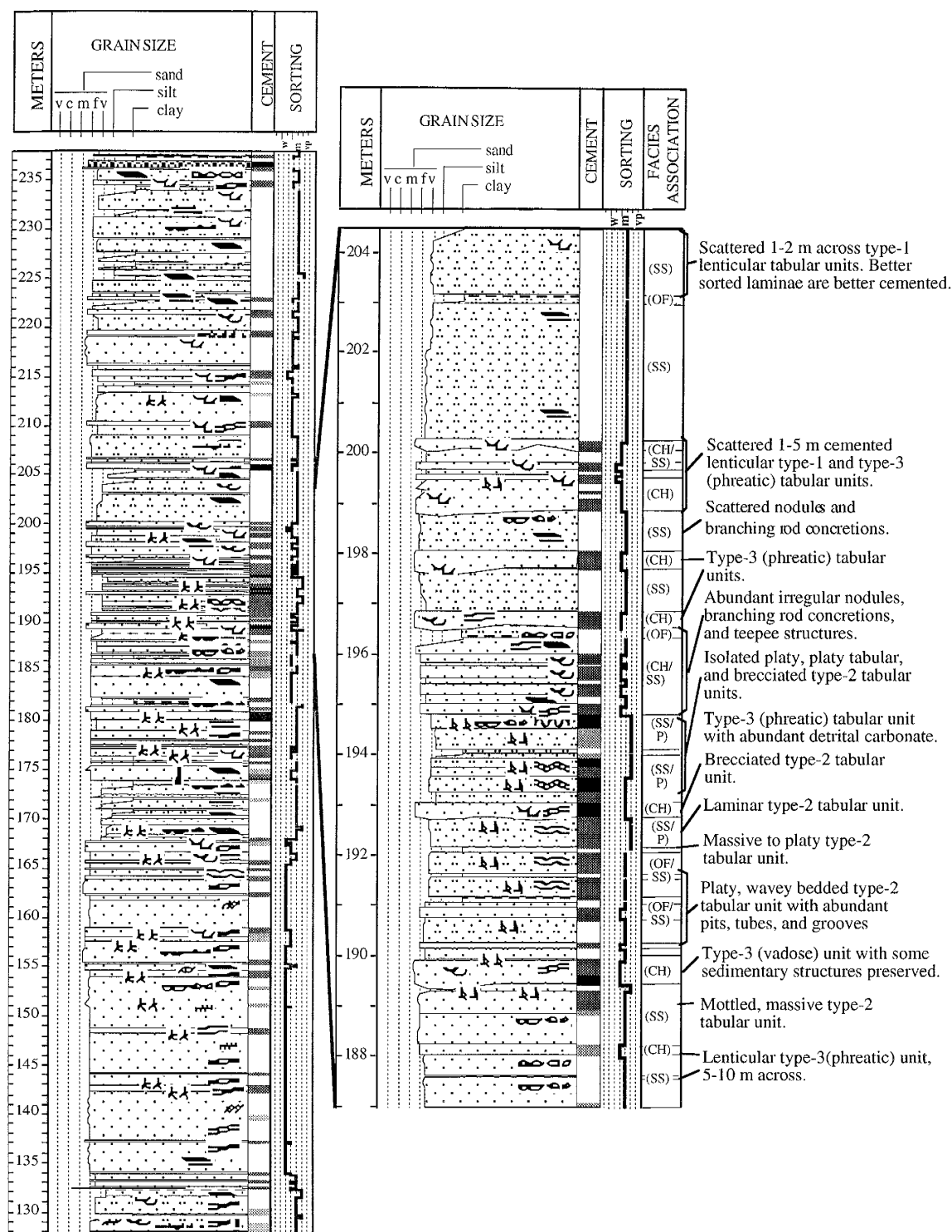
Figure 1.9. Stratigraphic column of fluvial, fluvial-eolian, and eolian sediments in the lower half of the Unnamed Member. Note the correlation between coarser and better sorted channel (CH) associations and good cementation at 190, 193, 196, and 199 meters. Sheet sand (SS) and overbank fine (OF) sediments are associated with laminated and brecciated laterally extensive paleosol horizons (P).   Nodular, platy and rod shaped concretions are associated with small channels (CH), sheet sand (SS), and overbank fine (OF) sediments. For explanation of symbols and patterns see Figure 1.6.

21
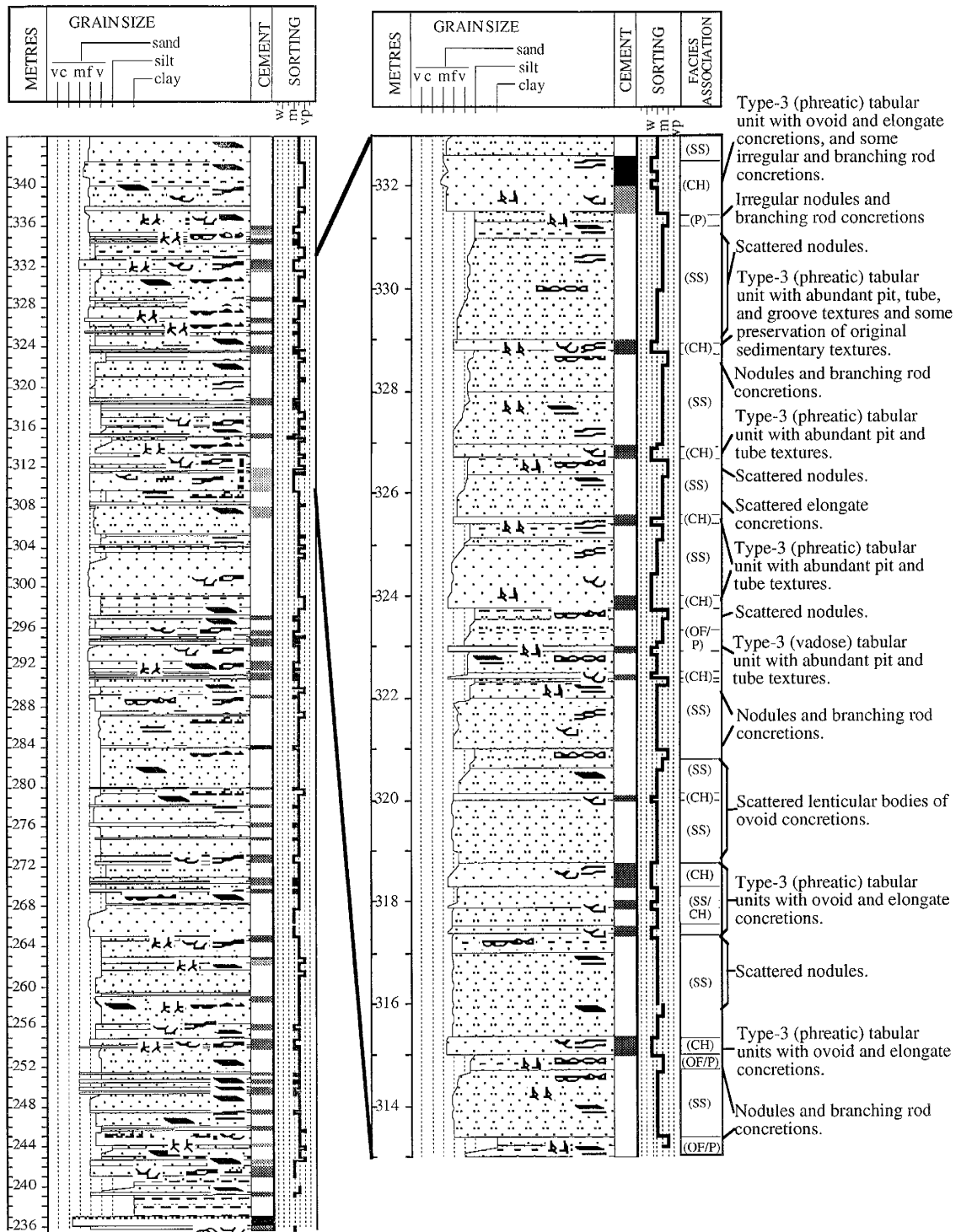
Figure 1.10. Stratigraphic column of fluvial sediments in the upper half of the Unnamed Member. Note correlation of coarser and better sorted channel (CH) associations with good cementation. The finer, poorer sorted sections of sheet sand (SS) and overbank fine (OF) sediments are associated with nodules and rod-shaped concretions. For explanation of symbols and patterns see Figure 1.6.

22
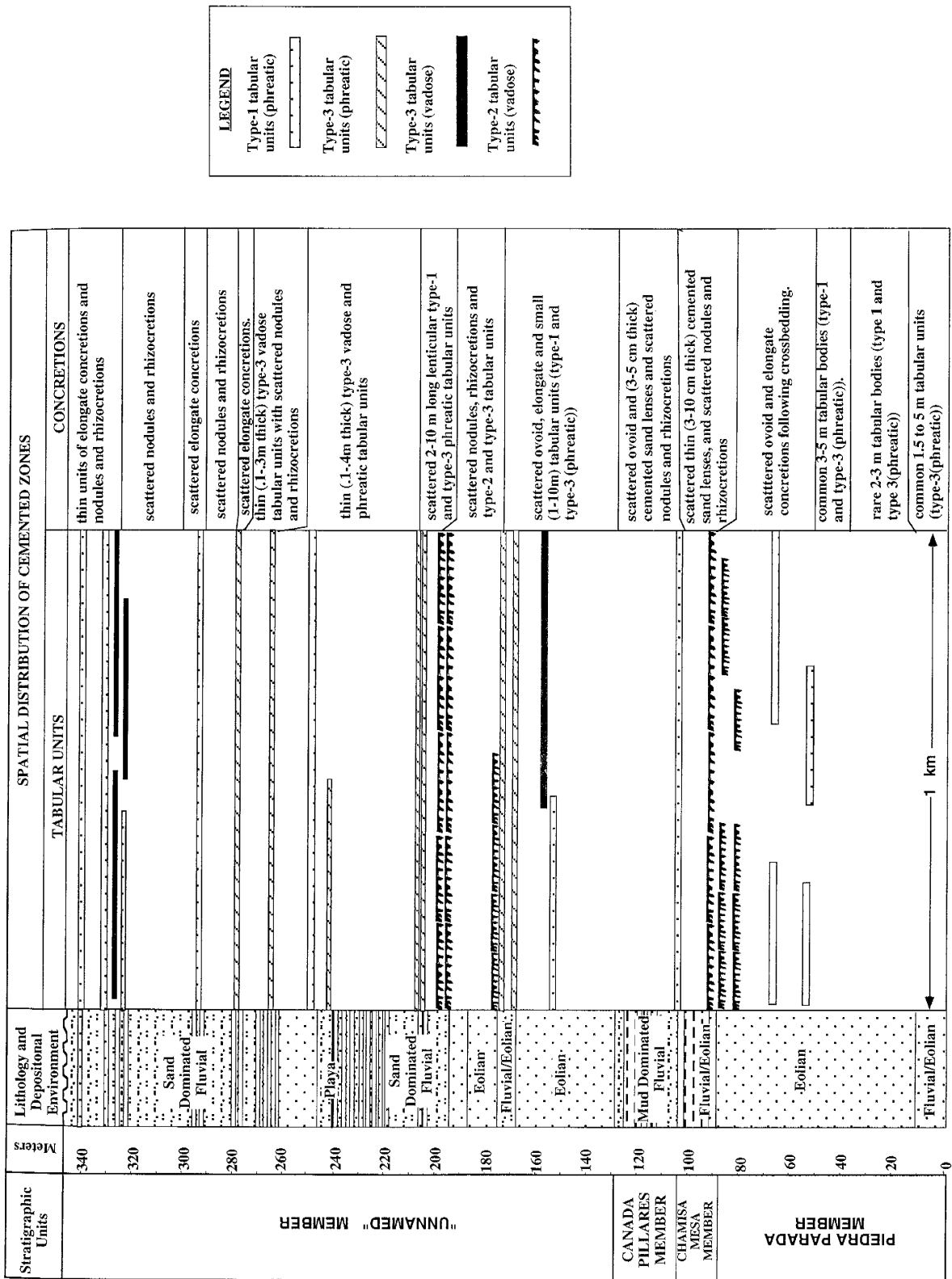
Figure 1.11. Spatial distribution of cementation types in the Zia Formation. Note the association of laterally extensive phreatic units with sand lithologies. Laterally extensive vadose units are not associated with any particular depositional environment.

Concretions

Nodules

Nodules can be subdivided into two types. The first type consists of small (0.1-5 cm diameter) subspherical to irregular forms (Fig. 1.12A). These types are common in reddened clays and clay-rich silty sands in overbank fine (OF), and paleosol (P) horizons (Table 1.1; Figs. 1.7-1.10). Some of the first kind of nodules exhibit two stages of concentric zonation, distinguished by a color change from grey or greenish grey in the middle to pink on the outside. Dense micrite forms the usual matrix, and crystallaria (with some circumgranular forms) are common (Fig. 1.12B). The second type of nodule is roughly the same size and shape, but is also characterized by oval grooved and tubular surface pitting (Fig. 1.12C). This type of nodule is more common in the silts and silty sands of sheet sand deposits (SS), overbank fines (OF), and paleosols (P)) in the upper Unnamed Member (Figs. 1.9, 1.10). This type of nodule exhibits a micritic matrix, circumgranular cracking, micrite-spar, and some alveolar textures as well (Fig. 1.12D). A micrite-spar microtexture is where grains or groups of grains are coated with micritic cements, and the areas in between are filled with spar (16-50μ diameter).

Ovoid and Elongate Concretions

These concretions range from small (1-4 cm diameter) ovoid and oblate forms, to elongate cemented masses (Figs. 1.13A-1.13C). Ovoid concretions are found isolated or coalesced in botyroidal masses (0.2-1 m diameter). Elongate concretions are cemented masses (generally <10 m long) in which the long axis of the concretion is oriented subparallel to bedding. Elongate concretions also occur alone or in irregularly shaped groups with similar orientations. Most ovoid to elongate concretions are covered with millimeter sized wart-like structures (hereafter referred to as warts). Where it is possible to tell, ovoid to elongate concretions seem to form in coarser units with better

Figure 1.12 A. Irregular micritic nodules in a clay-rich silt from the Chamisa Mesa Member. Divisions on scale are in centimeters. **B.** Photomicrograph of a nodule showing micritic matrix, crystallaria (large spar vein through middle of photo), and circumgranular cracking (arcuate shapes in upper center). **C.** Nodule with pitted, tubular pores (shown by arrows), and grooved surface textures. Tubular structures are filled with spar calcite in the center of the nodule. Divisions on scale are in centimeters. **D.** Photomicrograph of previous nodule showing a micritic matrix, and a complex mixture of alveolar textures and circumgranular cracking. Alveolar textures are more rounded than circumgranular cracking, and not necessarily associated with framework grains.
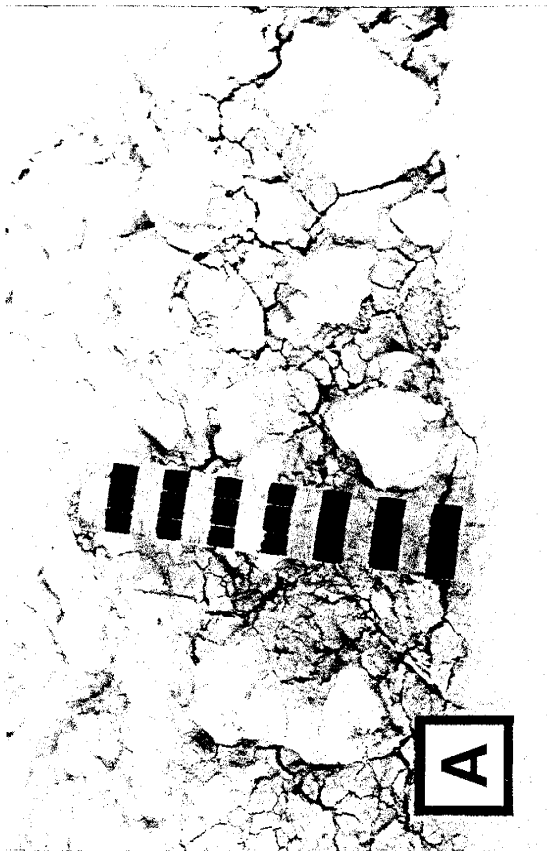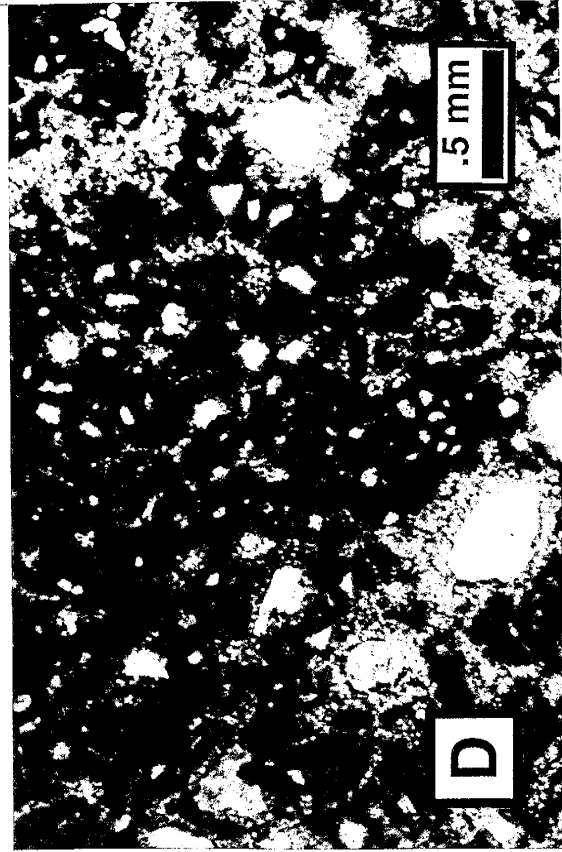
Figure 1.13 A. Isolated and groups of ovoid concretions from the Piedra Parada Member. Divisions on the scale are in centimeters. **B.** Elongate concretions that seem to be constructed from ovoid concretions. These concretions show concentric internal zonation. **C.** Elongate concretions from the upper part of the Unnamed Member. Note the consistency of the orientation. Scale applies to foreground only. **D.** Concentric ovoid concretion from the upper part of the Unnamed Member. Divisions on the scale are in centimeters.

sorting than beds either above or below them. This relationship is not well demonstrated in the cross-stratified dune (EC), or eolian sand sheet (ES) deposits (Table 1.1; Figs. 1.7, 1.8), but is more evident in channel (CH) sand bodies (Table 1; Figs. 1.8-1.10). Calcite cements in ovoid concretions are poikilotopic to blocky spar (15 μm-1.0 mm diameter). Although most ovoid to elongate concretions are not zoned, some exhibit internal zonation, of which two types can be recognized. The first type consists of two concentric zones, differentiated by only a color change from grey (inner zone) to pink (outer zone). The second type consists of six or more concentric layers of radial spar cement (layers vary from 0.5 to 3 mm in thickness; Fig. 1.13D).

Platy Concretions

Platy concretions are small (5-50 cm diameter), flat, irregularly shaped masses, that commonly occur in groups or masses with a consistent planar orientation and are subparallel to bedding. This type of concretion is commonly associated with sheet sand deposits (SS), overbank fines (OF), paleosol horizons (P), and interdune (ID) deposits (Table 1.1; Figs. 1.7-1.10). Surfaces of platy concretions commonly have 1-3 cm diameter pits, tubes, or grooves (Fig. 1.14A), although smooth surfaces are also found. Platy concretions with pitted, tubed or grooved surfaces commonly have a micritic matrix, with micrite-spar and alveolar textures (Fig. 1.14B), whereas those with smooth upper and lower surfaces commonly have a microspar (7-15μ diameter) matrix.

Rod Concretions

Tube and rod concretions are small (0.1 - 5 cm diameter, 3 - 50 cm long) horizontal to vertical masses, that occur both individually and in groups. These concretions are associated with overbank fines (OF), paleosol horizons (P), eolian sand sheet deposits (ES), and interdune (ID) deposits (Table 1.1; Figs. 1.7-1.10). They commonly branch, and most thin downwards (Fig. 1.14C). Some rod concretions have pitted, tubular and grooved surface textures; most are smooth. Calcite cements associated with these

Figure 1.14 A. Platy concretion from the middle of the Unnamed Member with millimeter sized pits, tubular pores (arrows) and groove structures. Divisions on the scale are in centimeters. **B.** Photomicrograph of alveolar textures (A) from a platy concretion. **C.** Rod-shaped concretions from eolian sands in the Chamisa Mesa Member. Note that several of them branch and thin downwards. Divisions on the scale are in centimeters. **D.** Radial spar microtexture resembling microcodium.
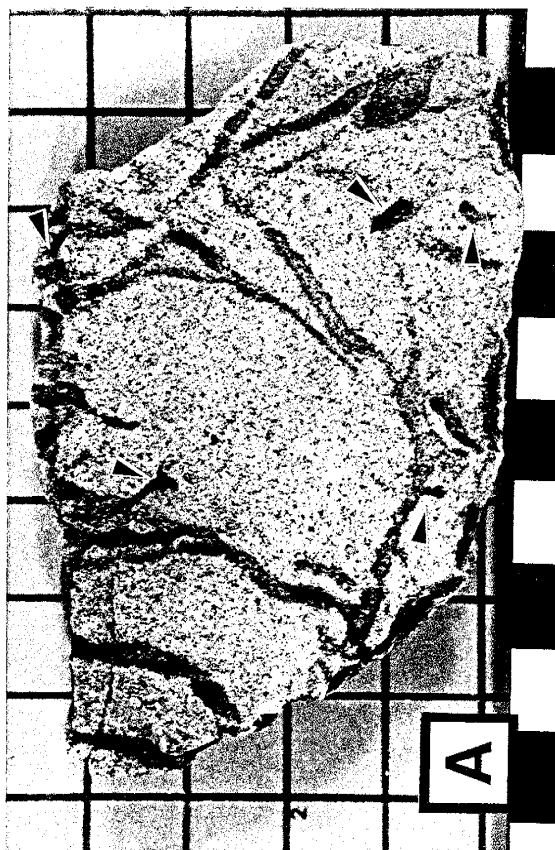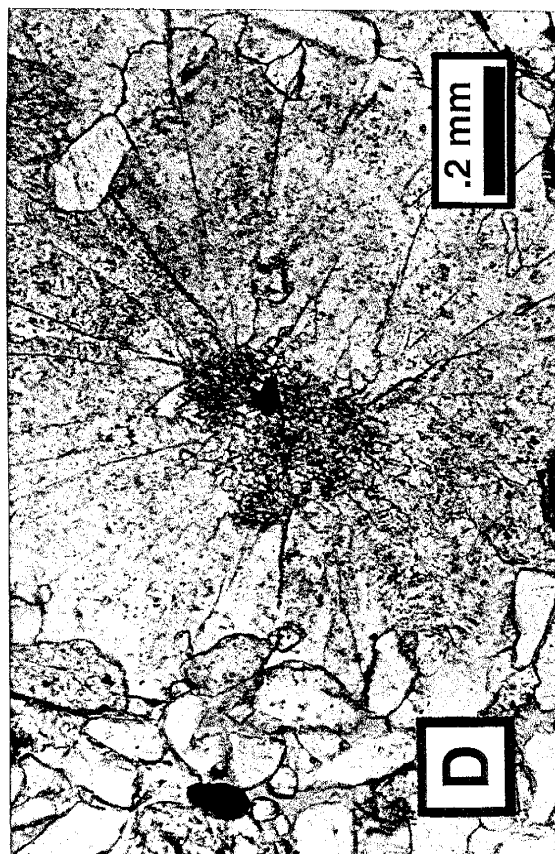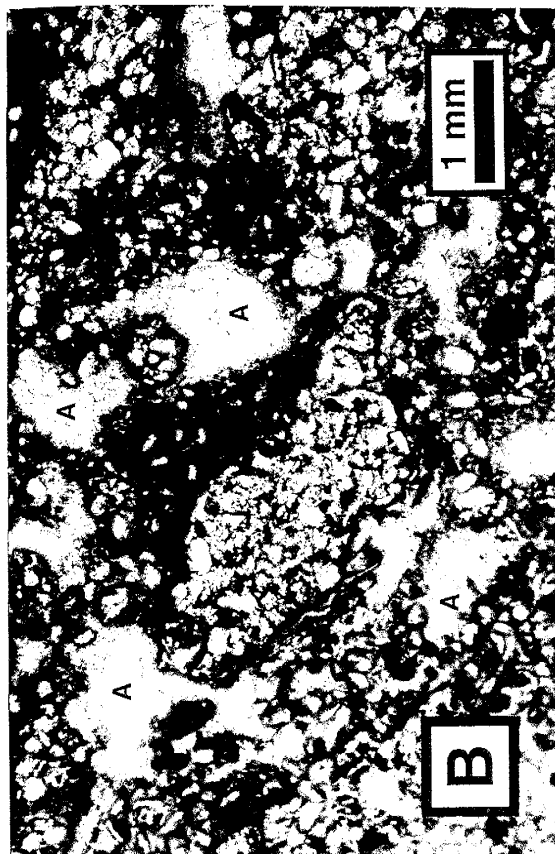
concretions are dominantly micritic and exhibit circumgranular cracking, alveolar, micrite-spar, and meniscus microtextures. Radial spar microtexture is present locally. This microtexture is characterized by bladed radial spar, formed around a micritic nucleus (Fig. 1.14D).

Tabular cemented units

Tabular cemented units are 0.2 to 3 m thick bodies that commonly extend for hundreds of meters or more laterally. These units can be divided into three types: those with original sedimentary structures preserved (type 1); those in which sedimentary structures are not preserved, with tube, grove and pitted surfaces textures (type 2); and those in which some of type-1 and type-2 characteristics are present (type 3).

Type 1 (sedimentary structures preserved)

Sedimentary structures such as trough and planar crossbedding are common features of type-1 tabular cemented units (Fig. 1.15A). These cemented units are coarser grained and better sorted than units immediately below and above (Figs. 1.8-1.10). Lower contacts are commonly sharp and locally erosive. Upper contacts are commonly sharp. Bed outlines can be lenticular, wavy, and irregular, depending on the original sedimentary structures preserved. These units are commonly associated with channel associations (CH), and coarser, better sorted units in sheet sand deposits (Table 1.1, Figs. 1.7-1.10). These units vary from 0.2 to 3 meters in thickness and can be of great lateral extent (>1 km; Fig. 1.11). Calcite cementation textures are mainly blocky spar. Coalesced ovoid to elongate concretions are commonly found on the tops of these units. These coalesced concretionary beds are commonly less than one meter in thickness and can extend for tens of meters laterally (Fig. 1.11).

Type 2 (no sedimentary structures preserved)

Type-2 tabular units lack original sedimentary structures, and are commonly associated with reddened clays and clayey sands from overbank fine (OF), paleosol (P), and interdune (ID) deposits (Table 1.1; Figs. 1.7-1.10). Micritic calcite is the main cement, and micrite-spar textures, grain dissolution, alveolar structures, circumgranular

cracking, and meniscus cement are common. Type-2 tabular units are subdivided by outcrop morphology into: massive, platy, wavy bedded, fractured, and laminar bed-forms.

The most common type-2 morphology is characterized by massive bedding, with abundant branching or isolated rod structures, and pitted, tubular and grooved surface textures (Fig. 1.15B). Lower contacts are commonly gradational. This morphology is generally 0.3 - 1 m thick, and occasionally can be of great lateral extent (> 1 km; Fig. 1.11).

Some outcrops are thin (10-20 cm), platy or wavy bedded, with pitted, tubular and grooved surfaces (0.5 to 3 cm diameter). These thin bedded units are generally less than 10 m in lateral extent.

Other outcrops are characterized by millimeter sized calcite-filled fractures that are in places irregular, unoriented, and fenestral, and sometimes resemble small folds (Fig. 1.15C). Original sedimentary structures are generally not preserved. These units may also be associated with tubular, rod and platy concretions. These outcrops exhibit alveolar and fenestral microtextures, and displacement laminae in thin section.

Some outcrops have an irregular wavy laminar (3-10 cm thickness) morphology. Individual laminae are vary from 1 to 2 mm in thickness. These units commonly have sharp upper and lower contacts. These forms exhibit abundant alveolar and fenestral micro-textures (Fig. 15D).

Type 3 (tabular units with mixed features)

The above descriptions are of pure end-member cementation types. However, most tabular cemented units in the Zia Formation show a mixture of characteristics of these end-members. Units that are closest in appearance to the type-1 end-member have excellent preservation of sedimentary structures, with rare pit and tube structures (Type 3; Fig. 1.16A). The most common, thickest and most laterally extensive units (> 2 km) are those that are close in appearance to type-1 tabular units (Fig. 1.11). Mixed feature cements near the type-2 end-member are associated with more poorly sorted, finer grained layers and pit,

Figure 1.15 A. Type-1 tabular unit from the middle of the Unnamed Member. Note the good preservation of sedimentary structures. Units on the scale are in decameters. **B.** Type-2 tabular unit from the Piedra Parada Member. Note absence of sedimentary structures. Units on the scale are in decameters. **C.** Structures resembling small folds from the middle of the Unnamed Member. Units on the scale are in centimeters. **D.** Photomicrograph of fenestral/laminar microtextures common in tabular units with laminar, brecciated, and teepee outcrop morphologies.
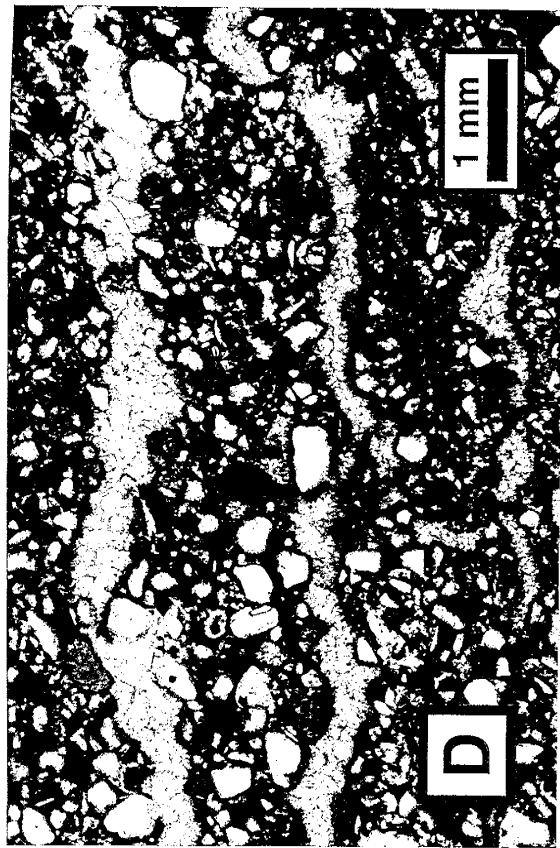
tubes, and rod structures, with some evidence of the original sedimentary structures (Type 3; Figure 1.16B).

Type-3 units also show a mixture of cement textures, including floating grain and micrite-spar types. Floating grain microtextures are commonly characterized by grains surrounded by drusy to isopachous sparry cements, with the remaining void spaces filled with micrite or microspar (Fig. 1.16C). This type of cement is commonly found in units near the type-1 end-member. The micrite-spar micro-texture is most common in mixed units near the type-2 end-member (Fig. 1.16D. In these units, the spar is generally equal or more abundant than the micrite cements.

Cathodoluminesence and Elemental Composition

Authigenic calcite varies from bright orange to non-luminescent, whereas detrital carbonate is a dull orange. Poikilotopic and blocky spar associated with ovoid and elongate concretions and type-1 tabular units are typically a dull orange to non-luminescent. Some type-1 tabular units, and most type-3 show some zonation (bright orange, to dull orange-red, and non-luminescent). In most cases this zonation is not visible under plane polarized light. Micritic cements are either a dull orange-red or non-luminescent. Spar filled alveolar and fenestral textures associated with these micrites are only luminescent along the very edges. Oscillatory zoning (regular and irregular) in this spar occurs rarely. Although zonation is visible under cathodoluminesence, it is not visible using back-scattered electron imaging. Microprobe analysis shows that the cements, regardless of microtexture, are very near the calcite end-member composition (Fig. 1.17). Magnesium is the main impurity, and even this is rarely over 1 mol %. Cements from the Sand Hill Fault at the top of the section show slightly more magnesium than Zia Formation samples (Mozley and Goodwin, 1995b; Fig. 1.17).

Figure 1.16 A. Type-3 (phreatic) tabular unit. Although there is good preservation of sedimentary structures, a branching downwards tube is shown by the arrows. Hammer is approximately 18 centimeters long. **B.** Type-3 (vadose) tabular unit. Arrows point to relict sedimentary structures. Divisions on the scale are in decimeters. **C.** Spar-micrite microtexture from a type-3 (phreatic) unit. Framework grains are coated in displasive isopachous spar, and the space in-between is filled with micrite. **D.** Micrite-spar microtexture from a type-3 (vadose). Grains and groups of grains are coated with micrite, and the space in-between is filled with spar.
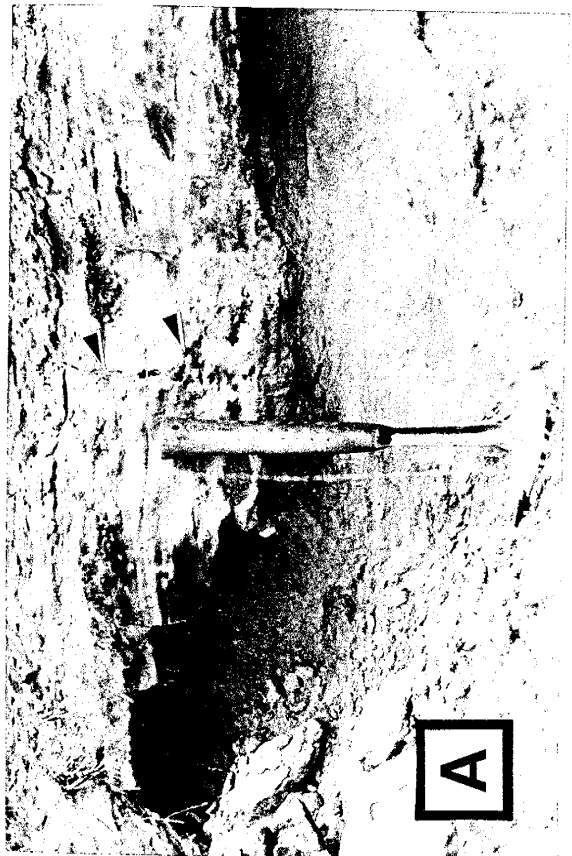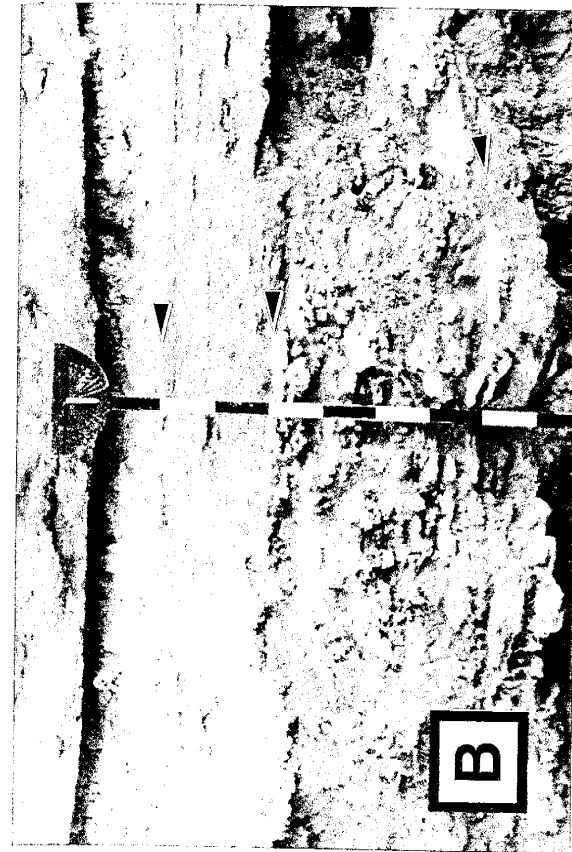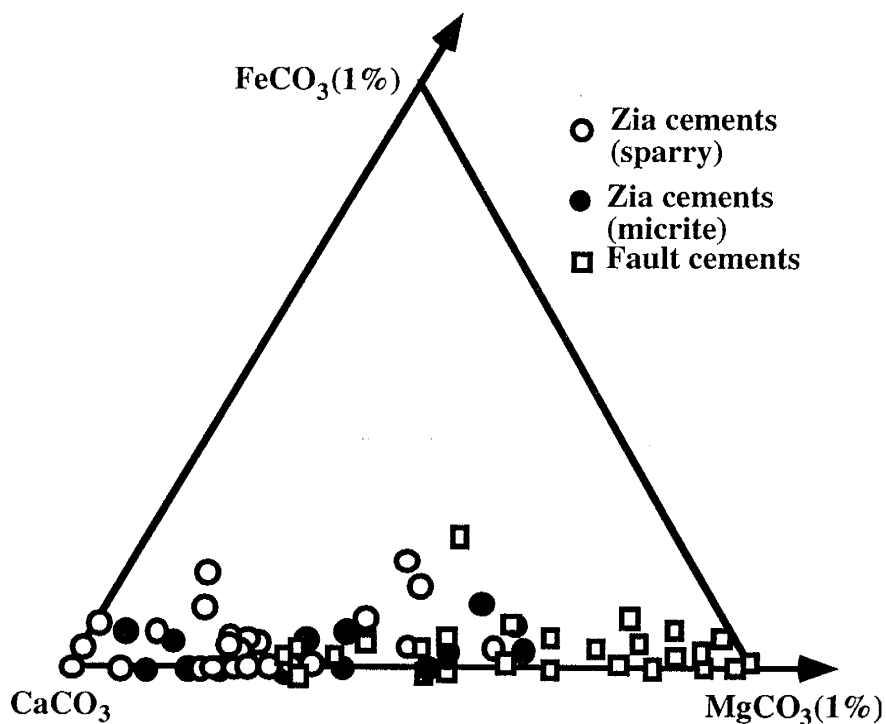
Figure 1.17. Ternary diagram showing composition of micrite, spar and Sand Hill fault cements from the study area. The scale of the plot is at 99% CaCO3 (mol %). Data for fault cements from Mozley and Goodwin (1995b).

Isotope Geochemistry

The isotopic composition of the various calcite types does not vary greatly. Carbon isotope values ($\delta^{13}C$) range from -3.0 to -5.5 $^o/_{oo}$ PDB, whereas oxygen isotope values ($\delta^{18}O$) range from -7.3 to -13.6 $^o/_{oo}$ PDB (Table 1.3). $\delta^{13}C$ values for nodular, platy, and rod shaped concretions, and type-2 tabular units are generally heavier than other types regardless of stratigraphic position (Fig. 1.18). There is also a weak upward stratigraphic trend of increased $\delta^{13}C$ values in the Unnamed Member for type-1 and type-3 tabular units. $\delta^{18}O$ values for the lower part of Zia Formation show no definite trend with stratigraphic position, but there is an increase in $\delta^{18}O$ values in type-1 and type-3 tabular units higher in the section within the Unnamed Member (Fig. 1.18). The highest value for Zia Formation cements (-7.3 $^o/_{oo}$ PDB) approaches the average value of the fault cements (-7.1 $^o/_{oo}$ PDB; Mozley and Goodwin, 1995b). Samples collected along a 500 meter lateral traverse of a single cemented horizon that intersects the fault have similar $\delta^{18}O$ values (Fig. 1.19). The sample closest to the fault (0.5 m) has the closest value to the fault cements

(-7.3 $^o/_{oo}$ PDB). Type- 2 tabular units and nodular, platy, and rod shaped concretions are generally more enriched in ^{13}C and depleted in ^{18}O than those associated with type-1 and type-3 tabular units and ovoid and elongate concretions (Fig. 1.20).

● Type-2 tabular units, and nodules, rod-shaped and platy concretions (Vadose)

○ Type-3 units with mostly type-2 characteristics (Type-3 (Vadose))

■ Type-1 tabular units and ovoid and elongate concretions (Phreatic)

□ Type-3 units with mostly type-1 characteristics (Type-3 (Phreatic))

▲ Fault cements
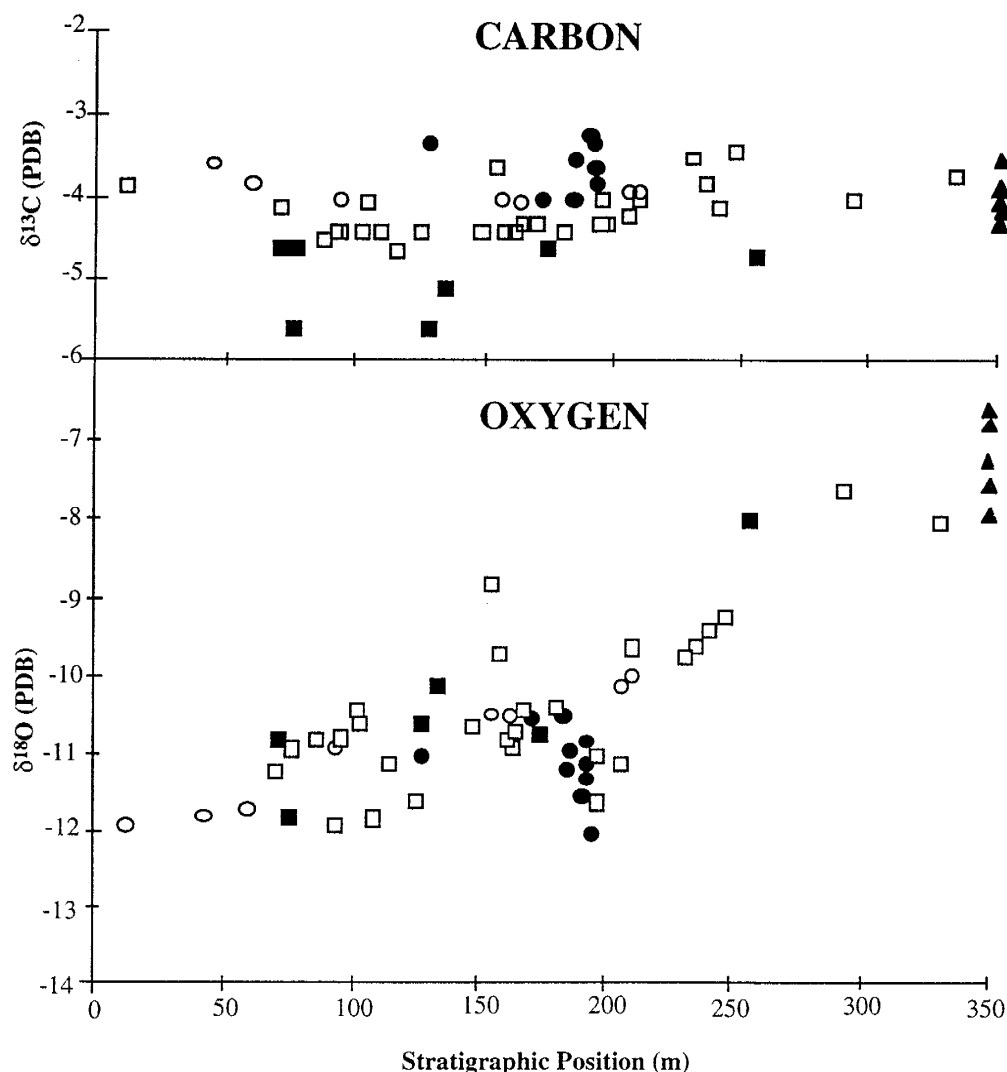
Figure 1.18. Plot of carbon and oxygen isotope values versus stratigraphic position. δ^{13} C values exhibit significant scatter even within a single horizon (see 180-190 m). Phreatic carbon values however, do plot consistently below those of vadose values, regardless of stratigraphic position. δ^{18}O values show more scatter than carbon values, and increase in the upper 2/3 of the Unnamed Member.
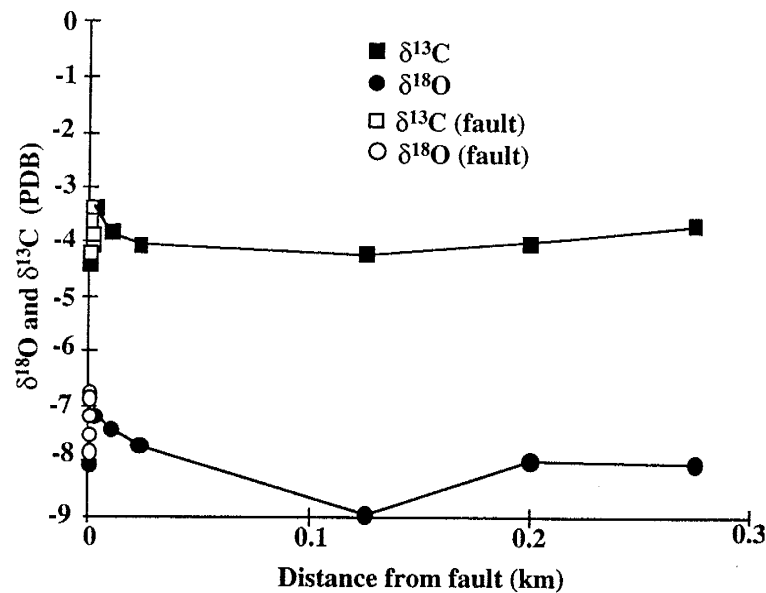
Figure 1.19. Plot of $\delta^{13}C$ and $\delta^{18}O$ values versus distance from the Sand Hill Fault. These samples were taken from a single laterally extensive stratigraphic horizon.
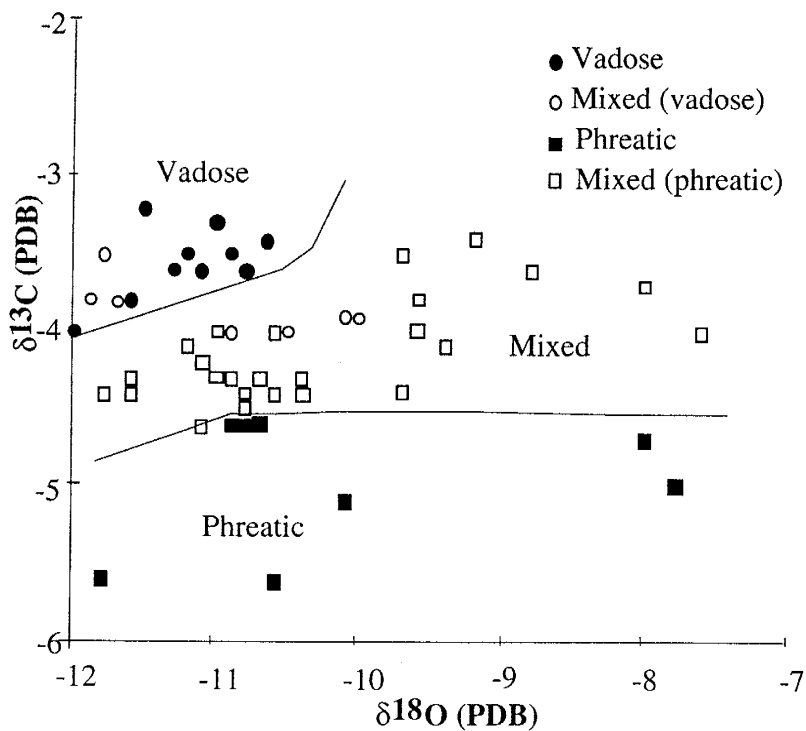
Figure 1.20. Plot of $\delta^{13}C$ versus $\delta^{18}O$, with individual points identified by cementation types. Vadose types include nodule, platy, and rod concretions, as well as type-2 tabular units. Phreatic types include ovoid to elongate concretions as well as type-1 tabular units. In general vadose cements have heavier carbon values and lighter oxygen values than phreatic cements. Phreatic and type-3 (phreatic) units that plot with oxygen values greater than -10 are from the upper part of the Unnamed Member.

Table 1.3. Carbon and oxygen isotope values for cemented units in the Zia Formation Stratigraphic location of samples indicated on Figure 2.2; -phr indicates mostly phreatic; -vad indicates mostly vadose; * indicates units with abundant detrital carbonate.

Sample No.	% CaCO$_3$	$\partial^{13}C$ PDB	$\partial^{18}O$ PDB	Cementation Type	Sample No.	% CaCO$_3$	$\partial^{13}C$ PDB	$\partial^{18}O$ PDB	Cementation Type
8394-1	26	-3.8	-11.9	type-3vad	81994-18	31	-4.1	-9.4	type-3phr
8394-2	39	-3.5	-11.8	type-3vad	81994-19	39	-3.4	-9.2	type-3vad
8394-3	42	-3.8	-11.7	type-3vad	81994-20	49	-4.7	-8.0	elongate
8394-4	31	-4.1	-11.2	type-3phr	122394-1	50	-3.2	-11.5	type-3vad
8394-5	31	-5.6	-11.8	elongate	122394-2	70	-3.5	-11.2	type-2
8394-6	52	-3.0	-11.4	type-3phr*	122394-3	60	-3.5	-10.9	type-2
8394-7	32	-4.0	-10.6	type-3phr	122394-4	34	-4.0	-10.5	type-2
8594-1	29	-4.6	-10.8	ovoid	122394-5	66	-4.4	-10.4	type-3phr
8594-2	29	-4.6	-10.9	elongate	122394-6	31	-4.6	-10.7	type-3phr
8594-3	29	-4.5	-10.8	type-3phr	122394-7	62	-4.0	-10.5	type-2
8594-4	25	-4.0	-10.9	type-2	122394-8	28	-4.3	-10.4	type-3phr
8594-5	27	-4.4	-11.9	type-3phr	122394-9	32	-4.3	-10.7	type-3phr
8594-6	52	-4.4	-10.8	type-3phr	122394-10	38	-4.0	-10.5	type-3vad
8594-7	40	-4.4	-10.4	type-3phr	1395-1	30	-4.3	-10.9	type-3phr
8594-8	61	-4.4	-11.8	type-3phr	1395-2	20	-4.4	-10.8	type-3phr
8594-9	36	-4.6	-11.1	type-3phr	1395-3	38	-4.4	-9.7	type-3phr
8594-10	39	-4.4	-11.6	type-3phr	1395-4	39	-4.0	-10.5	type-3phr
8594-11	71	-3.6	-10.8	type-2	1395-6	37	-3.6	-8.8	type-3vad
8594-12	55	-3.3	-11.0	type-3vad	1395-7	30	-4.4	-10.6	type-3phr
8594-13	70	-3.9	-10.1	type-3vad	1395-9	34	-5.1	-10.1	type-1
8594-14	64	-3.9	-10.0	type-3vad	1395-11	6	-5.6	-10.6	type-1
8594-15	34	-3.5	-9.7	type-3phr	6295-4	-	-4.0	-7.6	elongate
8594-16	26	-3.8	-9.6	type-3phr	72195-1	-	-3.3	-11.0	nodule
81994-1	45	-3.6	-11.3	type-2	72195-2	-	-3.5	-9.0	nodule
81994-2	66	-3.6	-11.1	type-2	72195-3	-	-3.9	-9.3	nodule
81994-3	42	-3.5	-11.0	type-3phr*	72895-1	-	-3.7	-8.0	type-3phr
81994-4	38	-3.8	-11.6	nodule	72895-2	-	-4.0	-8.0	type-3phr
81994-5	44	-4.0	-12.0	type-2	72895-3	-	-4.3	-9.0	type-3phr
81994-6	38	-4.0	-11.0	type-3phr	72895-4	-	-4.0	-8.0	type-3phr
81994-7	35	-4.3	-11.6	type-3phr	72895-5	-	-3.7	-7.5	type-3phr
81994-8	43	-4.3	-11.0	type-3phr	72895-6a	-	-3.6	-7.3	type-3phr
81994-9	67	-4.2	-11.1	type-3phr	72895-6b	-	-4.4	-8.2	type-3phr
81994-14	42	-4.0	-9.6	type-3phr	72895-7	-	-4.6	-9.2	nodule
81994-15	50	-3.8	-10.0	type-3phr					

DISCUSSION

Environments of Cement Formation

We have inferred the environments of cement formation in the Zia Formation by comparing microscopic and macroscopic characteristics to those of cements of known origin described in the literature. In this section, we discuss known characteristics of vadose and phreatic cements, and use this as the basis for identification of cementation environments in the Zia Formation.

Characteristics of Vadose Cementation

Despite the complexities and variations in surficial environments of precipitation, vadose zone cements in arid environments have a number of distinctive characteristics:

(1) A dense micritic fabric, crystallaria, and circumgranular cracking have been associated with pedogenic (Weider and Yaalon, 1982; Esteban and Klappa, 1983; Wright, 1990; Wright and Tucker, 1991; Mora et al., 1993), and non-pedogenic vadose cementation. Microcodium, which exhibits a radial spar microtexture, is associated with either root filaments, casts of fruiting, or resting stages of soil fungi (Klappa, 1978; Klappa, 1979; Esteban and Klappa, 1983; Wright, 1990; Monger et al, 1991; Wright and Tucker, 1991; Mora et al., 1993).

(2) Permeability in the vadose zone tends to be higher in finer sediments, because flow occurs preferentially along grain surfaces rather than the center of large pores. Finer sediments have more surfaces for vadose flow to occur (Palmquist and Johnson, 1962; Hillel, 1980; Jury et al., 1991; Mozley and Davis, 1996). If cementation is limited by the supply of Ca^{2+} and/or HCO_3^- to the precipitation site, vadose cements should occur preferentially in the finer sediments (Mozley and Davis, 1996).

(3) Vadose cements are commonly associated with soil zonation and the alteration of parent material during soil development resulting in reddened clays and clay-rich sands in which there is little or no preservation of original sedimentary structures (Retallack, 1990; Mack et al., 1993; Mora et al., 1993).

(4) Vadose cementation is intimately associated with rhizocretions, which record the orientation and position of former root systems, as root casts or molds (Klappa, 1980b; Esteban and Klappa, 1983; Retallack, 1988; Retallack, 1990).

(5) Vadose cementation is sometimes associated with distorted or disrupted bedding such as brecciation and teepee structures. Brecciation can result from cracking and drying during de-watering, or cracking and dissolution when well-indurated carbonate layers are disturbed by growing roots (Gile et al., 1966; Klappa, 1980a; Esteban and Klappa, 1983). Growing roots also play a role in the formation of some teepee structures, when expansion along a single layer forces sediment upwards (Klappa, 1980a). Teepee structures can also arise from expansive calcite and/or evaporite mineral growth at the surface (Watts, 1977; Warren, 1982; Goudie, 1983).

(6) Cementation in the vadose zone can also result in irregular, wavy, laminar cement morphologies. Laminar cemented zones with abundant root traces and alveolar and fenestral microtextures are thought to result from root mats forming in the zone of capillary rise (Cohen, 1982; Warren, 1983; Semeniuk and Searle, 1985; Wright et al., 1988). Laminar units high in the vadose zone may have etched upper surfaces due to exposure (Semeniuk and Meager, 1981), or have fewer and more vertically oriented rhizocretions (Cohen, 1982).

Vadose Cementation in the Zia Formation

Nodules, platy concretions, rod shaped concretions, and type-2 tabular units all have micritic matrices, alveolar microtextures, circumgranular cracks, and crosscutting fractures. Cementation is associated with finer-grained layers in reddened clays and clay-rich sands in which there is very little or no preservation of original sedimentary structures. The radial spar microtexture associated with some concretions resemble microcodium. All of this implies that these cementation types are vadose. Micrite-spar cement textures could have initially formed in the vadose zone as pendant and meniscus envelopes around grains or groups of grains (Jacka, 1974; Reeves, 1976; Warren, 1983). These initial vadose

cements would provide sites for further calcite precipitation, and the unfilled voids could be subsequently filled with sparry calcite in the phreatic zone (Jacka, 1974; Funk, 1979).

Platy concretions are described by several authors as resulting from initial disruption of relict bedding, while similar rod concretions are described as rhizocretions (Klappa, 1980b, Esteban and Klappa, 1983; Retallack, 1988).

Irregular, unoriented, and fenestral millimeter sized calcite-filled fractures found in some units are interpreted as brecciation structures. Structures that resemble small folds are probably teepee structures because they are associated with rhizocretions and alveolar microtextures. There is not enough clay in these units to cause expansion, although expansive calcite growth cannot be ruled out. The laminar cemented units in the Zia Formation have abundant root traces and alveolar textures, and thus are interpreted as root mats associated with the zone of capillary rise.

Characteristics of Phreatic Cementation

Cementation in a terrestrial phreatic environment also has several distinctive characteristics:

(1) Calcite precipitation under phreatic conditions can continue uninterrupted by an air-water interface (Morse and Mackensie, 1990). Thus, isopachous or drusy, poikilotopic and blocky spar cements, are generally associated with precipitation in the phreatic zone (Jacka, 1970, Folk, 1974; Morse and Mackenzie, 1990; Retallack, 1990; Burns and Matter, 1995). Sparry cements can also form in the vadose zone as calcans or crystic nodules, but they are associated with soil zonation, highly dense micritic cements and nodules (Weider and Yaalon, 1982). Because these cements are not associated with such features they are unlikely to represent calcans or crystic nodules.

(2) As previously discussed, if cementation is limited by the supply of Ca^{2+} and/or HCO_3^- to the precipitation site, and supply is limited by flow; phreatic cements should be associated with coarser, more permeable sediments (Mozley and Davis, 1996; Lynch, 1996). Studies by Lynch (1996) indicates that preferential cementation of coarser more permeable sediments operates on the scale of a thin section and outcrop.

(3) Pedogenesis commonly destroys original structures, so the preservation of original sedimentary structures such as crossbedding is evidence of a non-pedogenic origin, and has been attributed to phreatic-groundwater cementation by others (Wright and Tucker, 1991; Spötl and Wright, 1992, Mora et al., 1993).

(4) Phreatic cementation is very rarely associated with rhizocretions (Wright and Tucker, 1991; Spötl and Wright, 1992; Mora et al., 1993). The lack of rhizocretions indicates that cementation occurred below the zone in which plants had their roots, in the phreatic zone.

Phreatic Cementation in the Zia Formation

Ovoid and elongate concretions, and type-1 tabular units appear to have formed principally in the phreatic zone because they have poikilotopic and blocky spar cements, are associated with coarser, better sorted units, show preservation of original sedimentary structures, and are not associated with rhizocretions. Elongate concretions have been noted by other authors and attributed to groundwater flow in the phreatic zone (McBride et al., 1994; McBride, et al., 1995; Mozley and Davis, 1996). Orientations of these elongate concretions tend to be uniform within a single outcrop, generally on the scale of several kilometers, as would be unexpected in vadose zone cementation (Mozley and Davis, 1996).

Mixed Vadose and Phreatic Cementation

Most cemented tabular units in the Zia Formation are difficult to classify as strictly pedogenic, vadose non-pedogenic, or phreatic carbonates. Cementation in these units forms a continuum between vadose and phreatic end-members. The most common type of mixed unit is near the phreatic end-member. In these units, vadose influence is indicated by the rare occurrence of rhizocretions in outcrop. Vadose influence on cements may also be indicated by the presence of sparry, floating grain microtextures. Floating grain microtextures appear to be the result of initial vadose cementation (grain-coating micrite), followed by circumgranular cracking, and then expansive phreatic cementation (spar) caused by burial below the water table (Fig. 1.16C). Expansive calcite growth is a common feature of some phreatic carbonates (Wright and Tucker, 1991; Mora et al.,

1993), and there is no evidence of grain or cement dissolution as described by Tandon and Friend (1989).

Cements near the vadose end-member are associated with typical vadose features. However, these features are less apparent than in type-2 tabular units, and sparry void filling cements are sometimes more abundant than micrite. As stated previously, micrite-spar cement textures could have initially formed in the vadose zone as pendant and meniscus envelopes around grains or groups of grains (Jacka, 1974; Reeves, 1976; Warren, 1983; McBride and Honda, 1994). Upon burial, these initial vadose cements would provide sites for further calcite precipitation, and the unfilled voids could be subsequently filled with sparry calcite in the phreatic zone (Jacka, 1974; Funk, 1979). The vadose contribution to cementation may have been overlooked in the past because of this overprinting.

Cathodoluminesence and Elemental Composition

Phreatic cements in the Zia Formation consist of large crystals of almost pure calcite, which show no zoning in cathodoluminescence. This lack of zoning suggests that the cements formed in a relatively short time during which pore-water chemistry was relatively constant (Burns and Matter, 1995).

Although vadose cements in the Zia Formation are typically non-luminescent, occasionally multiple complex irregular zonations do occur. Wright and Peeters (1989) suggest that such zonations result from multiple stages of crystal growth, complex crystal dissolution, and re-precipitation. For the most part floating grain textures in the Zia Formation seem to be the result of expansive calcite growth, and not grain dissolution as described by Tandon and Friend (1989).

Cements from type-3 tabular (vadose) units are similar to vadose cements in luminescent characteristics. Cements from type-3 tabular (phreatic) units sometimes exhibit regular zoning in cathodoluminsence. Generally no zonation is present in calcite crystals under plain light, implying that crystal growth may not be multi-generational.

Isotope Geochemistry

The environment of precipitation has a direct effect on carbon and oxygen isotope values for vadose and phreatic zone carbonates. Units interpreted to be of vadose origin have generally higher $\delta^{13}C$ values and lower $\delta^{18}O$ values than cemented units inferred to have formed dominantly in the phreatic zone (Fig. 1.20). Type-3 units (mixed features) typically have $\delta^{13}C$ and $\delta^{18}O$ values between phreatic and vadose units (Fig. 1.20). Further complications arise because $\delta^{13}C$ values for "mostly phreatic" mixed units resemble vadose values, whereas their $\delta^{18}O$ values resemble the phreatic values.

Higher $\delta^{13}C$ values for vadose cement are attributed by other authors to either greater diffusion of heavy atmospheric carbon, or a larger relative percentage of isotopically heavier C_4 or CAM plant biomass (Talma and Netterberg, 1983; Pendal and Amundson, 1990). Lower $\delta^{18}O$ values for vadose cement have several possible explanations: (1) The main mechanism for the precipitation of calcite in the vadose zone was transpiration-induced drying, and not evaporation (transpiration does not fractionate oxygen, evaporation does, Quade et al., 1989; Cerling and Quade, 1993). Evaporation removes the lighter oxygen (by fractionation), making the $\delta^{18}O$ values in the vadose cement heavier. (2) Waters that recharged the aquifer had undergone water-rock interaction, mixing oxygen values from meteoric waters with those derived from dissolution of ^{18}O-enriched minerals in the rock. Dissolution of framework grains, particularly volcanic rock fragments and feldspar, is common in the Zia Formation (Fig. 5). (3) Main recharge events that penetrated into the phreatic zone occurred during the summer when isotopic values are heavier (Quade et al., 1989; Cerling and Quade, 1993; Wang et al., 1993).

Stratigraphic variation in isotopic compositions may also mask the relationship between isotopic values and environment of precipitation. Changes in the local vegetation, precipitation rates, or seasonal temperatures can effect isotope values (Mora et al., 1993; Wang et al., 1993). Currently, detailed age data for the Zia Formation is not available, and so the possible correlation of Zia Formation isotope changes with global changes is not possible. The isotopic signature of the vadose cement may also be contaminated by later phreatic cementation (or visa versa), especially in type-3 units. A similar complex variation

in isotope composition resulting from the mixing of vadose and phreatic (hydromorphic) cementation is observed in other fluvial settings (Slate et al., 1996). Also, bulk samples were analyzed, so possible isotopic differences between spar and micrite cements were not observed. Clearly, further data need to be collected on Zia Formation isotopes before any definite conclusions can be made.

TIMING OF CEMENTATION

Because most of the vadose cements appear to be pedogenic, they must have formed shortly after deposition of the host sediments (while the sediments were still exposed to surficial weathering). The exact timing of phreatic cementation is more difficult to determine. Evidence from some type-3 tabular units indicates that at least some of the phreatic cementation also occurred very early. The most common surface texture for type-3 tabular units is root molds (pits, tubes and grooves; Figs. 1.12C, 1.14A), indicating that the cement must have formed around the root while it was still physically present. Because phreatic cements generally do not fill the root molds, cementation must have occurred before the oxidation of the root. In an oxidizing, arid, alluvial environment, organic root material will not last long after burial, thus the phreatic cementation must have occurred very early.

CONTROLS ON THE SPATIAL DISTRIBUTION OF CEMENTATION: IMPLICATIONS FOR GROUNDWATER AND PETROLEUM RESOURCES

From the preceding discussion clearly the dominant types of cementation in the Zia Formation are pedogenic and phreatic. By definition, the spatial distribution of pedogenic carbonate is a function of the spatial distribution of paleosols, which is a function of facies architecture and the amount of time a particular surface is exposed. Most pedogenic carbonate in the Zia Formation is poorly developed, discontinuous and associated with finer grained sediments in overbank fines (OF), sheet sand (SS), and interdune (ID) facies associations (Table 1.1; Figs. 1.7-1.10). Unlike other vadose cements, the distribution of extensive, well-developed pedogenic units in the Zia Formation is primarily controlled by the duration of surface exposure and landscape stability.

Phreatic cementation is typically associated with coarser and better sorted facies associations such as fluvial channel deposits (CH), cross-stratified dune deposits (EC), eolian sandsheet (ES) deposits, and some interdune deposits (ID; Table 1.1; Figs. 1.7-1.10). This indicates that phreatic cements formed preferentially in initially high-permeability portions of the Zia Formation, presumably due to the initial high groundwater flow rates in such zones (i.e., permeable zones would have an abundant supply of dissolved Ca^{2+} and/or HCO_3^-). The distribution of styles of phreatic cementation can also be explained by groundwater flow effects. Where fluvial channel sand deposits are surrounded by silty sands, silts and shales, flow (and thus cementation) is focused into thinner more isolated sands (Lynch, 1996). In texturally more homogeneous sediments, flow is not focused and cementation is less extensive (Lynch, 1996), a feature we see in the eolian sediments of the Zia Formation. Where evidence of textural control on phreatic cementation is absent, vadose calcite is present and thus could have acted as a nucleus for later phreatic-zone precipitation.

Although our study is based upon outcrop samples, and consequently does not directly relate to groundwater or hydrocarbon production problems, the Zia Formation in the subsurface is an important local aquifer, and similar alluvial units form significant aquifers and hydrocarbon reservoirs elsewhere. Thus the cementation relationships observed in the Zia Formation are of more than local interest. Calcite cementation in the Zia Formation has adversely affected potential reservoir/aquifer quality in two main ways: (1) Phreatic-zone cementation occurred preferentially in units that had the highest primary permeabilities (i.e., coarser grained and better sorted layers). Thus extensive calcite cementation has resulted in a permeability inversion, in which zones of high primary permeability are now low permeability zones. (2) Type-3 and some type-1 tabular units are commonly laterally extensive, in some cases extending for over two kilometers (Fig. 11). These units would form significant barriers to vertical fluid flow, perhaps resulting in compartmentalization of the reservoir/aquifer. Such compartmentalization can result in

dramatically reduced production if wells are screened on only one side of the cemented layer (Kantorowicz et al., 1987).

CONCLUSIONS

Vadose cements in the Zia Formation are characterized by the presence of rhizocretions and associated microtextures (alveolar, fenestral, circumgranular cracking), and by a lack of primary sedimentary structures. Phreatic cements in the Zia Formation are characterized by poikilotopic and blocky spar cements, the preservation of original sedimentary structures, and the absence of rhizocretions and associated microtextures. They occur as isolated or groups of ovoid or elongate concretions, and as laterally extensive tabular bodies. Type-3 (mixed) units in the Zia Formation reflect characteristics of both phreatic and vadose zone cementation (e.g., preservation of sedimentary structures plus rhizocretions and alveolar microtextures). Type-3 (mixed) units may reflect movements of the water table, such that vadose cements are moved into the phreatic zone, or vice versa.

$\delta^{13}C$ values for vadose cements tend to be heavier and $\delta^{18}O$ values tend to be slightly lighter than phreatic cements. Type-3 units also have mixed isotope values, with $\delta^{13}C$ and $\delta^{18}O$ values in-between the end-member vadose and phreatic values.

Cementation in the phreatic zone occurred preferentially in zones of high primary permeability, whereas vadose cementation occurred principally in association with soil development. Pedogenic carbonates may have served as nucleation sites for later phreatic cementation, leading to complex zones of mixed pedogenic and phreatic cements.

Calcite cementation in the Zia Formation has greatly reduced potential reservoir/aquifer quality. Most permeable units are extensively cemented with phreatic calcite. Many tabular units are commonly laterally extensive forming significant barriers to vertical fluid flow, conceivably resulting in compartmentalization of the reservoir/aquifer. Such compartmentalization can result in substantially reduced production if wells are screened on only one side of a cemented layer.

REFERENCES

Allen, J. R. L., 1986, Pedogenic calcretes in the Old Red Sandstone facies (Late Silurian-Early Carboniferous) of the Anglo-Welsh area, Southern Britain, In Wright, V. P. (Ed.), 1986, Paleosols, their recognition and interpretation. Princeton, N. J., Princeton University Press, p. 58-86.

Anderson, M. P., 1989, Hydrogeologic facies models to delineate large-scale spatial rends in glacial and glaciofluvial sediments: Geological Society of America Bulletin, v. 101, p. 501-511.

Anderson, M. P.,1990, Aquifer heterogeneity--A geological perspective, In Bachu, S., ed., Fifth Canadian/American Conference on Hydrogeology, Proceedings: Dublin, Ohio, National Well Water Association, p. 3-22.

Arakel, A. V., and McConchie, D., 1982, Classification and genesis of calcrete and gypsite lithofacies in paleodrainage systems of inland Australia and their relationship to carnotite mineralization. Journal of Sedimentary Petrology, v. 52, p. 1149-1170.

Arakel, A. V., Jacobson, G., Salehi, M., and Hill, C. M., 1989, Silicification of calcrete in palaeodrainage basins of the Australian arid zone. Australian Journal of Earth Sciences, v. 36, p. 73-89.

Atkinson, C. D.,1986, Tectonic control on alluvial sedimentation as revealed by an ancient catena of the Capella Formation (Eocene) of Northern Spain. In Wright, V. P. (Ed.) Paleosols, their recognition and interpretation. Princeton, N.J., Princeton University Press, p. 139-179.

Burns, S. J., and Matter, A., 1995, Geochemistry of carbonate cements in surficial alluvial conglomerates and their paleoclimatic implications, Sultanate of Oman. Journal of Sedimentary Research, v. A65, no. 1, p. 170-177.

Carlisle, E.,1983, Concentration of uranium and vanadium in calcretes and gypcretes. In Wilson, R. C. I. (Ed.), Residual deposits: surface related weathering processes and materials, Geol. Soc. Lond. Spec. Pub., no. 11. p.185-195.

Cerling, T. E., and Quade, J., 1993, Stable carbon and oxygen isotopes in soil
    carbonates. In: Climate change in continental isotopic records. Geophysical
    Monograph 78, p. 217-231.

Cerling, T. E., Wang, Y., and Quade, J., 1993, Global change in the late Miocene;
    expansion of C_4 ecosystems. Nature, v. 361, p. 344-345.

Chan, M. A., 1989, Erg margin of the Permian White Rim Sandstone, SE Utah.
    Sedimentology, v. 36, p. 235-251.

Chapin, C. E., and Cather, S. M., 1994, Tectonic setting of the axial basins of the
    northern and central Rio Grande rift. In: Basins of the Rio Grande Rift: Structure,
    Stratigraphy, and Tectonic Setting (Ed. by Keller, G. R., and Cather, S. M.)
    Geological Society of America Special Paper 291, p. 5-25.

Cohen, A. S.,1982, Paleoenvironments of root casts from the Koobi Fora Formation,
    Kenya. Journal of Sedimentary Petrology, v. 52, no. 2, p. 401-414.

Davis, J. M., Lohmann, R. C., Phillips, F. M., Wilson, J. L., and Love, D. W., 1993,
    Architecture of the Sierra Ladrones Formation, central New Mexico: depositional
    controls on the permeability correlation structure: Geological Society of America
    Bulletin, v. 105, p. 998-1007.

Dreimanis, A., 1962, Quantitative gravometric determination of calcite and dolomite by
    using a Chittick apparatus. Journal of Sedimentary Petrology, v. 32, no. 3, p.
    520-529.

Esteban, M., and Klappa, C. F., 1983, Subaerial exposure environment, In: Carbonate
    Depositional Environments (Ed. by Scholle, P. A., Bebount, D. G., and Moore,
    C. H.) AAPG Mem., no. 33, p. 1-54.

Folk, R. L., 1974, The natural history of crystalline calcium carbonate; effect of
    magnesium content and salinity: Journal of Sedimentary Petrology, v. 44, p. 40-
    53.

Funk, J. M., 1979, Distribution of Carbonate Cements in Quaternary Alluvial-Fan Deposits, Birch Creek Valley, East-Central Idaho - Diagenetic Model. AAPG Bulletin, v. 63 (3), p. 454.

Gardner, L. E., Diffendal, R. F., and Williams, D. F., 1992, Stable isotope composition of calcareous paleosols and ground-water cements from the Ogallala Group (Neogene), western Nebraska. Contributions to Geology, University of Wyoming, 29, no. 2, 97-109.

Gawne, C. E., 1981, Sedimentology and stratigraphy of the Miocene Zia Sand of New Mexico: Summary. Geological Society of America Bulletin, Part 1, v. 92, p.999-1007.

Gile, L. H., Peterson, F. F., and Grossman, R. B., 1966, Morphological and genetic sequences of carbonate accumulation in desert soils: Soil Science, v. 101, p. 347-360.

Goudie, A. S., 1983, Calcrete. In: Chemical sediments and geomorphology: precipitates and residua in the near-surface environment (Ed. by Goudie, A. S., and Pye, K.) Academic Press, London, p. 93-131.

Hawley, J. W., and Haase, C. S., 1992, Hydrologic framework of the northern Albuquerque basin: New Mexico Resources Research Institute, Report WRRI 290.

Hillel, D., 1980, Fundamentals of Soil Physics: Sand Diego, Academic Press, Inc.

Jacka, A. D., 1970, Principles of cementation and porosity - occlusion in Upper Cretaceous sandstones, Rocky Mountain Region. Twenty-Second Annual Field Conference, Wyoming Geological Association Guidebook, p. 265-285.

Jacka, A. D., 1974, Differential cementation of Pleistocene carbonate fanglomerate, Guadalupe Mountains. Journal of Sedimentary Petrology, v. 44, no. 1, p. 85-92.

Jacobson, G., Arakel, A. V., and Yijian, C., 1988, The central Australian groundwater discharge zone: Evolution of associated calcrete and gypcrete deposits. Australian Journal of Earth Sciences, v. 35, p.549-565.

Jury, W. A., Gardner, W. R., and Gardner, W. H.,1991, Soil Physics (5th Edition): New York, John Wiley and Sons, Inc.

Kantorowicz, J. D., Bryant, I. D., and Dawans, J. M., 1987, Controls on the geometry and distribution of carbonate cements in Jurassic sandstones: Bridgeport Sands, southern England and Viking Group, Troll Field, Norway In: Diagenesis of sedimentary sequences (Ed. by Marshall, J. D.) Oxford, Blackwell, p. 103-118.

Klappa, C. F., 1978, Biolithogenesis of Microcodium; elucidation. Sedimentology, v. 25, p. 489-522.

Klappa, C. F., 1979, Calcified filaments in Quaternary calcretes: organo-mineral interactions in the subaerial vadose environment. Journal of Sedimentary Petrology, v. 49, p. 955-968.

Klappa, C. F., 1980a, Brecciation textures and teepee structures in Quaternary calcrete (caliche) profiles from eastern Spain: the plant factor in their formation. Geological Journal, v. 15, pt. 2, p. 81-89.

Klappa, C. F., 1980b, Rhizoliths in terrestrial carbonates: classification, recognition, genesis and significance. Sedimentology, v. 27, 613-629.

Klappa, C. F., 1983, A process-response model for the formation of pedogenic calcretes, In: Wilson, R. C. I. (Ed.), Residual deposits: surface related weathering processes and materials, Geol. Soc. Lond. Spec. Pub., no. 11, p. 221-233.

Kocurek, G.,1981, Significance of interdune deposits and bounding surface in aeolian dune sands. Sedimentology, v. 28, p. 753-780.

Kocurek, G., and Dott, R. H., 1981, Distinctions and used of stratification types in the interpretation of eolian sand. Journal of Sedimentary Petrology, v. 51, No. 2, p. 579-595.

Kraus, M. J., and Bown, T. M., 1986, Paleosols and time resolution in alluvial stratigraphy. In Wright, V. P. (Ed.) Paleosols, their recognition and interpretation. Princeton, N.J., Princeton University Press, p. 180-207.

Leeder, M. R., 1975, Pedogenic carbonates and flood sediment accretion rates: a quantitative model for alluvial arid-zone lithofacies. Geology Magazine, v. 112 (3), p. 257-270.

Lozinsky, R. P., 1994, Cenozoic stratigraphy, sandstone petrology, and depositional history of the Albuquerque Basin, central New Mexico, In: Keller, G. R., and Cather, S. M. (Eds.), Basins of the Rio Grande Rift: Structure, Stratigraphy, and Tectonic Setting: Boulder, Colorado, Geological Society of America Special Paper 291, p. 73-81.

Lynch, F. L., 1996, Mineral/Water Interaction, Fluid Flow, and Frio Sandstone diagenesis: evidence from the rocks. AAPG Bulletin, v. 80, No. 4, p. 486-504.

Machette, M. N., 1985, Calcic soils of the southwestern United States. Geological Society of America Special Paper 203, p. 1-21.

Mack, G. H., James, W. C., Monger, H. C., 1993, Classification of paleosols. Geological Society of America Bulletin, v. 105, p. 129-136.

Mann, A. W., and Horwitz, R. D., 1979, Groundwater calcrete deposits in Australia; some observations from Western Australia: Jour. Geol. Soc. Australia, v. 26, p. 293-303.

McBride, E. F., Picard, M. D., Folk, R. L., 1994, Oriented concretions, Ionian coast, Italy, evidence of groundwater flow direction. Journal of Sedimentary Petrology, v. A64, No. 3, p. 535-540.

McBride, E. F., and Honda, H., 1994, Carbonate cements in shallowly buried Pleistocene and Holocene sandstone and limestone, south Texas Gulf Coast. Transactions of the Gulf Coast Association of Geological Societies, v. XLIV, p. 467-476.

McBride, E. F., Milliken, K. L., Cavazza, W., Cibin, U., Fontana, D., Picard, M. D., Zuffa, Z. Z. (1995) Heterogeneous Distribution of Calcite Cement at the Outcrop Scale in Tertiary Sandstones, Northern Apennines, Italy. AAPG Bulletin, v.79, No. 7, p. 1044-1063.

Miall, A. D., 1990, Principles of Sedimentary Basin Analysis. 2nd edition, Springer-Verlag, NY, 668p.

Milnes, A. R., 1992, Calcrete In: Weathering, soils, and paleosols (Ed. by Martini, I. P., and Chesworth, W.) Elsevier, p. 309-347.

Monger, H. C., Daugherty, L. A., and Gile, L. H.,1991, A microscopic examination of pedogenic calcite in an aridisol of southern New Mexico. in: Occurrence, characteristics, and genesis of carbonate, gypsum, and silica accumulations in soils. Soil Science Society of America, Special Publication 26, p. 37-59.

Mora, C. I., Fastovsky, D. E., Driese, S. G., 1993, Geochemistry and stable isotopes of paleosols: University of Tennessee Department of Geological Sciences, Studies in Geology 23, 65 p.

Morse, J. W., and Mackenzie, F. T., 1990, Geochemistry of Sedimentary Carbonates. Developments in Sedimentology, v. 48, Elsevier.

Mozley, P., and Davis, J. M., 1996, Relationship between oriented calcite concretions and permeability correlation structure in an alluvial aquifer, Sierra Ladrones Formation, New Mexico. Journal of Sedimentary Research, v. A66, p. 11-16.

Mozley, P., and Goodwin, L., 1995a, Patterns of cementation along a Cenozoic normal fault: a record of paleoflow orientations. Geology, v. 23, p. 539-542.

Mozley, P., and Goodwin, L., 1995b, Patterns of cementation along the Sand Hill Fault, Albuquerque Basin, NM: Implications for paleoflow orientation and mechanisms of fault-related cementation, In: Characterization of hydrogeologic units in the northern Albuquerque Basin (Ed. by Haneberg, W. C., and Hawley, J. W.) New Mexico Bureau of Mines and Mineral Resources Open-File Report, 402-C, p. 3-11-3-23.

Netterberg, F.,1969, The interpretation of some basic calcrete types: South Africa. Arch. Bull., v. 24, p. 117-122.

Netterberg, F., and Caiger, J. H., 1983, A geotechnical classification of calcretes and other pedocretes. In: Residual deposits: surface related weathering processes and materials (Ed. by R. C. I. Wilson), pp. 235-243. Geol. Soc. Lond. Spec. Pub. 11, p 235-243.

Palmquist, W. N., and Johnson, A. I., 1962, Vadose flow in layered and nonlayered materials: United States Geological Survey Professional Paper, 450-c, p. C142 C143.

. Pendall, E., and Amundson, R.,1990, The stable isotope chemistry of pedogenic carbonate in an alluvial soil, in Punjab. Soil Science, v. 149, p. 199-211.

Porter, M. L., 1987, Sedimentology of an ancient erg margin: the Lower Jurassic Aztec Sandstone, southern Nevada and southern California. Sedimentology, v. 34, p. 661-680.

Powers, M. C., 1953, A new roundness scale for sedimentary particles. Journal of Sedimentary Petrology, v. 28, p. 108-110.

Quade, J., Cerling, T. E., and Bowman, J. R., 1989, Systematic variations in the carbon and oxygen isotopic composition of pedogenic carbonate along elevation transects in the southern Great Basin, United States. Geologic Society of America Bulletin, v. 101, p. 464-475.

Rabenhorst, M. C., Wilding, L. P., and West, L. T.,1984, Identification of pedogenic carbonates using stable carbon isotope and microfabric analyses. Soil Sci. Soc. A. Jour., v. 48, p. 125-132.

Read, J. F.,1974, Calcrete deposits and Quaternary sediments, Edel Province, Shark Bay, Western Australia. In: Evolution and Diagenesis of Quaternary Carbonate Sequences , Shark Bay, Western Australia (Ed. by Logan, B. W.) Am. Assoc. Petroleum Geologists Memoir 22, p. 250-282.

Reeves, C. C., 1976, Caliche: Origin, classification, morphology and uses. Lubbock, Texas, Estacado Books.

Retallack, G. J., 1988, Field recognition of paleosols. Geological Society of America, Special Paper 216, p. 1-20.

Retallack, G. J., 1990, Soils of the past. Unwin-Hyman, Boston.

Semeniuk, V., and Meagher, T. D., 1981, Calcrete in Quaternary coastal dunes in southwestern Australia: a capillary-rise phenomenon associated with plants. Journal of Sedimentary Petrology, v. 51, no. 1, p. 47-68.

Semeniuk, V., and Searle, D. J., 1985, Distribution of calcrete in Holocene coastal sands in relationship to climate, Southwestern Australia. Journal of Sedimentary Petrology, v. 55, No. 1, p. 86-95.

Slate, J. L., Smith, G. A., Yang, W., and Cerling, T. E., 1996, Carbonate-paleosol genesis in the Plio-Pleistocene St. David Formation, Southeastern Arizona. Journal of Sedimentary Research, v. 36, p. 85-94.

Spötl, C., and Wright, V. P., 1992, Groundwater dolocretes from the Upper Triassic of the Paris Basin, France: a case study of an arid, continental diagenetic facies. Sedimentology, v. 39, p. 1119-1136.

Talma, A. S., and Netterberg, F., 1983, Stable isotope abundances in calcretes. In: Residual deposits (Ed. by R. C. I. Wilson) Geol. Soc. Lond. Spec. Pub., no 11. p. 221-233.

Tandon, S. K., and Friend, P. F., 1989, Near-surface shrinkage and carbonate replacement processes, Arran Cornstone Formation, Scotland. Sedimentology, v. 36, p. 1113-1126.

Tedford, R. H., 1982, Neogene stratigraphy of the northwestern Albuquerque basin. New Mexico Geological Guidebook, 33rd Field Conference, Albuquerque Country II, p. 273-278.

Wang, Y., Cerling, T. E., Quade, J., Bowman, J. R., 1993, Stable isotopes of paleosols and fossil teeth as paleoecology and paleoclimate indicators: an example from the St. David Formation, Arizona. In: Climate change in continental isotopic records. Geophysical Monograph 78, p. 241-249.

Warren, J. K.,1982, The hydrological significance of Holocene teepees, stromatolites, and boxwork limestones in coastal salinas in south Australia. Journal of Sedimentary Geology, v. 52, No. 4, p.1171-1201.

Warren, J. K.,1983, Pedogenic calcrete as it occurs in Quaternary calcareous dunes in coastal South Australia. Journal of Sedimentary Petrology, v. 53, no. 3, p. 787-796.

Weber, K. J., 1982, Influence of common sedimentary structures on fluid flow in reservoir models: Journal of Petroleum Technology, v. 34, p. 665-672.

Weider, M., Yaalon, D. H.,1982, Micromorphological fabrics and developmental stages of carbonate nodular forms related to soil characteristics. Geoderma, v. 28, p. 203-220.

Wright, V. P, and Peters, C., 1989, Origins of some early Carboniferous calcrete fabrics revealed by cathodoluminescence: implications for interpreting the sites of calcrete formation. Sedimentary Geology, v. 65, p. 345-353.

Wright, V. P., Platt, N. H., and Wimbledon, W. A.., 1988, Biogenic laminar calcretes: evidence of calcified root-mat horizons in paleosols. Sedimentology, v. 35, p. 603-620.

Wright, V. P., 1990, A micromorphological classification of fossil and recent calcic and petrocalcic microstructures. In: Soil Micromorphology: a basic and applied science (Ed. Douglas, L. A.). Developments in Soil Science, 19, Elsevier, 401-407.

Wright, V. P., and Tucker, M. E., 1991, Introduction. In: Calcretes. (Ed. by Wright, V. P., and Tucker, M. E.). Int. Ass. Sediment., Reprint Series 2, 1-22.

Part 2

Sandstone Petrology of the Zia Formation, Lower Santa Fe Group, Albuquerque Basin, New Mexico

ABSTRACT

The Miocene Zia Formation consists of gravels, sands, and muds deposited in fluvial, eolian and playa lake environments.   Zia Formation sands can be subdivided into two distinct groups based on composition. The lower Zia Formation (Piedra Parada, Chamisa Mesa, and Canada Pillares Members) changes composition up section from felspathic litharenites to lithic arkoses. The upper Zia Formation (Unnamed Member) is mainly differentiated from the lower by greater amounts of feldspar. Compositional changes in the lower part of the Zia Formation are due to grainsize reduction without a change in provenance (e.g., reworking of polycrystalline quartz, volcanic, and chert rock fragments into smaller grains of quartz and feldspar). A change in provenance is suggested for the transition from lower to upper Zia Formation because of changes in the amount and type of feldspar (e.g., more total feldspar; increase in microcline), an increase in mafic volcanic rock fragments, and a decrease in chert. This change may be the result of additional detrital input from the Santa Fe block, Nacimiento block, or northern volcaniclastic sources.

The primary diagenetic process that affected the Zia Formation was calcite cementation.   Micritic calcite with alveolar textures and circumgranular cracking are interpreted to result from vadose cementation, whereas those exhibiting drusy to poikilotopic spar cements are interpreted as resulting from phreatic cementation. Most cemented units in the Zia Formation show the influence of both environments. Clay matrix and pore cement are only significant in units that are not cemented with calcite. Intergranular porosity is the dominant porosity type in cemented and uncemented units. Most porosity in phreatic units results from incomplete cementation. In vadose units porosity is caused by grain and cement dissolution, and circumgranular cracking.

INTRODUCTION

Primary sedimentary depositional characteristics such as grain size and sorting, as well as diagenetic alterations such as compaction and cementation, control the hydrological properties of sedimentary rocks. Petrographic study of sandstone composition and diagenetic features can provide valuable information necessary to understanding the controls on aquifer quality. Furthermore, petrographic analysis can provide valuable data for provenance studies which can be used to understand the spatial distribution of sedimentary packages. Although other studies have looked at Zia Formation petrography (Gawne, 1973, 1981; Lozinsky, 1988), none have looked at diagenesis in any detail.

This paper includes petrographic data on the provenance and diagenetic history of sediments in the Zia Formation. The Zia Formation is the basal rift filling unit in the Albuquerque basin, part of the 1000 km long Rio Grande rift of Colorado and New Mexico. Sediments in the basin are divided into the upper and lower Santa Fe Group (Lozinsky, 1994). The 10 to 30 Ma Zia Formation makes up the lower Santa Fe group in the northern part of the basin (Lozinsky, 1994).

PREVIOUS STUDIES

The study site is on the western margin of the Albuquerque basin, about 20 km northwest of Albuquerque, on the King Brothers Ranch. The area is located along the Rio Puerco Fault Zone (between the Llano de Albuquerque and the Rio Puerco), west of Rio Rancho (Fig. 2.1). The stratigraphy, lithology and structure of this area were first studied by Bryan and McCann (1937). Wright (1946) measured several stratigraphic sections along the Ceja del Rio Puerco, and studied the Sand Hill fault zone. Galusha (1966) proposed the term Zia Sand Formation for outcrops along the Ceja del Rio Puerco, and the Jemez River. He also defined the Piedra Parada and Chamisa Mesa Members. Galusha and Blick (1971) further refined the stratigraphy, adding a Tesuque Formation equivalent above their Zia sand. Gawne (1973, 1981) examined the stratigraphy and mapped the Zia exposures along the
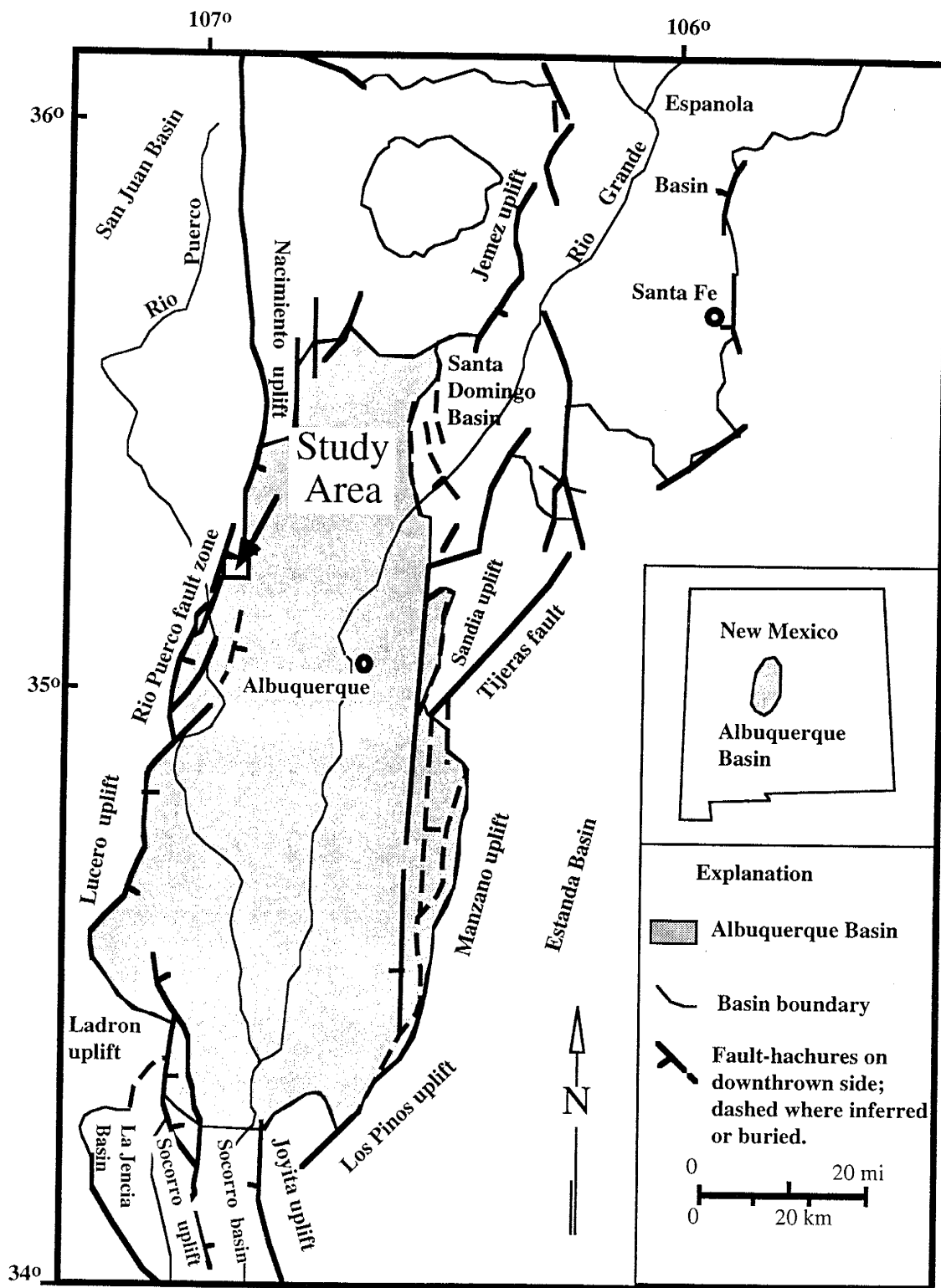
Figure 2.1. Map of the Albuquerque Basin showing the King brother's ranch study area. Map modified from Lozinsky (1993).

Canada Pillares and Canada Moquino drainages on the King Ranch. Gawne used and expanded the nomenclature used by Galusha (1966), but did not examine what she called "Tesuque Formation equivalent" in any detail. Tedford (1982), expanded the Zia formation to include Gawne's Tesuque equivalent, renaming it the Unnamed Member. The stratigraphic divisions of Tedford (1982) are used in the descriptions of the Zia Formation for this study (Fig. 2.2). The latest study of the Zia was by Lozinsky (1988), who examined a few thin sections from the King Ranch area.

STRATIGRAPHY

The Zia Formation can be divided into a sand-dominated eolian lower member (Piedra Parada), a fluvial/eolian member (Chamisa Mesa), a mud-dominated fluvial member (Canada Pillares Member), and the upper sand-dominated eolian/fluvial Unnamed Member (Gawne, 1981; Tedford, 1982; Fig. 2.2). The lower contact of the Zia is unconformable with the Eocene Galisteo Formation and the Cretaceous Mesaverde Formation (Hunt, 1936; Gawne, 1981; Tedford, 1982). The upper contact is the Sand Hill fault, a major normal fault that offsets the Zia and units of the Upper Santa Fe Group by about 600 meters (Hawley et al., 1995). This area is bounded on the West by the Moquino fault.

The Piedra Parada Member is the lowest member of the Zia, and is between 86 and 88 meters thick in the King ranch area. The basal contact is fluvial, with polished and faceted ventifacts of quartz and intermediate volcanic composition (Gawne, 1973, 1981). The main body of the Piedra Parada is primarily composed of medium to coarse grained, moderately to well sorted, massive to crossbedded eolian sand. Most of this member is poorly cemented to uncemented, although local preferential cementation of mainly coarser layers defines large tabular and trough crossbed sets. The upper contact of the Piedra Parada Member is a well cemented, laterally extensive, rhizocretionary unit.

The Chamisa Mesa Member is 16 to 20 meters thick in the King ranch area. This unit generally fines upwards from well sorted, gray to pink, fine grained, buff weathering sand,

Figure 2.2. Generalized stratigraphic column of the Zia Formation showing ages, lithologies, depositional environments, and locations of samples. Terminology and ages from Tedford (1982) and Lozinsky (1988).

into massive to laminated, pink to gray, buff weathering, interbedded sands, silts, and clays. Large tabular crossbed sets, defined by rhizocretionary cemented bounding surfaces, are common in the lower part of this unit. In the middle of this unit is a rhizocretionary, well cemented, laterally extensive sand, with an erosional upper surface. The upper part of this member is made up of interbedded sands, silts, and reddish brown clays. The upper contact is placed at the top of a laterally extensive, thinly bedded, coarse to fine grained sand unit. The lower part of the Chamisa Mesa Member is eolian, but the upper portions are fluvial (Gawne, 1973, 1981; Tedford, 1982).

The Canada Pillares Member is 28 to 30 meters thick in the King ranch area. This unit consists of pink to red clay and silt, and gray to pink fine to medium grained sand. The Canada Pillares Member is interpreted as mud dominated fluvial deposits (Gawne, 1973, 1981; Tedford, 1982), and has only been recognized along the Ceja del Rio Puerco. The upper contact is placed at the top of a reddish brown to buff silty sand unit.

The Unnamed Member unconformably overlies the Canada Pillares Member, and varies from 130 to 200 meters thick in the King ranch area. The lower contact is an erosional unconformity and placed at the bottom of a 40 to 50 meter thick, poorly cemented pinkish gray to pale red, fine to medium grained silty sand with tabular and trough crossbeds. Medium to coarse grained, well cemented sandstones, are locally present, as well as silty sand and clay interbeds. This lower section is interpreted as largely eolian (Lozinsky, 1988). The upper portion of the Unnamed Member consists of 290 to 300 meters of pinkish gray to pale red fine to medium grained sand, silty sand, silt and clay. Two green clay beds are found in this unit, the uppermost of which contains algal tufa heads (Lozinsky, 1988). Paleosol horizons and volcanic ash beds are found throughout the Unnamed Member. The upper part of the Unnamed Member is interpreted as a sand dominated fluvial environment (Lozinsky, 1988). The upper contact of the Unnamed Member is the Sand Hill fault.

METHODS

This paper was part of a larger study on calcite cementation in the Zia Formation. Because of this, most samples collected for study come from calcite cemented concretions and tabular units. Sixty-nine thin-sections were made from cemented and uncemented samples taken from four measured sections. Laterally continuous units were sampled in more than one area to examine variations in petrographic characteristics. The location of each sample is indicated on the generalized column (Fig. 2.2). Thin sections were impregnated with a blue-dyed epoxy to differentiate true porosity from that formed during the thin-section preparation (i.e., plucking of grains). All thin sections were stained for potassium feldspar using methods outlined by Miller (1988). These thin sections were analyzed for textures and mineralogy using a standard petrographic microscope, under plain light, crossed-polars, and cathodoluminesence. A MAAS/Nuclide model ELM-3 Luminoscope was used to gather cathodoluminsence data.

The modal composition and total porosity of the samples were determined by point counting (300 points) on a standard petrographic microscope equipped with a Swift automated point counting device. When estimating microporosity, half of the count was put into porosity, and half was put into the appropriate cement or grain category. The mean grain size, degree of roundness and sorting were estimated using visual comparators.

PETROLOGY

Composition

Zia sediments in the King Ranch area range in composition from arkoses to litharenites (Fig. 2.3; Folk, 1974a). Most of the sediments are classified as lithic arkoses. In the King Ranch area, samples plot in two distinct domains on the QFL diagram. One domain contains the lower Zia (Piedra Parada, Chamisa Mesa, and Canada Pillares Members), the other domain contains the upper Zia (Unnamed Member). The lower Zia becomes more quartz-rich up section (with decreasing age; Fig 2.3). The Piedra Parada member is classified entirely as a felspathic litharenite; the Chamisa Mesa and Canada Pillares members are mostly

lithic arkoses. The Unnamed Member has a variable composition, but is differentiated from the lower members by greater feldspar abundance.
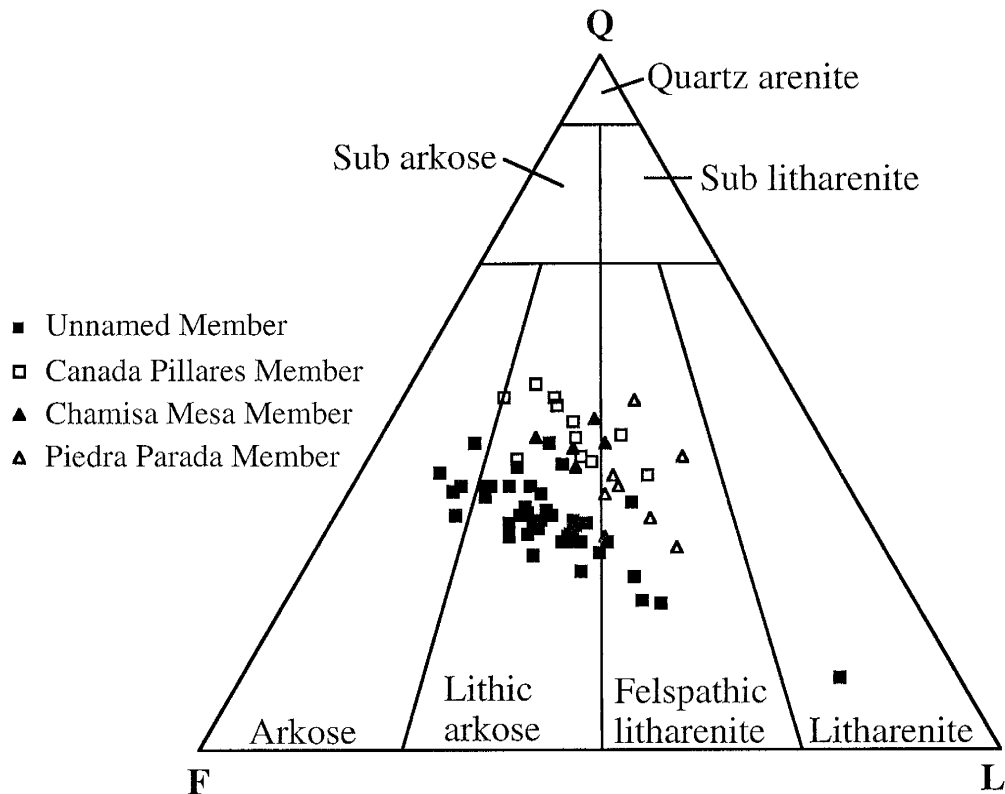
Fig. 2.3. Ternary diagram showing the relative proportions of quartz (Q), feldspar+granitic/gnessic fragments (F) and lithic fragments (L) in thin sections. Data is from Table B.1, sandstone classification is from Folk (1974a).

Quartz

Monocrystalline quartz is the most common quartz type throughout the Zia. Lozinsky (1988) reported polycrystalline quartz to total quartz ratio (Qp/Q) averages of .07 for the lower Zia at King Ranch. My samples have a Qp/Q ratio average of .14, very close to the West Mesa Well values of .15 for the same section (Lozinsky, 1988). The Qp/Q ratio average for the Unnamed Member is .10. In general, greater amounts of polycrystalline quartz correspond to greater grain size (Fig. 2.4).

Feldspar

In general feldspar percentages increase up section (Fig. 2.3), something also noted by Lozinsky (1988). Plagioclase is the most common detrital feldspar grain for most of the
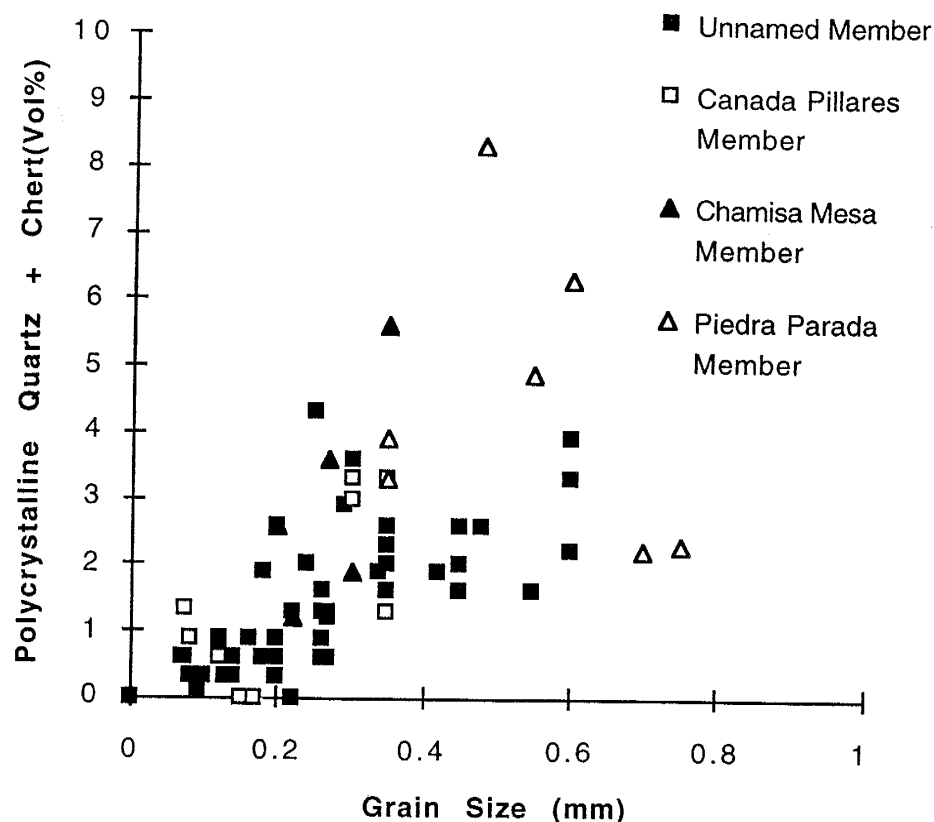
Fig. 2.4. Plot of abundance of polycrystalline quartz and chert versus mean grain size for cemented sandstones in the Zia Formation. In general coarser grained sandstones contain for polycrystalline quartz than finer grained sandstones. Data from Tables B.1 and B.4.

Zia (Table B.1). Lower Zia members (Piedra Parada, Chamisa Mesa, Canada Pillares) in the King ranch area generally show equal percentages of plagioclase and potassium feldspar (Table B.1). In this study I did not systematically differentiate between different types of plagioclase or potassium feldspars during point counting. Other studies indicate that plagioclase grains range in composition form oligoclase to labradorite, are commonly twinned, and sometimes display oscillatory zoning (Fig. 2.7A; Gawne, 1973; Gawne, 1981; Lozinsky, 1988). Orthoclase and Sanidine are the most common potassium feldspars

(Lozinsky, 1988). Microcline and perthite are consistently present in the lower Zia and percentages increase up-section (Lozinsky, 1988).

Rock Fragments

Volcanic rock fragments are generally the most abundant lithic fragments in the Zia at the King Ranch area, averaging between 70 to 90 % of all rock fragments (Figs. 2.5; 2.6A; 2.7A). Volcanic grains typically exhibit porphyritic textures, with phenocrysts of plagioclase, ferromagnesian silicates, and magnetite in glassy or microcrystalline groundmasses. Volcanic rock fragments are mostly intermediate in composition. Larger clasts were
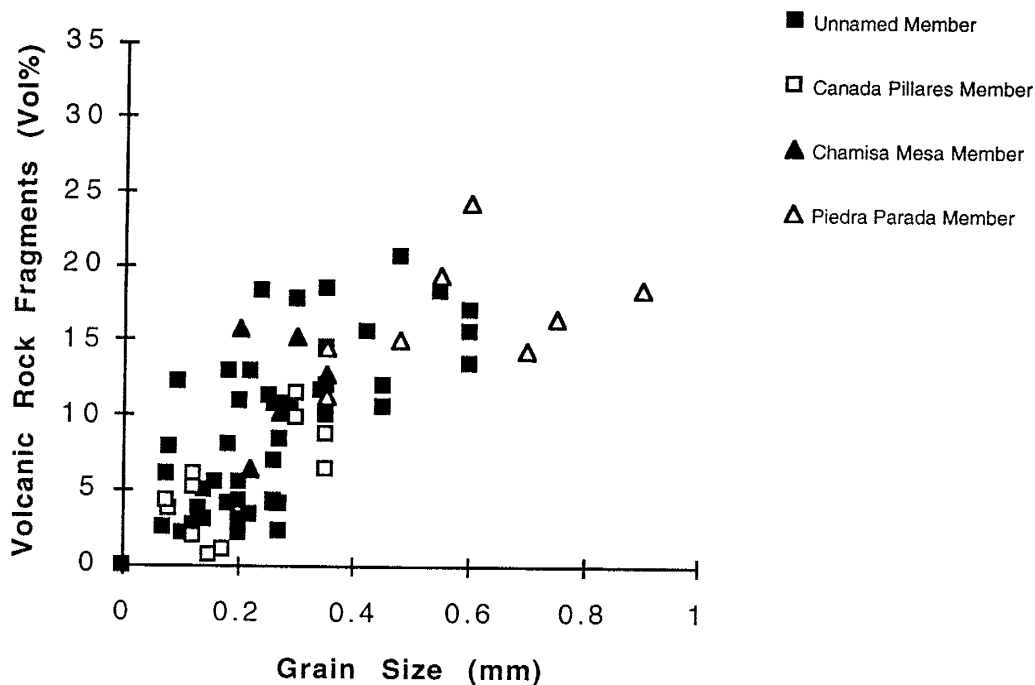
Fig. 2.5. Plot of abundance of volcanic-rock fragments versus mean grain size for cemented sandstones in the Zia Formation. In general, coarser-grained sandstones contain more volcanic-rock fragments than finer-grained sandstones. Data from Tables B.2 and B.4.

identified as pyroxene andesites and hornblende rhyodacites by Gawne (1973; 1981). As noted by Lozinsky, mafic volcanics become more common up section. In general, coarser grained units contain more volcanic rock fragments than finer grained sandstones (Fig. 2.5). Chert is the most common sedimentary rock fragment (Table B.2; Fig. 2.6B). Chert is especially common in the Piedra Parada Member (Table B.2; Fig. 2.7A). This study indicates that units with abundant carbonate rock fragments are associated with paleosols and

pedogenic features (Fig. 2.7B). This implies that these fragments are intraformational

recycled pedogenic carbonate. Other carbonate rock fragments appear to be micritic
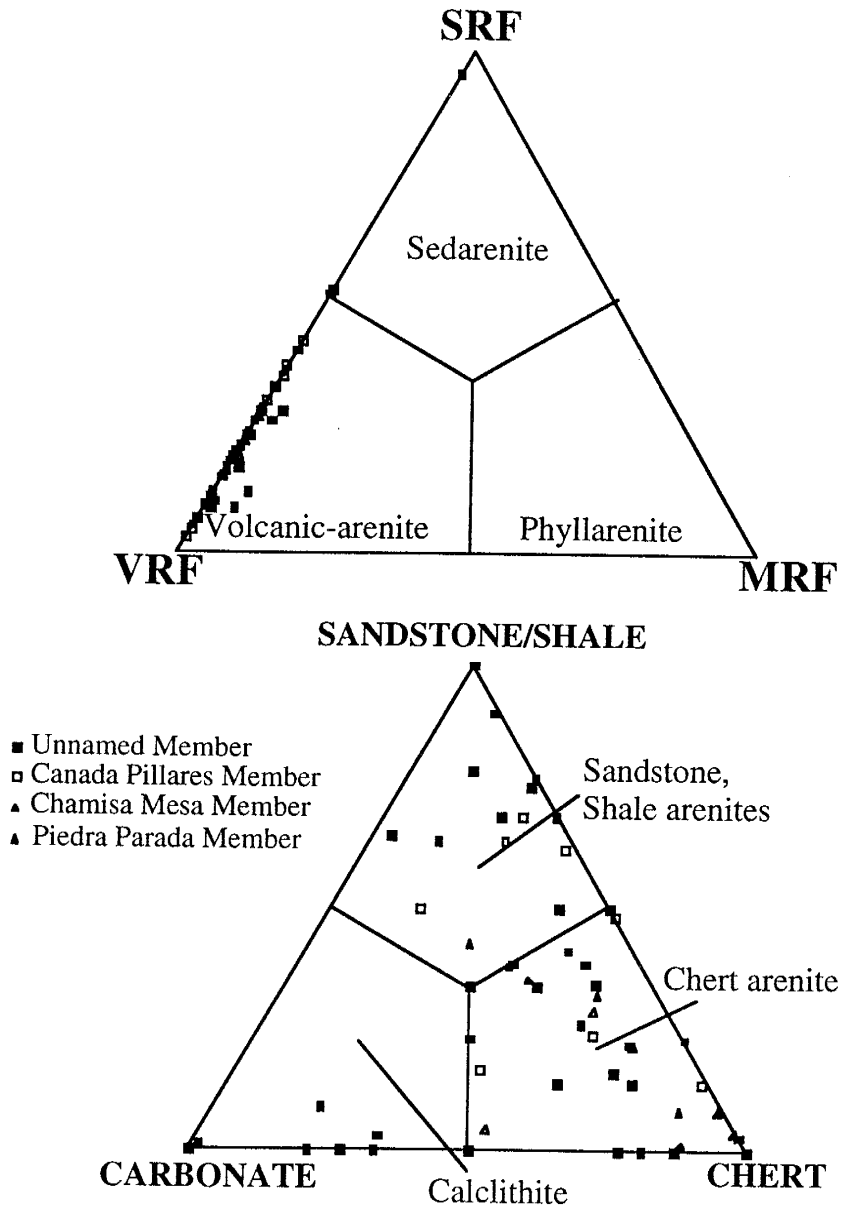
Fig. 2.6. Top: Ternary diagram showing the relative proportions of sedimentary (SRF), volcanic (VRF), and metamorphic (MRF) rock fragments in sandstones in the Zia Formation. Bottom: Ternary diagram shows the relative proportions of sandstone and shale, detrital carbonate, and chert in sandstones from the Zia Formation. Data from Table B.2. Sandstone classification from Folk (1974a).

Fig. 2.7 A. Photomicrograph of typical framework grains, including monocrystalline quartz (Qm), chert (CHT), Plagioclase (P), K-spar (K) , and volcanic rock fragments (V). Note the poikilotopic calcite cement. Crossed-nichols. Eolian sandstone from the Piedra Parada Member. **B.** Detrital carbonate grain found in a fluvial sandstone from the Unnamed Member. Plain polarized light. The cement is dominantly drusy calcite spar, however some micritic grain coatings are present in the upper right corner.
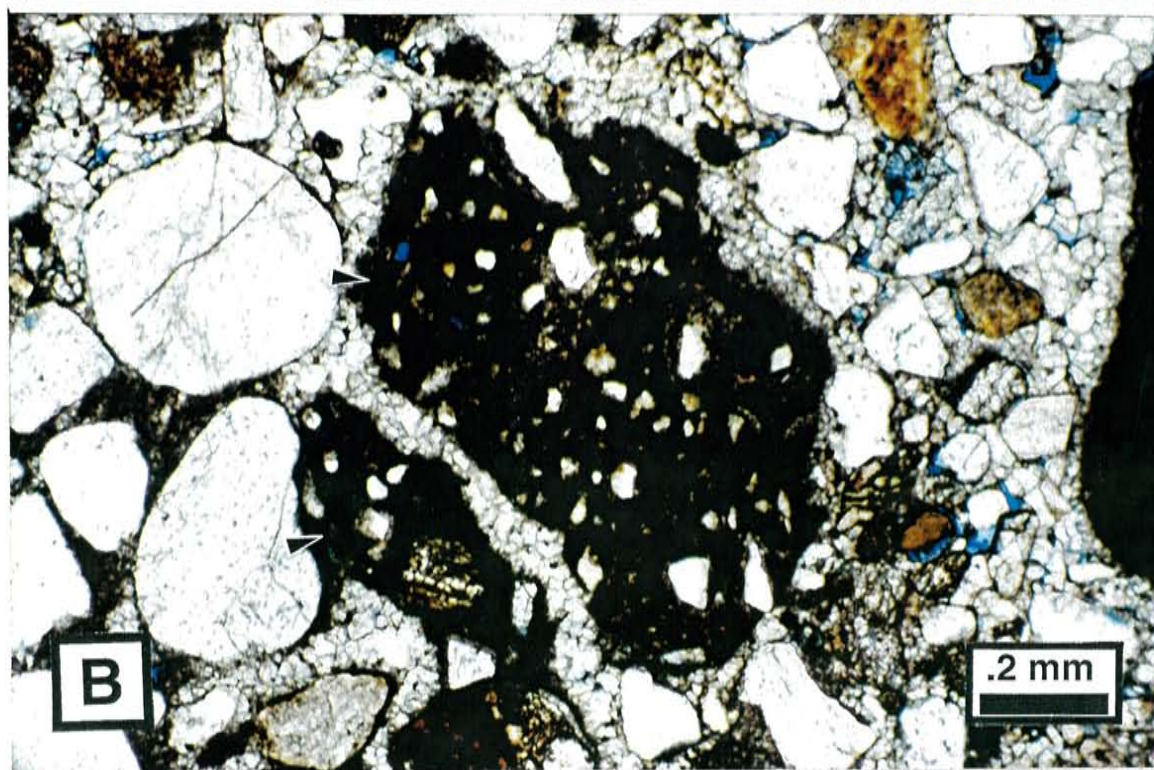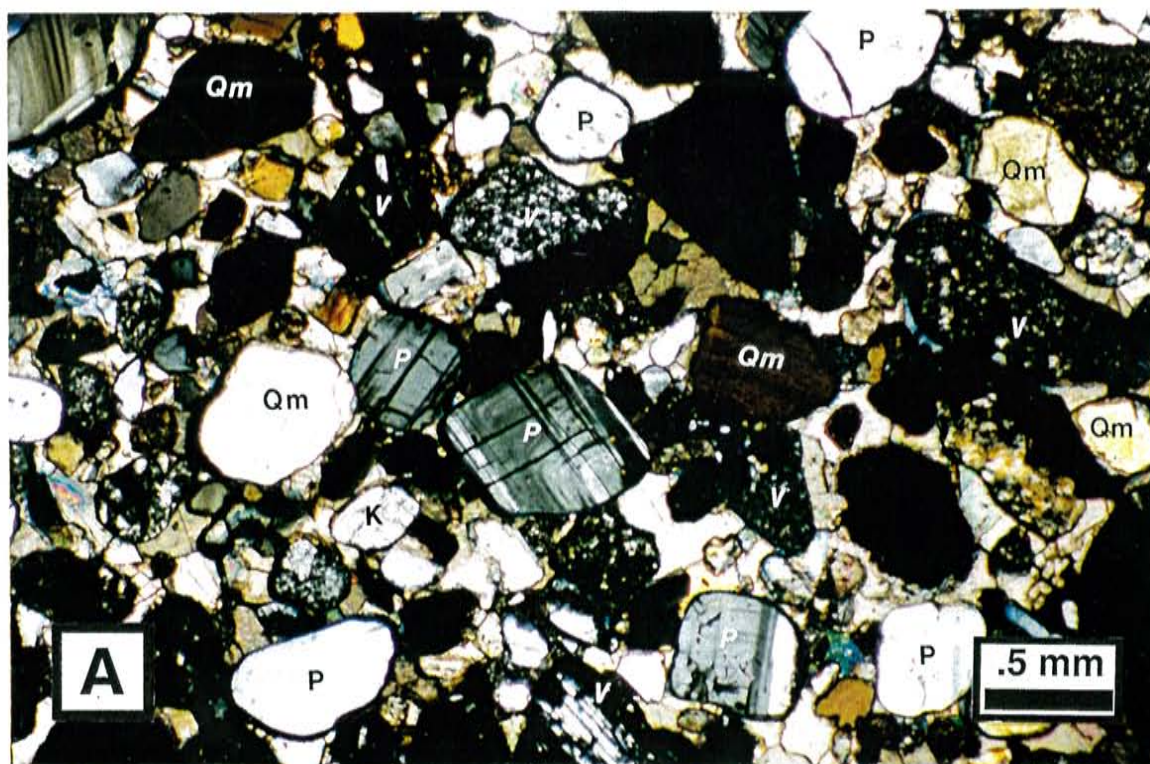
limestone. Very low percentages of metamorphic lithic fragments were noted, and are most common in the upper part of the Unnamed Member (Fig. 2.6A; Lozinsky, 1988).

This study, as well as work by previous authors (Gawne, 1981; Tedford, 1983) noted that muscovite, biotite, and heavy minerals such as hornblende are generally more common in the Unnamed Member (Table B.2).

PROVENANCE

Zia sediments were derived mostly from volcanic and sedimentary source areas. Metamorphic sources only contributed minor amounts to the Zia Formation, and then mostly in the upper Unnamed Member. Silicic to intermediate volcanics are the main source for the lower Zia rock fragments. There is a slight increase in mafic volcanic rock fragments in the Unnamed Member. In the lower Zia, plagioclase percentages are about equal to potassium feldspar percentages, however, plagioclase is dominant in the Unnamed Member. As noted before, there is also an increase in abundance of all feldspars from the lower Zia to the Unnamed Member. Microcline also becomes more common. These changes in feldspar composition indicate an additional source area for the Unnamed Member.

The predominant direction of wind transport was from the west (Gawne, 1973; 1981). Paleocurrent data from fluvial sands at the base of the Zia, the Canada Pillares Member, and the Upper Unnamed member indicate fluvial transport was to the southeast (See Part-3). Cretaceous and Tertiary sandstones may have provided the sedimentary fragments found in the lower Zia (Spiegel, 1961; Gawne, 1981; Lozinsky, 1988). A western source for the volcanic grains in the eolian lower Zia is implied from paleocurrent analyses (Part-3; also Gawne, 1973, 1981). The source could be from older volcaniclastic deposits, or the San Juan or Datil volcanic fields (Gawne, 1974; Ingersoll, 1987; 1990). Ratios and types of quartz and feldspars in the Zia Formation are similar to those described in "Interval 1" from age equivalent Upper Abiquiu (> 26 Ma; Smith, 1995). More samples and a detailed petrographic analysis of Zia Formation volcanic rock fragments would be necessary to make

any definite correlation. The shift in composition from the Piedra Parada Member to the Canada Pillares Member (Fig. 2.3) correlates with a reduction in percent polycrystalline quartz, chert, and volcanic rock fragments with decreasing grain size (Figs. 2.4, 2.5). Because there are no changes in types of volcanic clasts, types and percentages of feldspars, and heavy minerals, the most likely mechanism for this shift is grain size reduction during transport (Davies et. al., 1978; Ingersoll et. al., 1984; Cather and Folk, 1991).

The composition of the Unnamed Member has little overlap with the lower members of the Zia Formation. The increase in total percent feldspar, as well as changes in heavy minerals cannot be accounted for by grain size reduction, and may be the result of additional detrital input from the Santa Fe block, Nacimiento block, or northern volcaniclastic sources such as the Jemez volcanic field (Wright, 1946; Spiegel, 1961; Ingersoll, 1990). There are some compositional similarities in volcanic rock fragments from the Zia Formation to the Keres Group lavas and tuffs (13-6 Ma) to the northeast (Ellisor et al., 1996; Lavine et al., 1996). However, a more detailed petrographic and chemical analysis of Zia Formation volcanic rock fragments would be necessary to make any definite correlation.

DIAGENESIS

Diagenetic alterations affecting Zia Formation sediments can be divided into chemical and mechanical processes. Chemical processes include cementation, and grain and cement dissolution. Mechanical processes included compaction, grain fracturing, and infiltration of clays.

Chemical Processes

Cementation

Calcite (Poikilotopic spar to dense micrite) is the most common cement filling intergranular areas. Cements in the Zia can be divided into three basic groups: those exhibiting vadose characteristics, those exhibiting phreatic characteristics, and those with mixed characteristics (see Part 1). Cements with a micritic matrix, circumgranular cracking, alveolar microtextures, and the presence of rhizocretions are assumed to result from

pedogenic (vadose) processes (Fig. 2.8A; Esteban and Klappa, 1983; Wright and Tucker, 1991; Mora. et al., 1993). Phreatic cements are those in which blocky to drusy spar cements (Figs. 2.7A, 2.7B, 2.8B, 2.9A, 2.9B; Folk(b), 1974; Retallack, 1990; Burns and Matter, 1995) are associated with preservation of primary sedimentary textures (Wright and Tucker, 1991; Mora et al., 1993). Most cemented units show characteristics of both vadose and phreatic influences, including floating grain textures that could be the result of initial vadose cementation (micritic grain coatings) followed by circumgranular cracking, and expansive spar growth (Fig. 2.8C). Expansive calcite growth is a common feature of some phreatic carbonates (Wright and Tucker, 1991; Mora et al., 1993). Micritic grain-coating cements associated with void-filling spar may be the result of phreatic cementation after burial below the water table (Jacka, 1974; Funk, 1979).

Zeolites are present in the intergranular areas of some eolian sandstones (Figs. 2.8 B, 2.9B). Zeolites are typically present in rocks containing significant amount volcanic detritus and precipitated from alkaline pore waters (Hay and Shepard, 1977). The Zia samples fit both these criteria.

Because this study is biased towards calcite cemented units, only a few units were found where clay matrix was significant (i.e., 8594-1A, 8594-10, 81994-5, 1395-10, 1395-11, 81895-1, 81895-3; Table B2.3; Figs. 2.10, 2.11) With the exception of some vadose units, there is an inverse relationship between degree of calcite cementation and clay content (Fig. 2.11). Clays occur as sedimentary units, detrital clasts, thin rims on framework grains, and as pore filling matrix. Clays in the Zia Formation are commonly detrital, either as the main constituent of the original sediment (detrital), or as rip up clasts deposited along with other grains.

Grain Dissolution

Chemical alteration has removed unstable phenocrysts such as hornblende from many volcanic grains, leaving euhedral cavities. Less commonly entire grains are dissolved (Fig.

Fig. 2.8 A. Typical vadose cement with micritic calcite matrix, and alveolar texture (A) from a pedogenic unit in the Unnamed Member. Note the porosity (blue) developed from cement dissolution. If this area had been pore space when the latest stage of spar cementation occurred, then it would have been filled with spar as well. Plain polarized light. **B.** Drusy spar calcite typical of phreatic cementation, from a fluvial unit in the Unnamed Member. Note the coarsening of calcite crystal size towards the center of the pore. Also note the grain dissolution porosity (blue). Note the zeolites in the dissolved grain (Z). Plain polarized light. **C.** Floating grain textures, and alveolar-septal structures similar to those described by Wright (1990), from a fluvial unit in the Unnamed Member. In this unit initial vadose cementation was followed by later phreatic spar cementation and expansive calcite growth. The porosity (blue) is caused by incomplete cementation. Plain polarized light.
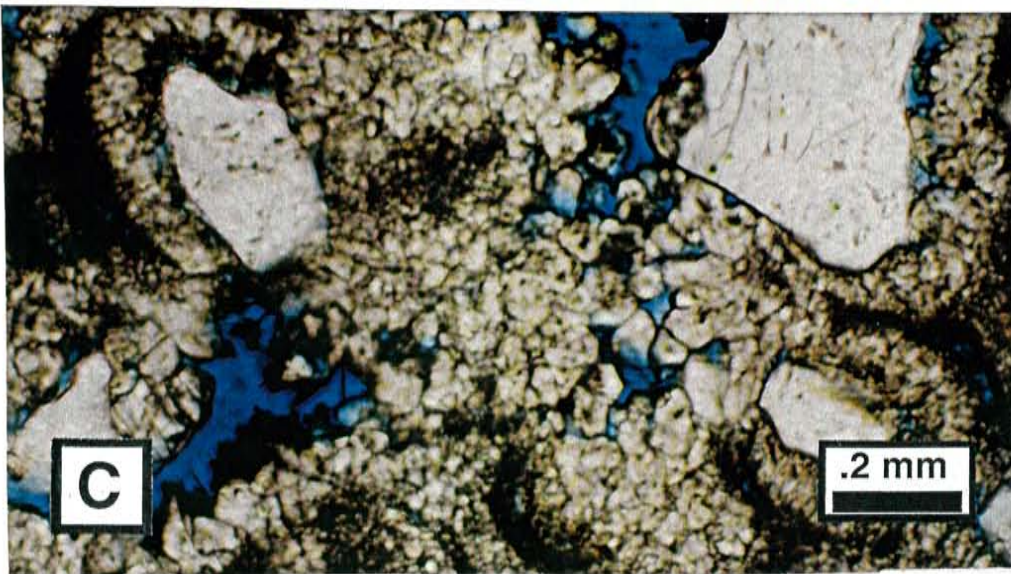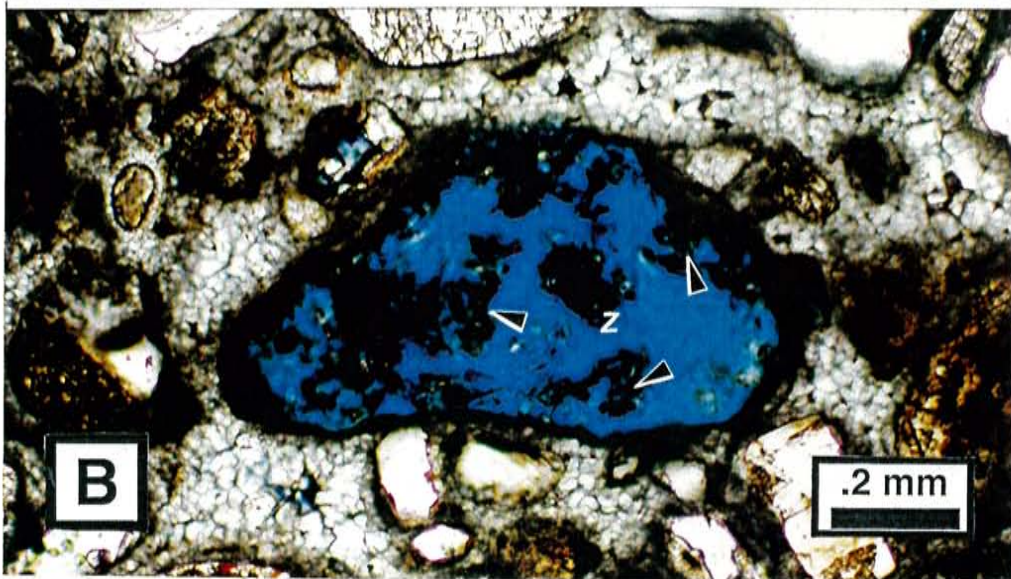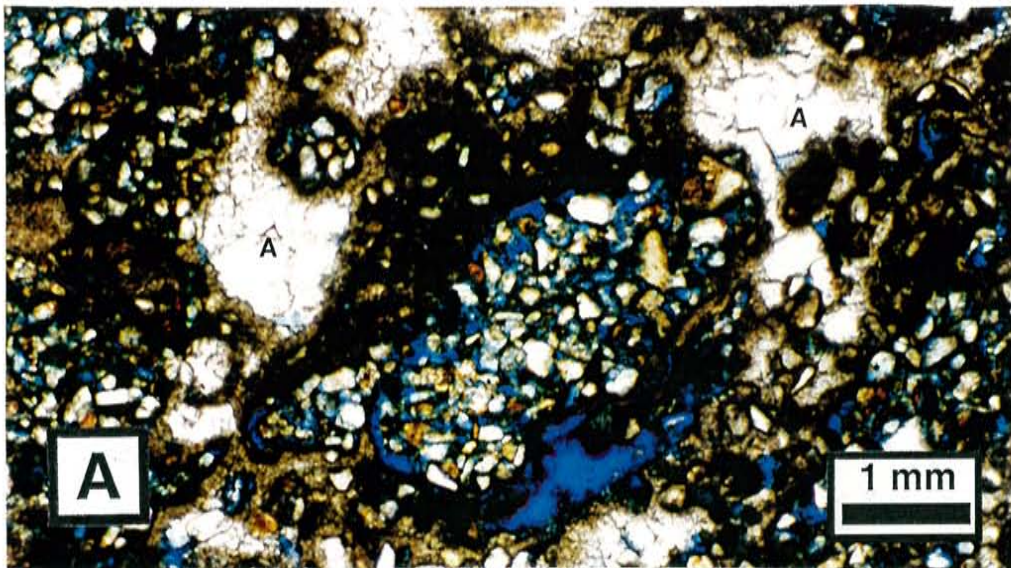
Fig. 2.9 A. Intergranular porosity (blue) from a eolian unit in the lower Unnamed Member. Note that the coarser grains are well cemented while the finer grains are not. Cement is poikilotopic calcite. Plain polarized light. **B.** Intragranular porosity (blue) probably resulting from fracturing during sample preparation or collection, from a eolian unit in the Piedra Parada Member. Note that pore boundaries match grain shapes exactly. Also note zeolites (Z). Plain polarized light. **C.** Porosity (blue) from circumgranular cracking in a pedogenic unit from the Unnamed Member. This unit also has abundant clays. Plain polarized light.
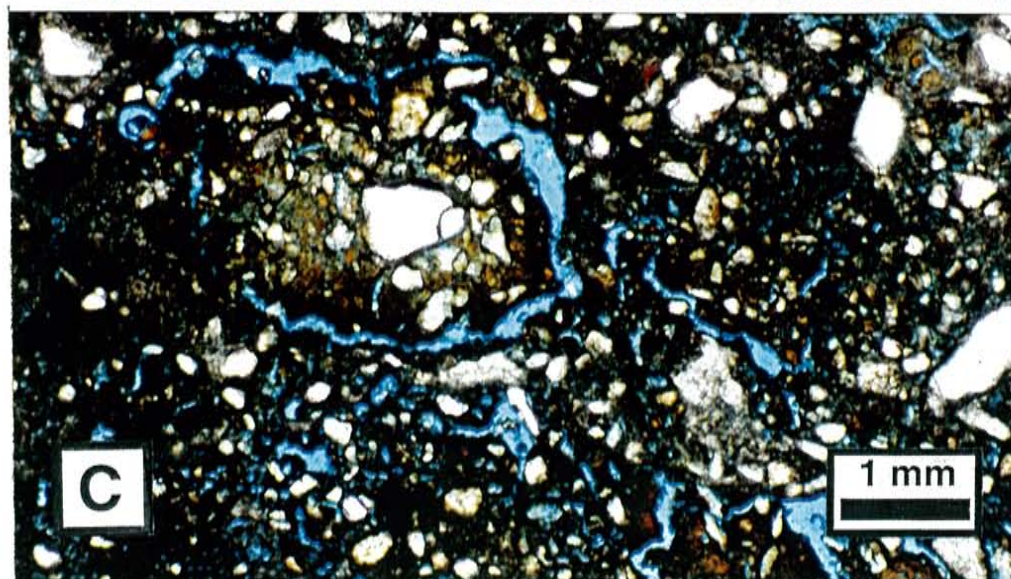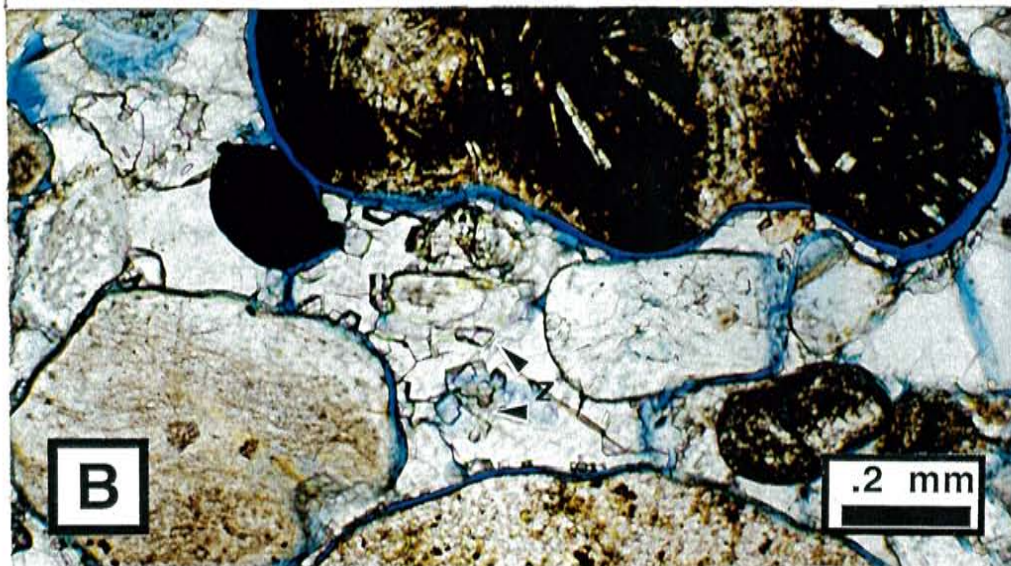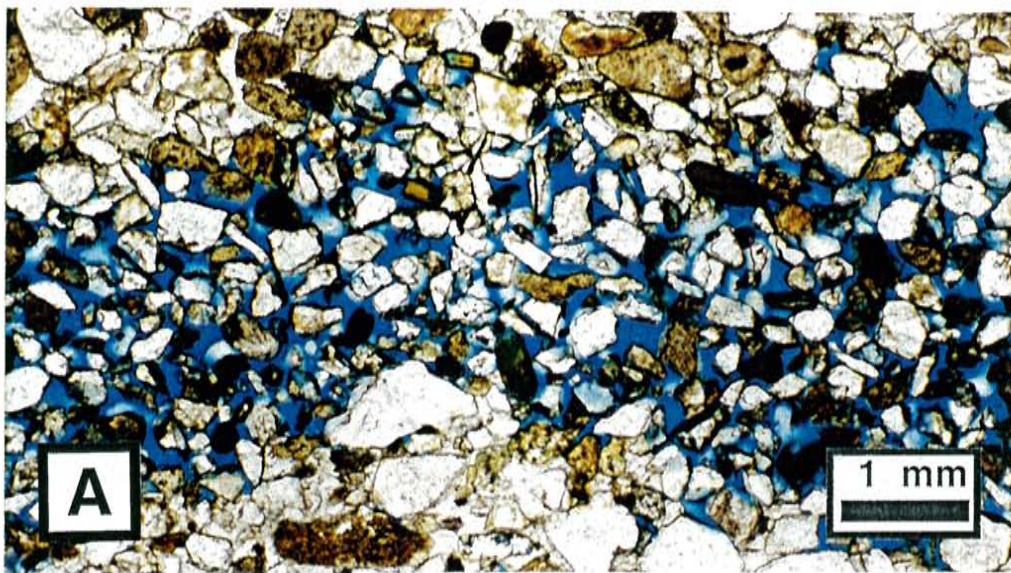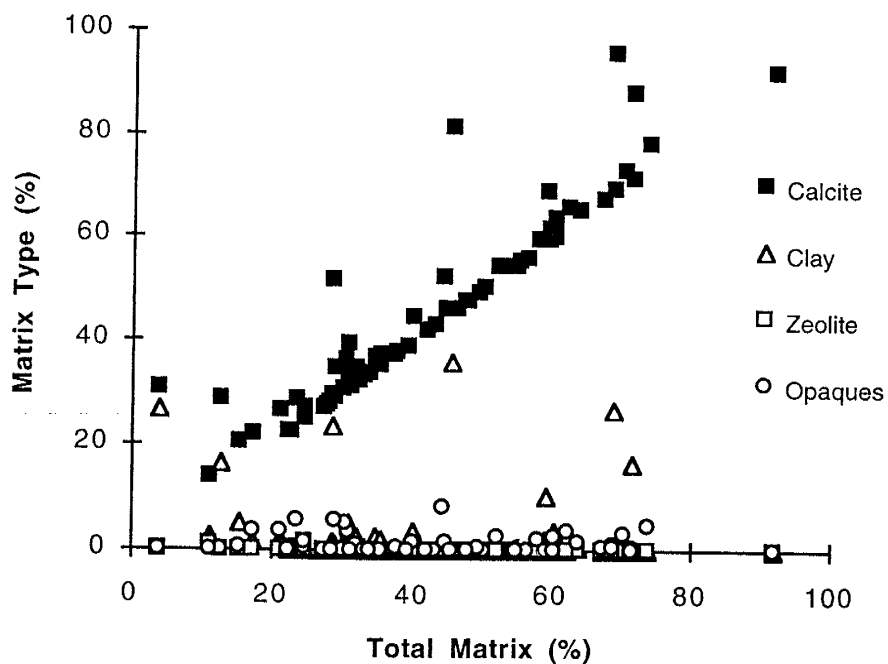
Fig. 2.10. Plot of total matrix versus percentages of calcite, clay, zeolite and opaque matrices. Note that calcite cement is the most common matrix material. Data from Table B.3.
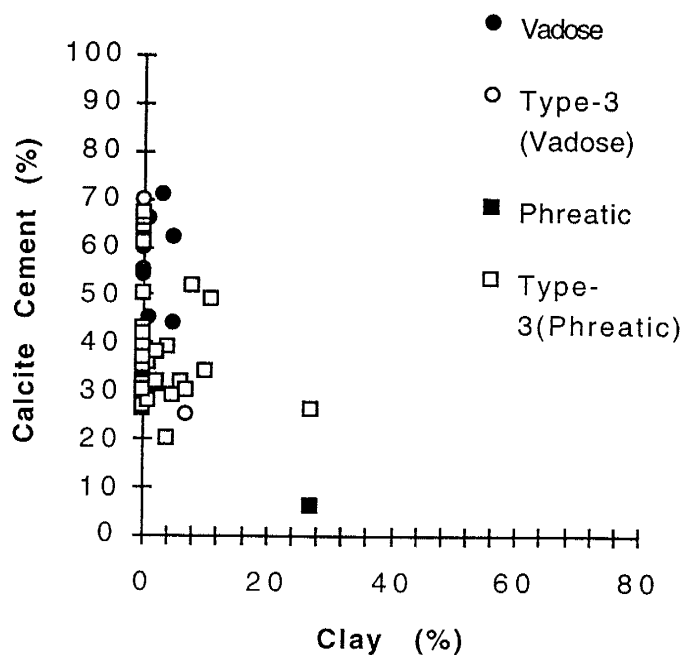
Fig. 2.11. Plot of calcite cement versus clay (rim and pore-filling). Notice that most cemented units do not contain any clay. With the exception of some vadose and some type-3 phreatic units with floating grain textures, higher clay contents are associated with lower amounts of calcite cements. Data from Table B.3.

2.8B). More irregular cavities indicate alteration of an originally glassy groundmass. In the Zia Formation, chert grains were generally more unstable than other quartz types.

Cement Dissolution

Dissolution of micritic cements is a common feature of vadose units in the Zia Formation and is commonly associated with circumgranular cracking and grain dissolution (Fig. 2.8A, 2.9C). Dissolution is distinguished from incomplete cementation by irregular boundaries on cement crystals, and the presence of partially floating framework grains surrounded by veins of sparry calcite (i.e.., if the areas were incompletely cemented, they would have been infilled by sparry calcite after burial below the water table; Fig. 2.8A).

Mechanical Processes

Intergranular fracturing can be divided up into two separate catagories: the first is common in the coarser grained poikilotopically sands from the Piedra Parada and lower Unnamed Members (Fig. 2.9B), and probably the result of breaking during sampling or sample preparation. The edges of these fractures fit the framework grains exactly, and there is no evidence of cement or grain alteration. The second type of fracturing is called circumgranular cracking, and results from repeated wetting and drying of the host sediment (Wright, 1990). Most circumgranular cracks in the Zia Formation are filled with sparry calcite (Fig. 2.9C).

Calcite filled intragranular fractures (fractures through framework grains) are associated with floating grain microtextures. These fractures could be the result of spar infilling a previously fractured grain, or grain-fracturing due to expansive calcite growth.

Compaction

There is no evidence of significant compaction (grain re-arrangement, bending or fracturing of grains, or ductile deformation) in the Zia Formation in either cemented or uncemented units.

Clay Infiltration

Although few clay-rich units were sampled, data indicates that most pore-filling clays without euhedral crystals, and a grain supported matrix (as opposed to grains floating in a clay matrix), are probably the result of mechanical infiltration (Wilson and Pittman, 1977). Also, the colors and textures of clays in sands and silty sands in the Zia Formation resemble clay units above them.

Porosity

The main control on porosity in most samples is the amount of cement and clay matrix, and intergranular macroporosity is the dominant porosity type in most samples (Table B.5; Figs. 2.12, 2.13). This intergranular macroporosity is divided into three main types: (1) porosity resulting from incomplete cementation, (2) fracture macroporosity, and (3) dissolution macroporosity. In general samples containing significant amounts of clay and cement have low macroporosity, whereas samples (incompletely cemented) with low clay and cement have higher porosity (Fig. 2.12).

Fracture macroporosity resulting from circumgranular cracking is very important in some pedogenic units(Figs. 2.9C, 2.13). Other fracture porosity is probably the result of fracturing during sample collection or preparation (Fig. 2.9B).

Dissolution macroporosity results from the dissolution of both framework grains and cements. As stated before, in many units chemical dissolution has resulted in the removal of unstable phenocrysts in volcanic rock fragments, leaving both euhedral and irregular cavities. These types of porosities do not contribute significantly to permeability due to poor interconnection, and/or small pore diameter (Pittman, 1979). In some vadose units, however, cement dissolution has also contributed to significant macroporosity (Figs. 2.12, 2.13).

Intragranular and cement microporosity are only important in samples that have low total porosity (Table B.6; Fig. 2.13). Cement microporosity is common in vadose cements, and can be either the result of incomplete cementation or of cement dissolution. Cement dissolution causes ragged irregular crystal boundaries.
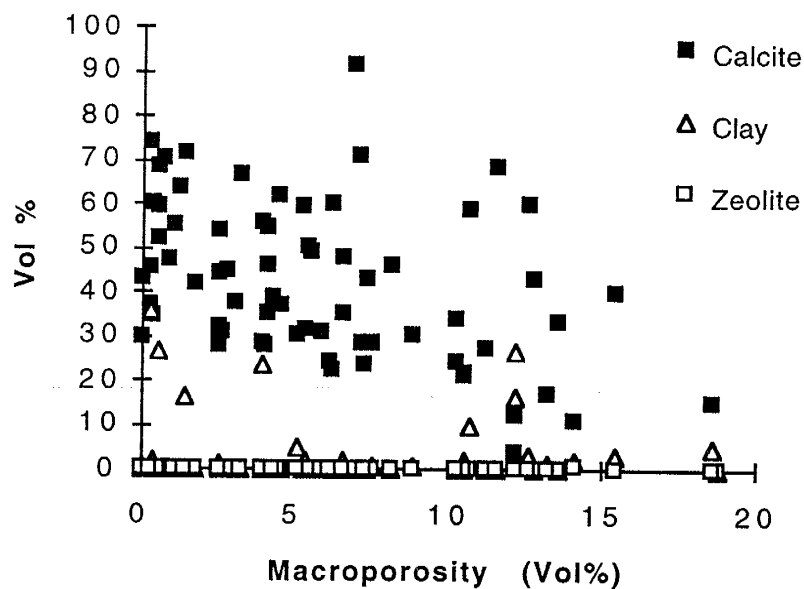
Fig. 2.12. Plot of macroporosity versus percentages of calcite, clay and zeolite for cemented sandstones in the Zia Formation. Data from Tables B.3 and B.5. Note that few units have significant clay or zeolite content. Some vadose units have high porosity relative to percent calcite due to dissolution of cements and circumgranular cracking
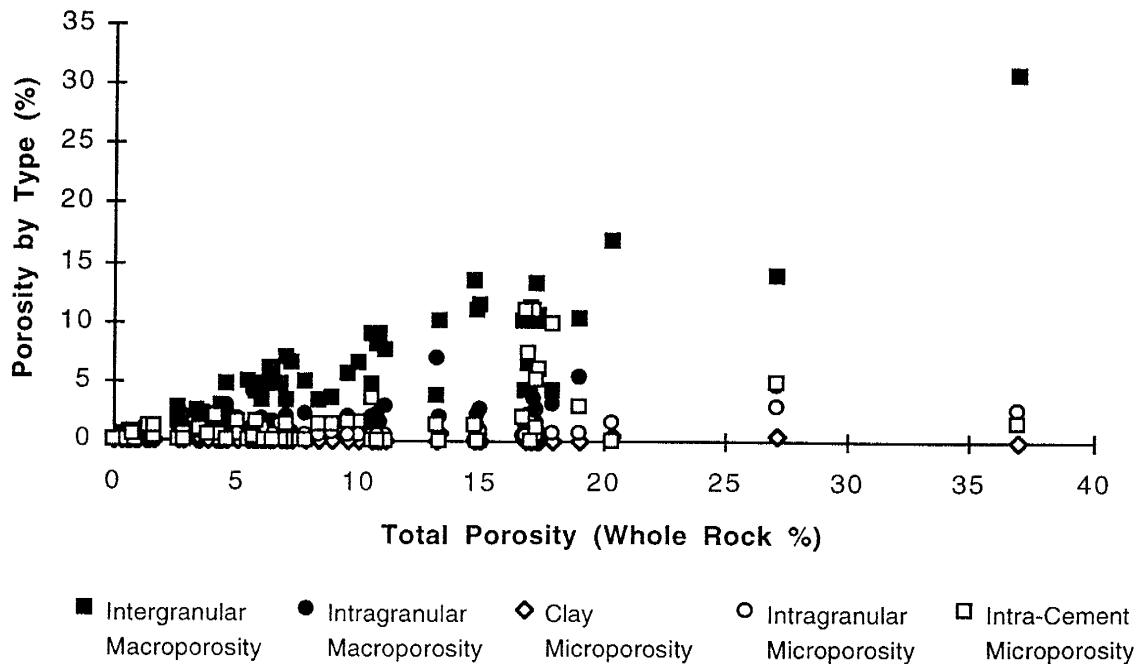
Fig. 2.13. Plot of total porosity versus individual porosity types. Intergranular macroporosity is the main porosity type in most samples. Note that intra-cement microporosity resulting from cement dissolution can be significant in some samples. Data from Table B.5.

CONCLUSIONS

Zia sands can be subdivided into two distinct groups on the basis of composition. The composition of the lower Zia changes from a felspathic litharenite (Piedra Parada Member) to lithic arkoses (Chamisa Mesa, Canada Pillares Members). The Unnamed Member is differentiated from the lower members by greater amounts of feldspar. The linear nature of the composition change for the lower Zia Formation, as well as correlation of percentages of volcanic and chert grains with grain size suggests that the changes are due to a fining upwards sequence without a change in provenance. The change in types and amounts of feldspar and lithic fragments suggests that the change from the lower Zia to the Unnamed Member represents not only a change in sedimentary processes but also a change in provenance.

The primary diagenetic process that affected the Zia Formation was authigenic calcite cementation. Calcite cementation can be divided by petrological characteristics into vadose, phreatic, and mixed types. Most cemented units in the Zia Formation have mixed characteristics. Intergranular porosity is the dominant porosity type in cemented and uncemented units. Porosity in phreatic units is primarily the result of incomplete cementation, whereas porosity in vadose units is due to cement and grain dissolution, and circumgranular cracking.

REFERENCES

Bryan, K., and McCann, F. T., 1937, The Ceja del Rio Puerco: A border feature of the Basin and Range province in New Mexico: Journal of Geology, v. 45, p. 801-828.

Burns, S. J., and Matter, A., 1995, Geochemistry of carbonate cements in surficial alluvial conglomerates and their paleoclimatic implications, Sultanate of Oman. Journal of Sedimentary Research, v. A65, no.1, p. 170-177.

Cather, S. M., and Folk, R. L., 1991, Pre-diagenetic sedimentary fractionation of andesitic detritus in a semi-arid climate: an example from the Eocene Datil Group, New Mexico. In: Sedimentation in volcanic settings, SEPM Special Publication, no. 45, p. 211-226.

Chapin, C. E., and Cather, S. M., 1994, Tectonic setting of the axial basins of the northern and central Rio Grande rift. In: Basins of the Rio Grande Rift: Structure, Stratigraphy, and Tectonic Setting (Ed. by Keller, G.R., and Cather, S.M.) Geological Society of America Special Paper 291, p. 5-25.

Davies, D. K., Vessell, R. K., Miles, R. C., Foley, M. G., and Bonis, S. B., 1978, Fluvial transport and downstream sediment modifications in an active volcanic region, in Miall, A.D. (Ed.) , Fluvial Sedimentology: Canadian Society of Petroleum Geologists Memoir 5, p. 61-84.

Ellisor, R., Wolff, J., and Gardner, J. N., 1996, Outline of the petrology and geochemistry of the Keres Group lavas and tuffs. New Mexico Geological Society Guidebook, 47th Field Conference, Jemez Mountains Region., p. 237-242.

Esteban, M, and Klappa, C. F., 1983, Subaerial exposure environment, In: Carbonate Depositional Environments (Ed. by Scholle, P.A., Bebount, D.G., and Moore, C.H.) AAPG Mem., no. 33, p. 1-54.

Folk, R. L., 1974(a), Petrology of sedimentary rocks., Austin, Hemphill, 182 pp.

Folk, R. L.,1974(b), The natural history of crystalline calcium carbonate; effect of magnesium content and salinity: Journal of Sedimentary Petrology, v. 44, p. 40-53.

Funk, J. M., 1979, Distribution of Carbonate Cements in Quaternary Alluvial-Fan Deposits, Birch Creek Valley, East-Central Idaho - Diagenetic Model. AAPG Bulletin 63 (3), p. 454.

Galusha, T., and Blick, J. C., 1971, Stratigraphy of the Sante Fe Group, New Mexico: American Museum of Natural History Bulletin, v. 144, p 1-128.

Gawne, C. E., 1973, Faunas and sediments of the Zia Sand, middle Miocene beds of New Mexico. New York, Columbia University, unpublished Ph.D. thesis, 352p.

Gawne, C. E. , 1981, Sedimentology and stratigraphy of the Miocene Zia Sand of New Mexico: Summary. Geological Society of America Bulletin, Part 1, v. 92, p. 999-1007.

Hawley, J. W., and Haase, C. S., 1992, Hydrologic framework of the northern Albuquerque basin: New Mexico Water Resources Research Institute, Report WRRI 290, p. 37-55.

Hay, R. L., 1978, Geologic occurrence of Zeolites. in Natural Zeolites, Occurrence, Properties, Use. Sand, L.B., and Mumpton, F.A., (Eds.), Pergamon Press, p. 135-143.

Hay, R. L., and Shepard, R. A., 1977, Zeolites in open hydrologic systems, In: Mineralogy and geology of natural zeolites, Mumpton, F., (Ed.), Reviews in Mineralogy, v. 4. Washington D.C., Mineralogical Society of America, p. .93-102.

Hunt, C. B., 1936, Geology and Fuel Resources of the Southern Part of the San Juan Basin, New Mexico. U.S. Geologic Survey Bulletin, v. 860-B, p. 1-80.

Jacka, A. D., 1974, Differential cementation of Pleistocene carbonate fanglomerate, Guadalupe Mountains. Journal of Sedimentary Petrology, v. 44, no. 1, p. 85-92.

Ingersoll, R. V., Bullard, T. F., Ford, R. L., Grimm, J. P., Pickle, J. D., and Sares, S. W., 1984, The effect of grain size on detrital modes: A test of the Gazzi-Dickinson point-counting method, Journal of Sedimentary Petrology, v. 54, p. 103-116.

Ingersoll, R. V., Cavazza, W., Baldridge, W. S., and Shafiqullah, M., 1987, Oligocene-Miocene volcaniclastic petrofacies and basin evolution in northern New Mexico: Implications for initiation of the Rio Grande rift: Geological Society of America Abstracts with Programs, v.19, p. 712.

Ingersoll, R.V., Cavazza, W. Baldridge, W. S., and Shafiqullah, M., 1990, Cenozoic sedimentation and paleotectonics of north-central New Mexico: Implications for

initiation and evolution of the Rio Grande rift. Geological Society of America Bulletin, v. 102, p. 1280-1296.

Ingersoll, R.V., Cavazza, W., 1991, Reconstruction of Oligo-Miocene volcaniclastic dispersal patterns in north-central New Mexico using sandstone petrofacies. In: Fisher, R.V., and Smith, G.A., eds. Sedimentation in volcanic settings. Society of Economic Paleontologists and Mineralogists Special Publication 45, p. 227-236.

Lavine, A., Smith, G., Goff, F., and Macintosh, W.C., 1996, Volcaniclastic rocks of the Keres Group: insights into mid-Miocene volcanism and sedimentation in the southeastern Jemez mountains. New Mexico Geological Society Guidebook, 47th Field Conference, Jemez Mountains Region., p. 211-218.

Leonard, M. L., 1982, Provenance of the Zia Sand Formation between San Ysidro and Bernalillo, New Mexico. Compass of the Sigma Gamma Epsilon. p. 61-71.

Lozinsky, R. P.,1988, Stratigraphy, sedimentology, and sand petrology of the Santa Fe Group and pre-Santa Fe Group Tertiary deposits in the Albuquerque basin, central New Mexico: Unpublished PhD dissertation, Socorro, New Mexico, New Mexico Institute of Mining and Technology, 298 pp.

Lozinsky, R. P., 1994, Cenozoic stratigraphy, sandstone petrology, and depositional history of the Albuquerque Basin, central New Mexico, in Keller, G. R., and Cather, S. M., (Eds.), Basins of the Rio Grande Rift: Structure, Stratigraphy, and Tectonic Setting: Boulder, Colorado, Geological Society of America Special Paper 291, p. 73-81.

Lucas, S. G., 1980, Stratigraphy and age of the Galisteo Formation and the structural history of the Rio Puerco fault Zone, north-central New Mexico. Abstracts with Programs, Geological Society of America, vol. 12; 6, p. 279.

Mora, C. I., Fastovsky, D. E., Driese, S. G. , 1993, Geochemistry and stable isotopes of paleosols: University of Tennessee Department of Geological Sciences, Studies in Geology 23, 65 p.

Morse, J. W., and Mackenzie, F. T. , 1990, Geochemistry of Sedimentary Carbonates. Developments in Sedimentology, v. 48, Elsevier. p.

Mozley, P. S., Beckner, J. B., and Whitworth, T. M., 1995, Spatial distribution of calcite cement in the Santa Fe Group, Albuquerque Basin, NM: implications for ground-water resources. New Mexico Geology, v. 17, No. 4, p. 88-93.

Pittman, E.D., 1979, Porosity, diagenesis and productive capability of sandstone reservoirs, In: Aspects of diagenesis. P. A. Scholle and P. R. Schluger, (Eds.), SEPM Special Publication No. 26, p. 159-173.

Powers, M.C., 1953, A new roundness scale for sedimentary particles. Journal of Sedimentary Petrology, v. 28, p. 108-110.

Retallack, G.J. ,1988, Field recognition of paleosols. Geological Society of America, Special Paper 216, p. 1-20.

Smith, G. A., 1995, Paleogeographic, volcanologic and tectonic significance of the Upper Abiquiu Formation at Arroyo del Cobre, New Mexico. New Mexico Geological Society Guidebook, 46th Field Conference, Geology of the Santa Region., p. 261-270.

Smith, G. A., and Lavine, A., 1996, What is the Cochiti Formation? New Mexico Geological Society Guidebook, 47th Field Conference, Jemez Mountains Region., p. 219-224.

Spiegel, Z., 1961, Late Cenozoic sediments of the lower Jemez River region. New Mexico Geological Society Guidebook, no. 12, p. 132-138.

Tandon, S. K., and Friend, P. F., 1989, Near-surface shrinkage and carbonate replacement processes, Arran Cornstone Formation, Scotland. Sedimentology, v. 36, p. 1113-1126.

Tedford, R. H., 1982, Neogene stratigraphy of the northwestern Albuquerque basin. New Mexico Geological Guidebook, 33rd Field Conference, Albuquerque Country II, p. 273-278.

Weider, M., and Yaalon, D. H. ,1982, Micromorphological fabrics and developmental stages of carbonate nodular forms related to soil characteristics. Geoderma, v. 28, p. 203-220.

Wilson, M. D., and Pittman, E. D., 1977, Authigenic clays in sandstones: recognition and influence on reservoir properties and paleoenvironmental analysis: Journal of Sedimentary Petrology, v. 47, p. 3-31.

Woodward, L. A., 1987, Geology and mineral resources of Sierra Nacimiento and vicinity, New Mexico. New Mexico Bureau of Mines and Mineral Resources, Memoir 42, 84p.

Wright, H. E., Jr., 1946, Tertiary and Quaternary geology of the lower Rio Puerco area, New Mexico: Geological Society of America Bulletin, v. 57, p. 383-456.

Wright, V. P. ,1990, A micromorphological classification of fossil and recent calcic and petrocalcic microstructures. In: Soil Micromorphology: a basic and applied science (Ed. Douglas, L.A.). Developments in Soil Science, no. 19, Elsevier, p. 401-407.

Wright, V. P., and Tucker, M. E. ,1991, Introduction. In: Calcretes. (Ed. by Wright, V.P., and Tucker, M.E.). Int. Ass. Sediment., Reprint Series 2, p. 1-22

Part 3

Relationship Between Concretion Orientation, Sedimentary Structures, and Paleo-Groundwater Flow in the Zia Formation, New Mexico

ABSTRACT

Both the fluvial and eolian deposits in the Miocene Zia Formation contain numerous oriented concretions that are interpreted to reflect paleo-groundwater flow orientation in the phreatic (saturated) zone. Paleocurrent directions from the eolian sediments of the Zia Formation indicate prevailing westerly winds , whereas paleocurrent data for fluvial facies in the Canada Pillares and Unnamed Members indicate an east to southeasterly transport direction. Concretion orientations for the eolian sediments in the Zia Formation are dominantly NE-SW, with azimuths ranging from 16-19°. Concretion orientations for fluvial sediments in the Zia Formation are dominantly southeasterly, with azimuths ranging from 161-169°. For fluvial sediments, concretion orientations are subparallel to paleocurrent directions (< 35° difference in mean vectors). For eolian sediments concretion orientations are consistently 60-90° from paleocurrent directions. Assuming that cementation is controlled by chemical transport, this difference in orientation implies that the direction and scale of permeability anisotropy in fluvial and eolian depositional systems are fundamentally different. Elongate concretions show much less scatter in orientation than paleocurrent data in both systems. Because of consistency of orientation and ease of measurement, concretion orientations in both fluvial and eolian sediments can provide a rapid means of estimating paleo-groundwater flow directions.

INTRODUCTION

Understanding the effect of primary sedimentary structures on permeability is of great importance in understanding controls on groundwater flow. Previous workers have explored the relationships between paleocurrent data, oriented calcite concretions, and permeability in a fluvial system (Davis et al., 1993; Mozley and Davis, 1996). In this study I have used paleocurrent data and oriented concretions to determine the relationships between primary sedimentary structures and paleo-groundwater flow in both fluvial and eolian sediments in the Zia Formation.

GEOLOGIC SETTING

The Zia Formation records initial sedimentation in the northern Albuquerque basin, the largest and deepest basin in the over 1000 kilometer long Rio Grande rift of Colorado and New Mexico (Lozinsky, 1994). The Zia Formation is exposed along an arc extending from the Ceja del Rio Puerco in the west, to the Jemez River area in the north, to the Espinaso Ridge, east of Albuquerque (Kelly, 1977; Gawne, 1981; Lozinsky, 1988; Fig. 3.1). The formation can be divided into a sand-dominated eolian lower member (Piedra Parada), a fluvial/eolian member (Chamisa Mesa), a mud-dominated fluvial member (Canada Pillares Member), and a sand-dominated fluvial/eolian member (Unnamed Member; Gawne, 1981; Tedford, 1982; Fig. 3.2). This study is concentrated on the Canada Pillares type area, along the Rio Puerco fault zone, on the King ranch area (Fig. 3.1).

ORIENTED CONCRETIONS

Elongate concretions in the Zia Formation are subhorizontal elongate cemented masses (generally <10 m long), commonly lacking internal structure (Figs. 3.3A-3.3C). Calcite cement in all types of elongate concretions in the Zia is blocky spar. These concretions exhibit very consistent orientations, normally within a few degrees variation within a single outcrop (Figs. 3.3A; 3.3B). Oriented concretions in fluvial deposits are
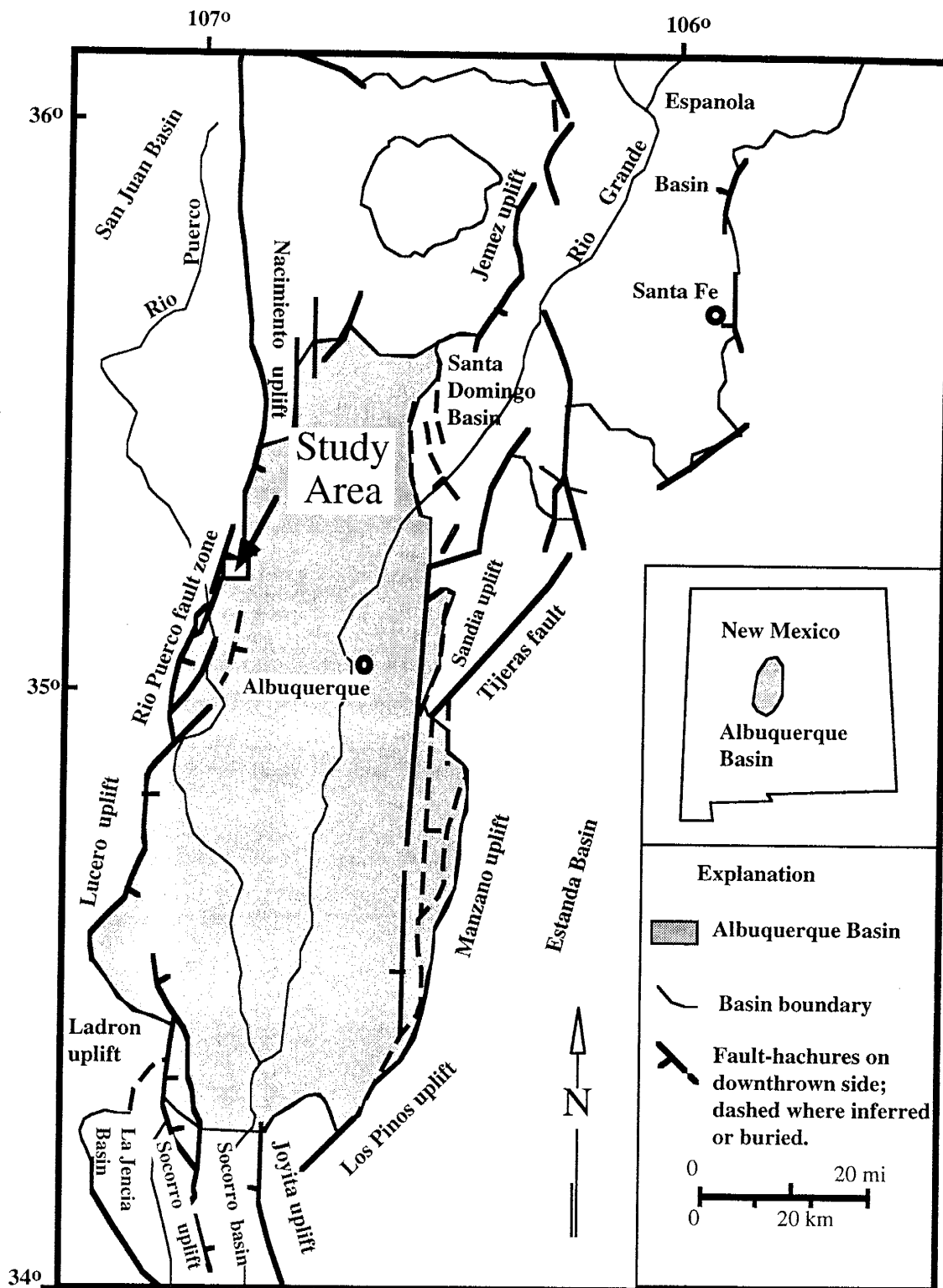
Figure 3.1. Map of Albuquerque Basin showing the King brother's ranch study area. Map modified from Lozinsky (1993).
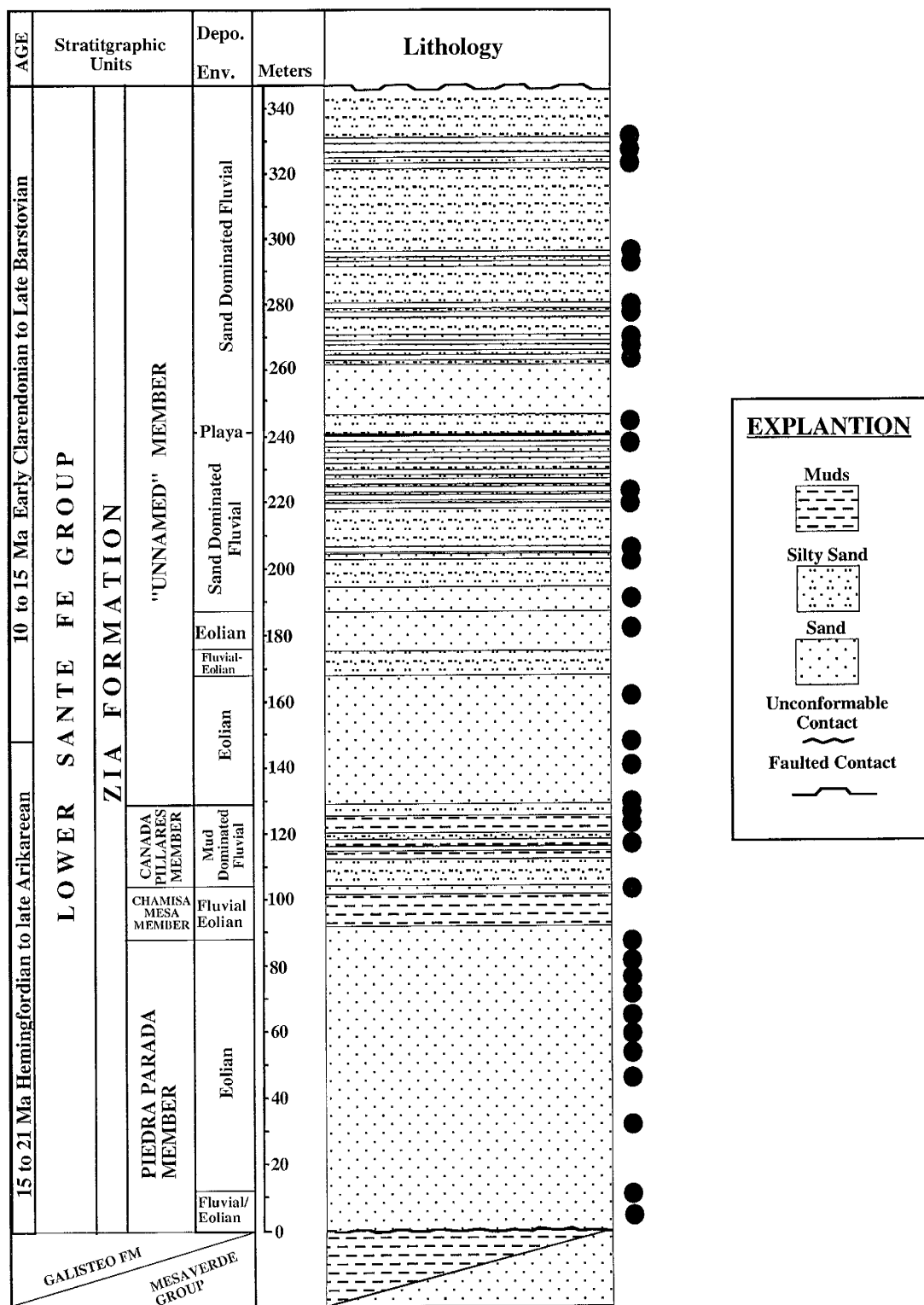
Figure 3.2. Generalized stratigraphic column of the Zia Formation showing ages, lithologies, and depositional environments. Black dots show approximate locations for orientation and paleocurrent data. Terminology and ages from Tedford (1982) and Lozinsky (1988).

Figure 3.3A. Large oriented concretions from a fluvial unit in the upper
Unnamed Member. Concretions in this unit forms a sheet subparallel to the
plane of bedding. Scale is in centimeters. **B.** Small finger-like oriented
concretions from a fluvial unit in the upper Unnamed Member. Note the mm
sized warts on the surface. The part of the pen showing is approximately 5 cm
long. **C.** Oriented concretion following crossbedding planes from an eolian unit
in the Piedra Parada Member. Scale is in decimeters.

associated with coarse to medium grained, well sorted, thin bedded channel deposits. Oriented concretions in fluvial systems are generally oriented subparallel to the bedding of the outcrop in which they are found (Fig. 3.3A), but have no apparent relationship to individual crossbedding planes. Oriented concretions in eolian deposits are associated with medium to fine grained, well sorted dune deposits, and are generally flattened and rounded in outline. Eolian concretions in few instances have partially cemented cores. Oriented concretions in eolian deposits are generally parallel to the plane of crossbedding (Fig. 3.3C), and are typically near the center of large tabular bodies, not at the base of dunes. Although elongate concretions in the Zia have been noted by previous workers (Galusha, 1966; Gawne, 1973, 1981; McBride et al., 1993), they are not well studied or understood.

Oriented concretions have been noted in a large number of other studies (Todd, 1903; Schultz, 1941; Meschter, 1958; Colton, 1967; Jacob, 1973; Raiswell and White, 1975; Parsons, 1980; Theakstone, 1981; Fastovsky and Dot, 1986; Pirrie, 1987; Johnson, 1989; McBride et al., 1994; Beik, 1994; McBride et al., 1995; Mozley and Davis, 1996). Many of these workers suggested that elongate concretions reflect the orientation of groundwater flow during precipitation (Schultz, 1941; Meschter, 1958; Raiswell and White, 1975; Parsons, 1980; Theakstone, 1981; Fastovsky and Dot, 1986; Pirrie, 1987; Johnson, 1989; McBride et al., 1994; Beik, 1994; McBride et al., 1995; Mozley and Davis, 1996). These studies also indicate a strong correlation between concretion orientation, paleocurrent direction, and primary depositional textures.

METHODS

For this study, measured sections of the Zia Formation in the King Ranch area were constructed along four transects to examine lateral and vertical variations in lithology, cementation, paleocurrent directions and concretion orientations. Concretion orientations and paleocurrent data were corrected for structural dip using Stereonet 4.0, and plotted using the Rosy 2.13 program. Trough directions were estimated from 2-D exposures using the relationship between characteristic asymmetry in basal scour surfaces and truncation of forset

laminae (DeCelles et al., 1983). It was not possible in several cases to get crossbedding measurements directly from the concretionary unit, so they were obtained from overlying and underlying units. All data are given using dip directions and dip angles (Tables C.1- C.10).

Paleocurrent data from the Canada Pillares area gathered by Gawne (1973) were also used in this study. Dip directions taken by Gawne were analyzed by the vector method of Curray (1956), without weighting by magnitude of dip. In this method data are treated as vectors with magnitude of unity. Because of low tectonic dip angles (<10°), Gawne and I both made the assumption that set boundaries were originally horizontal when correcting her data for the effects of tectonic dip. Data from Gawne's study was taken from steroplots, as the original tabulated data were not available.

Because I needed to directly compare concretion orientation data and paleocurrent direction data, and avoid inflating dispersion measurements, all orientation data were treated as directional data for the purpose of calculations. For fluvial deposits, a concretion oriented NW-SE would be assigned a direction of SE. This study and previous work on paleogeography and paleocurrent directions indicate that this is the preferred direction of fluvial deposition (Gawne, 1981; Ingersol et al., 1990). For eolian systems, a concretion oriented NE-SW is arbitrarily assigned a direction of NE.

RESULTS

Paleocurrent directions from the eolian sediments for the Zia Formation indicate prevailing westerly winds (Figs. 3.4A, 3.4C, 3.4E). Paleocurrent data for fluvial facies in the Canada Pillares and Unnamed Members indicates an east to southeasterly transport direction. (Figs. 3.5A, 3.5C). Concretion orientations for the eolian sediments in the Zia Formation are dominantly NE-SW, ranging from 16-19°. Concretion orientations for fluvial sediments in the Zia Formation are dominantly southeasterly, ranging from 161-169°.
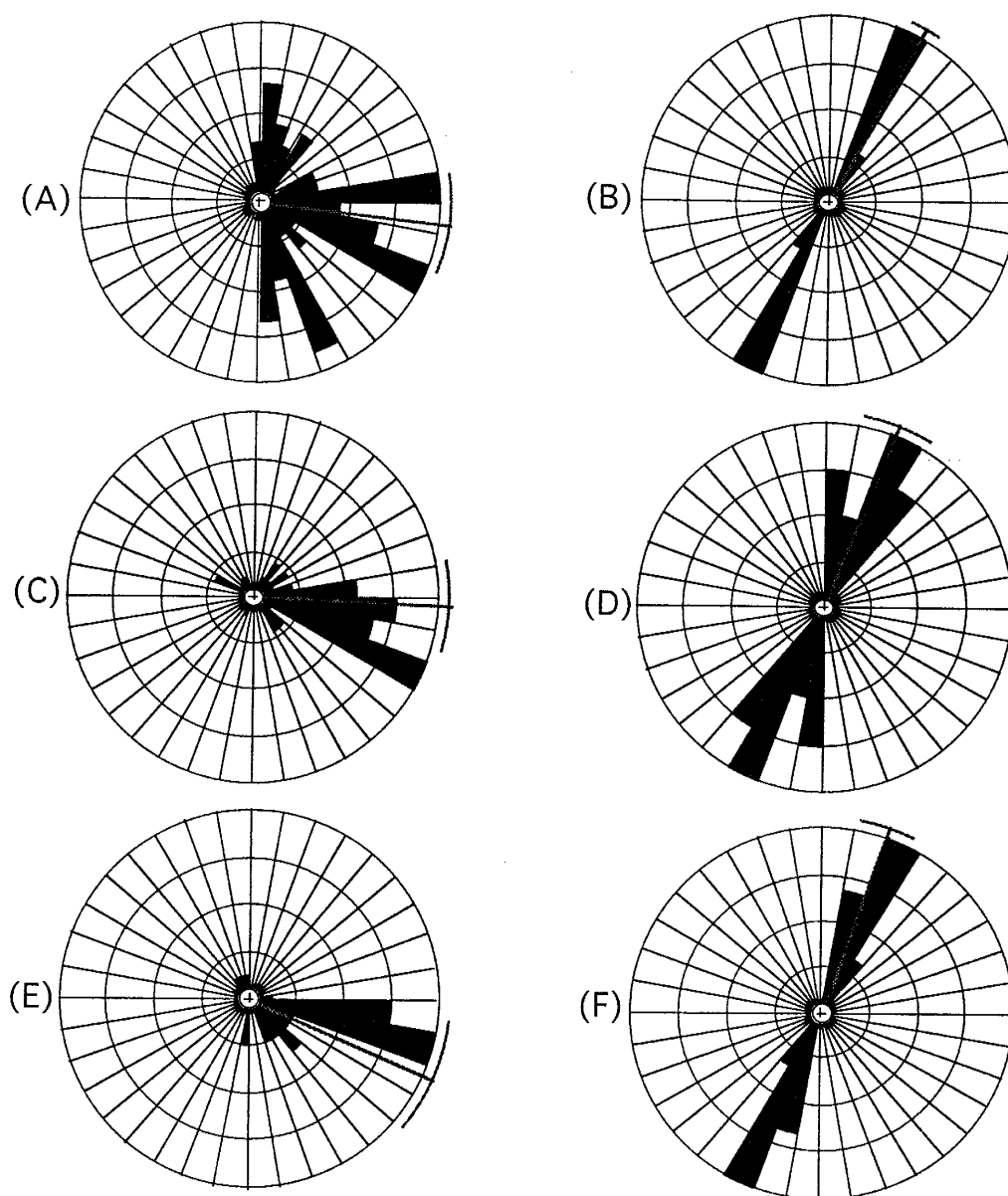
Figure 3.4 Rose diagram of paleocurrent directions and concretion orientations from eolian sediments in the Zia Formation. Grey line extending from the center of the rose diagrams indicates vector mean, the grey curved line outside the rose diagrams indicates confidence angle. **A.** Paleocurrent directions (N=88; vector mean=97°) from the eolian portions of the Piedra Parada Member, Canada Pillares type area. Data from Table C.1. **B.** Concretion orientations (N=13; vector mean=28°) from the eolian portions of the Piedra Parada Member, Canada Pillares type area. Data from Table C.2. **C.** Paleocurrent directions (N=46; vector mean=89°) from the eolian portion of the Chamisa Mesa Member, Canada Pillares type area. Data from Table C.3. **D.** Concretion orientations (N=12; vector mean=19°) from the eolian portion of the Chamisa Mesa Member, Canada Pillares type area. Data from Table C.4. **E.** Paleocurrent directions (N=32; vector mean=113°) from the eolian portion of the Unnamed Member, Canada Pillares type area. Data from Table C.7. **F.** Concretion orientations (N=12; vector mean=16°) from the eolian portion of the Unnamed Member, Canada Pillares type area. Data from Table C.8.
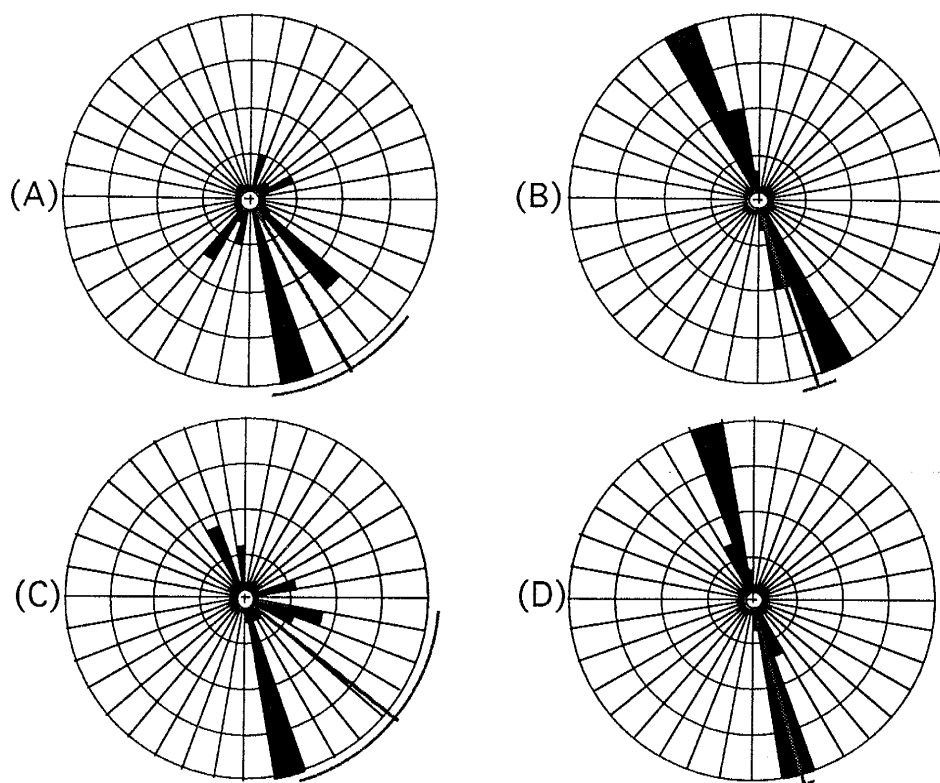
Figure 3.5 Rose diagram of paleocurrent directions and concretion orientations for fluvial sediments in the Zia Formation. Grey line extending from the center of the rose diagrams indicates vector mean, the grey curved line outside the rose diagrams indicates confidence angle. **A.** Paleocurrent directions (N=18; vector mean=120°) from the fluvial Canada Pillares Member, Canada Pillares type area. Data from Table C.5. **B.** Concretion orientations (N=10; vector mean=161°) from the fluvial Canada Pillares, Canada Pillares type area. Data from Table C.6. **C.** Paleocurrent directions (N=22; vector mean=128) from the fluvial portion of the Unnamed Member, Canada Pillares type area. Vector mean for just channels (not shown) is 160°. Data from Table C.9. **D.** Concretion orientation (N=54; vector mean=164) from the fluvial portions of the Unnamed Member, Canada Pillares type area. Data from Table C.10.

In all cases, whether eolian or fluvial, there is much more scatter in the paleocurrent data than in the concretion orientation data (e.g., Tables 3.1-3.10; Figs. 3.4 - 3.8). The resultant mean vector length is a measurement of dispersion, where large values (near 1.0) indicate that observations are tightly bunched together, and values near 0 indicate that the vectors are widely dispersed (Davis, 1986). The resultant mean vector length for elongate concretions in all systems is .975, whereas the resultant mean vector length for paleocurrent directions is .510. This is expected given the wide variation in paleocurrent orientations in most fluvial and eolian systems. Oriented concretions in eolian deposits show slightly more dispersion than those found in fluvial deposits, with resultant mean vectors of .952 and .984 respectively.

For the fluvial parts of the Canada Pillares and the Unnamed Member there is good agreement between concretion orientations and paleocurrents (Figs. 3.5A-3.5D). This indicates that concretion orientations may be good indicators of sediment transport directions in fluvial sediments. For eolian sediments, however, concretion orientations and paleocurrents differ between 60 and 90 degrees (Figs. 3.4A-3.4F). It is important to remember that while concretion orientations and paleocurrent directions for eolian sediments are near perpendicular, these concretions are generally subparallel to the plane of crossbedding of the host sediment. The relationship between concretion orientation and paleocurrent direction for both fluvial and eolian sediments is shown diagramatically in Figure 3.6.
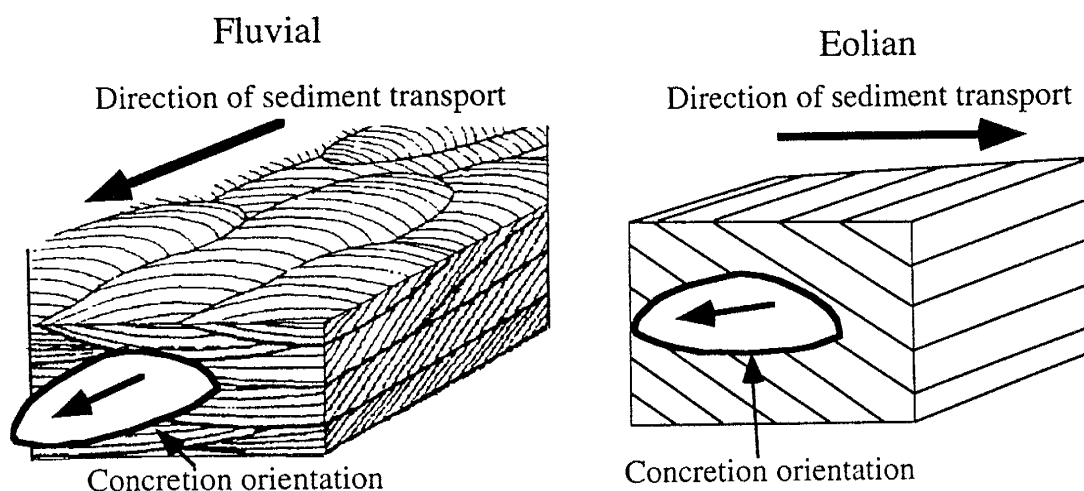
Figure 3.6. The relationship between concretion orientation and crossbedding in fluvial and eolian systems in the Zia Formation. Note that for fluvial systems concretion orientation is sub-parallel to sediment transport. For eolian systems concretion orientations are roughly perpendicular to the direction of sediment transport.

Discussion

For fluvial and eolian deposits in the Zia Formation there are important differences in the relationships between oriented concretions and stratification. First, concretion orientations in fluvial systems are sub-parallel to paleocurrent directions (i.e. commonly

cutting across cross-strata), while in eolian systems concretion orientations are roughly perpendicular to paleocurrent directions (i.e., aligned within sets of cross-strata).

Assuming that oriented concretions reflect paleo-groundwater flow directions, there are two possible explanations for the differences between concretion and paleocurrent directions in fluvial and eolian sediments:

1) There was a change in the direction of the overall hydraulic gradient between deposition of fluvial and eolian sediments in the Zia Formation. A change in the large-scale hydraulic gradient could occur if there were major changes in basin geometry between changes of depositional environment. This explanation seems unlikely as concretion orientations from fluvial sediments both below and above eolian sediments have a consistent orientation (Fig 3.5).

2) The relationship between permeability anisotropy and paleocurrent directions is different for eolian and fluvial-alluvial systems. For fluvial systems, previous studies indicate than the anisotropy and paleocurrent directions are sub-parallel (Davis et al., 1993; Mozley and Davis, 1996). In eolian systems, the anisotropy is dependent on the internal arrangement of stratification types within individual sets of crossbeds, and different types of crossbedding can have very different physical properties (Weber, 1987; Lindquist, 1988; Chandler et al., 1989). Flow is potentially greater along grain-flow strata than across strata as a result of the inverse grading that characterizes grain-flow strata (Lindquist, 1988; Chandler et al., 1989). Fluid flow in wind ripple cross strata may be even more restricted to strata-parallel flow because of the distribution of low permeability laminae, and second-order migrating interdune deposits (Lindquist, 1988; Chandler et al., 1989). These studies indicate that for eolian dune sediments, fluid flow should occur roughly parallel to strata, roughly perpendicular to crossbed directions (Fig. 3.7). Paleocurrent and concretion orientation data from eolian sediments in the Zia Formation, also indicate that paleocurrent directions and

Straight-crested   **Barchanoid**   **Barchan**
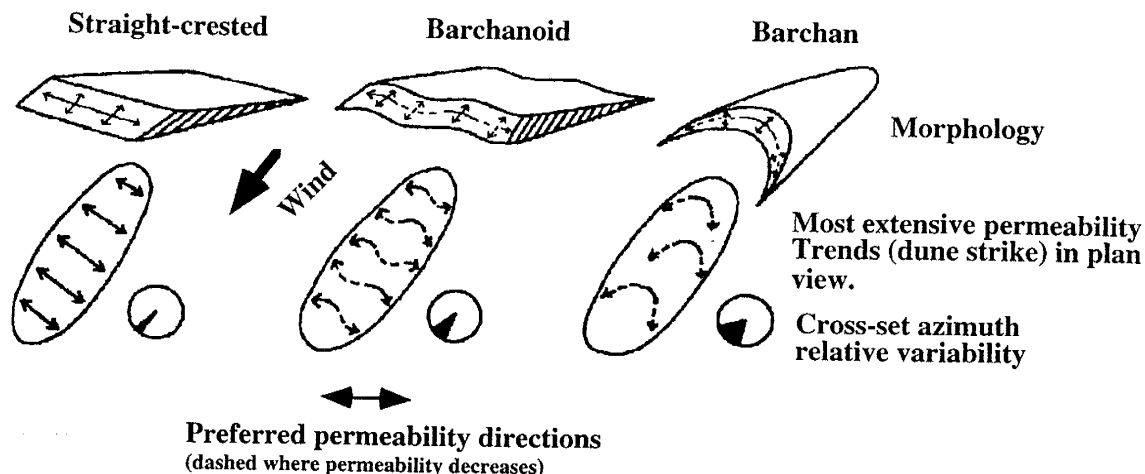
Figure 3.7. Preferred permeability directions for three common dune morphologies, with relative differences in azimuth variability for lee face cross-sets also shown (from Lindquist, 1988). Azimuth dip directions are roughly perpendicular to the trend of the most extensive permeability line.

fluid flow were perpendicular to each other (Figs. 3.4A-3.4F).

In some fluvial systems concretion orientations reflect overall paleo-groundwater flow, and are not influenced by small scale crossbedding (Mozley and Davis, 1996). However, for eolian facies in the Zia Formation concretion orientation and groundwater flow were apparently largely determined by crossbedding orientation. It is supposed that this difference in sensitivity to sedimentary textures could be the result of permeability anisotropy contrasts and overall sediment body geometry.

Fluvial sediments in the Zia Formation consist primarily of interbedded permeable channel sand bodies and impermeable overbank-splay deposits (Part 1). These channel bodies are typically elongate in the direction of sediment transport in aerial view . Because of the great permeability contrasts between the sediment types in fluvial sediments (between .2 and 3.9 darcies; Dreyer et al., 1990), early fluid flow would be focused in the channel deposits, and parallel to the direction of sediment transport (Fig. 3.8).

Eolian sediments in the Zia Formation mainly consist of thick tabular units of moderately to well-sorted medium to fine sands, bounded by thin clay-rich interdune and fluvial deposits (Fig. 3.8). Dune sediments have high permeabilities (1.3-3 darcies for wind-

ripple strata, and 4.9-6 darcies for grain-flow deposits; Chandler et al., 1989), and strong permeability contrasts such as those found in fluvial sediments are not present, allowing fluid to flow unfocused and at a slower rate. Groundwater flowing through the body would not be concentrated in any particular direction, and so heterogeneities in crossbedding could have a greater effect.
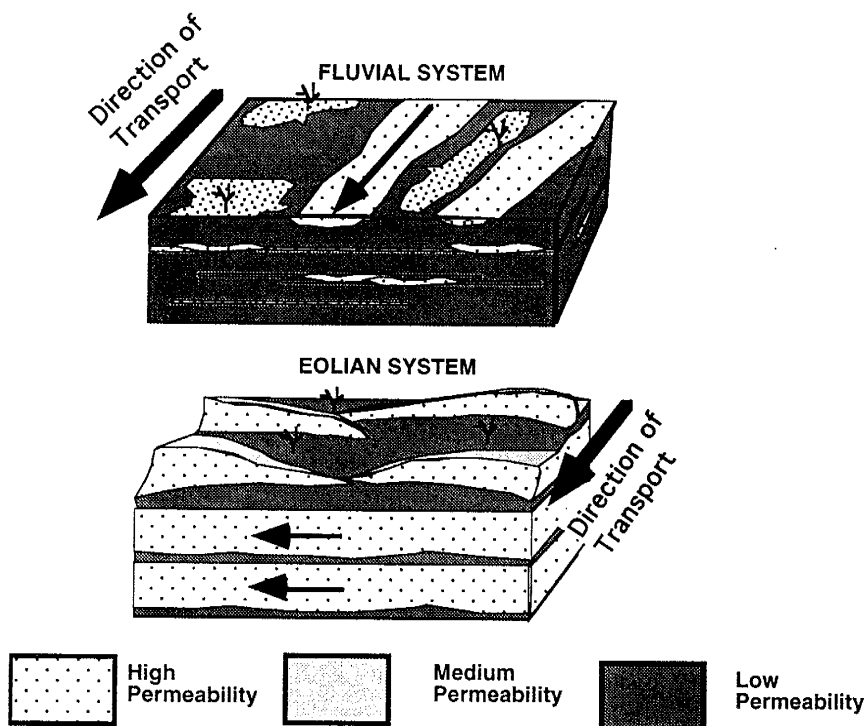
Figure 3.8. Schematic diagram of the differences between sediment body geometries in fluvial and eolian systems, and its effect on fluid flow. Arrows indicate preferred direction of fluid flow. Block diagrams based on data from stratigraphic columns, and sedimentary data in Appendix A. Estimation of fluid flow direction modified from Chandler, et al. (1989), Dryer, et al. (1990), and Larkin and Sharp (1992).

CONCLUSIONS

Elongate calcite concretions in the Zia Formation reflect paleo-groundwater flow orientations in the phreatic zone. For fluvial sediments, concretion orientations and paleo-groundwater flow are sub-parallel ($< 35^\circ$ difference in mean vectors), and are not affected by heterogeneities in crossbedding. For eolian sediments in the Zia Formation concretion orientations are $60-90^\circ$ from other paleocurrent indicators, implying that paleo-groundwater flow is affected by heterogeneities in crossbedding. This implies that the direction and scale of permeability anisotropy in fluvial and eolian depositional systems are fundamentally different. Elongate concretions in fluvial systems show much less scatter in orientation than paleocurrent data in all systems, implying that they reflect overall groundwater flow. Elongate concretions in eolian systems also show slightly more scatter in orientation, and are affected by small-scale anisotropies in primary depositional textures and permeabilities. Because of consistency of orientation, and the ease of measurement, concretion orientations in both fluvial and eolian sediments can provide a rapid means of estimating paleo-groundwater flow directions. Because of the differences in anisotropy in fluvial and eolian sediments, knowledge of the depositional environment, as well as traditional paleocurrent measurements are essential when estimating direction of sediment transport from concretion orientations.

REFERENCES

Beik, B., 1994, Concretions and nodules in North Dakota-Cannonballs, Logs, and other Oddities. North Dakota Geological Society Newsletter, v. 21, no. 2. p. 6-11.

Colton, G. W., 1967, Orientation of carbonate concretions in the Upper Devonian of New York: United States Geological Survey Professional Paper 575-B, p. B57-B59.

Chandler, M. A., Kocurek, G., Goggin, D. J., and Lake, L. W., 1989, Effects of stratification heterogeneity on permeability in eolian sandstone sequence, Page Sandstone, Northern Arizona: Bulletin of American Association of Petroleum Geologists, v. 73, no. 5, p. 658-668.

Curray, J. R., 1956. The analysis of two dimensional orientation data. Journal of Geology, v. 64, p 117-131.

Davis, J. C., 1986, Statistics and data analysis in geology. 2nd ed., John Wiley and Sons, 646p.

Davis, J. M., Lohmann, R. C., Phillips, F. M., Wilson, J. L., and Love, D. W., 1993, Architecture of the Sierra Ladrones Formation, central New Mexico: Depositional controls on the permeability correlation structure: Geological Society of America Bulletin, v. 105, p. 998-1007.

DeCelles, Peter, G., and Langford, R. P., 1983, Two new methods of paleocurrent determination from trough cross-stratification. Journal of Sedimentary Petrology, v. 53, No. 2, p. 629-642.

Dreyer, T., Schreie, A., and Walderhaug, O., 1990, Minipermeameter-based study of permeability trends in channel sand bodies: Bulletin of American Association of Petroleum Geologists, v. 74, p. 359-374.

Freeze, R. A., and Cherry, J. A., 1979, Groundwater: Englewood Cliffs, New Jersey, Prentis-Hall, 604 p.

Glennie, K. W., 1970, Desert sedimentary environments. Developments in sedimentology, v. 14, Amsterdam, London, and New York, Elsevier Pub. Co., 222 p.

Hartcamp, C. A., Arribas, J., and Tortosa, A., 1993, Grain size, composition, porosity and permeability contrasts within cross-bedded sandstones in Tertiary fluvial deposits, central Spain: Sedimentology, v. 40, p. 787-799.

Hillel, D., 1980, Fundamentals of Soil Physics: Sand Diego, Academic Press, Inc.

Ingersoll, R.V., Cavazza, W., Baldridge, W. S., and Shafiqullah, M., 1990, Cenozoic sedimentation and paleotectonics of north-central New Mexico: implications for initiation and evolution of the Rio Grande rift. Geological Society of America Bulletin, v. 102, p. 1280-1296.

Jacob, A. F., 1973, Elongate concretions as paleochannel indicators, Tongue River Formation (Paleocene), North Dakota: Geological Society of America Bulletin, v. 84, p. 2127-2132.

Johnson, M. R., 1989, Paleogeographic significance of oriented calcareous concretions in the Triassic Katberg Formation, South Africa: Journal of Sedimentary Petrology, v. 59, p. 1008-1010.

Jury, W. A., Gardner, W. R., and Gardner, W. H., 1991, Soil Physics (5th Edition): New York, John Wiley and Sons, Inc.

Kelly, V. C., 1977, Geology of the Albuquerque basin, New Mexico: New Mexico Bureau of Mines and Mineral Resources, Memoir 33, 60 pp.

Kochel, R. C., and Riley, G. W., 1988, Sedimentologic and stratigraphic variations in sandstones of the Colorado Plateau and their implications for groundwater sapping: NASA publications SP-491, Chapter 3, p. 57-62

Kortekaas, T. F. M., 1985, Water/oil displacement characteristics in cross-bedded reservoir zones: Society of Petroleum Engineers Journal, v. 25, No. 6, p. 917-926.

Larkin, R. G., Sharp, J. M., 1992, On the relationship between river-basin geomorphology, aquifer hydraulics, and ground water flow direction in alluvial aquifers. Geological Society of America Bulletin, v. 104, p. 1608-1620.

Leonard, M. L., 1982, Provenance of the Zia Sand Formation between San Ysidro and Bernalillo, New Mexico. Compass of the Sigma Gamma Epsilon. p. 61-71.

Lindquist, S. J., 1988, Practical characterization of eolian reservoirs for development: Nugget Sandstone, Utah-Wyoming thrust belt: Sedimentary Geology, v. 56, p. 315-339.

Lozinsky, R. P., 1994, Cenozoic stratigraphy, sandstone petrology, and depositional history of the Albuquerque Basin, central New Mexico, in Keller, G.R., and Cather, S.M., eds. Basins of the Rio Grande Rift: Structure, Stratigraphy, and Tectonic Setting: Boulder, Colorado, Geological Society of America,Special Paper 291, 73-81.

Lupe, R., and Ahlbrandt, T. S., 1979, Sediments of ancient eolian environments-reservoir inhomogeneity. In E. D. McKee (Ed.), A study of global sands seas. USGS Professional Paper 1052, p. 241-251.

McBride, E. F., Picard, M. D., Folk, R. L., 1993, Elongate concretions in sandstone: evidence of ancient flow directions in groundwater. AAPG Bulletin, v. 77 (8), p. 1455.

McBride, E.F., Picard, M.D., Folk, R.L., 1994, Oriented concretions, Ionian coast, Italy, evidence of groundwater flow direction. Journal of Sedimentary Petrology, v. A64, no. 3, p. 535-540.

Meschter, D. Y., 1958, A study of concretions as applied to the geology of uranium deposits: United States Atomic Energy Commission Technical Memorandum Report TM-D-1-14, 10p.

Mozley, P., and Davis, J. M. , 1996, Relationship between oriented calcite concretions and permeability correlation structure in an alluvial aquifer, Sierra Ladrones Formation, New Mexico. Journal of Sedimentary Research. v. A66 , p. 11-16.

Palmquist, W. N., and Johnson, A. I., 1962, Vadose flow in layered and non layered materials: United States Geological Survey Professional Paper, 450-C, C142-C143.

Parsons, M. W., 1980, Distribution and origin of elongate sandstone concretions, Bullion Creek and Slope Formations (Paleocene), Adams county, North Dakota [unpublished MS thesis]: University of North Dakota, Grand Forks, North Dakota, 133p.

Pirrie, D., 1987, Oriented calcareous concretions from James Ross Island, Antarctica: British Antarctic Survey Bulletin, v. 75, p. 41-50.

Raiswell, R., and White, N. J. M., 1978, Spatial aspects of concretionary growth in the Upper Lias of northeast England: Sedimentary Geology, v. 20, p. 291-300.

Tedford, R. H., 1982, Neogene stratigraphy of the northwestern Albuquerque basin. New Mexico Geological Guidebook, 33rd Field Conference, Albuquerque Country II, p. 273-278.

Theakstone, W. H., 1981, Concretions in glacial sediments at Seglvatnet, Norway: Journal of Sedimentary Petrology, v. 51, p. 191-196.

Todd, J. E., 1903, Concretions and their geological effects: Geological Society of America Bulletin, v. 14, p 353-368.

Weber, K. J., 1982, Influence of common sedimentary structures on fluid flow in reservoir models: Journal of Petroleum Technology, v. 34, p. 665-672.

Weber, K. J., 1987, Computation of initial well productivities in aeolian sandstone on the basis of a geologic model, Leman gas field, U.K., in R.W.Tillman and K.J. Weber, eds., Reservoir sedimentology: SEPM Special Publication 40, p. 333-354.

Appendix A

A Preliminary Study of Facies Associations in the Zia Formation

INTRODUCTION

The identification of facies associations in the Zia Formation was undertaken to understand the relationship between lithology and cementation, and to relate that understanding to the spatial distribution of cements. The term facies association is used to describe a grouping of commonly associated sedimentary characteristics, e.g., thickness, areal extent, and shape of lithologic units, rock types, sedimentary structures, and fauna types and abundances (Miall, 1990). Sediments can be divided into eight facies associations that are found throughout the formation. These associations represent channel and levee, sand sheet, floodplain, paleosol, eolian dune, eolian sand sheet, and interdune environments (Table 1.1). Facies association maps of fluvial and eolian depositional environments were constructed (using methods described in Miall, 1990) on several outcrops in the King ranch area along the Rio Puerco fault zone. These facies maps were used to define the facies associations for the Zia.

FACIES ASSOCIATION DESCRIPTIONS

Eight main types of facies association are defined in this study: channel (CH), sheet sand (SS), overbank fine (OF), paleosol (P), cross-stratified eolian dune (EC), eolian sheet sand associations (ES), interdune facies associations (ID), and playa associations (Pl). With the exception of the paleosol and overbank fine associations, the classification of fluvial associations follows that of Miall (1990). In this study paleosols are treated as a separate facies association because of their usefulness for studying cementation and alluvial depositional environments (Allen, 1974; Davis et al., 1993).

The terms facies and facies/lithofacies association are also used to define eolian sediments of particular geometry and sedimentary characteristics (Porter, 1987; Chan, 1989; Kocurek and Dott, 1981, Kocurek, 1981; Miall, 1990). Symbols used for eolian facies associations (e.g., EC, ES) were also developed for this study.

Channel Association (CH)

The channel association is subdivided into two groups based primarily on scale. The first category of channel association includes tabular to lenticular, fine to medium grained sand bodies, 3 to 5 meters thick, and up to 2 km in lateral extent (Fig. 4.1). Basal contacts of channels vary from scoured and erosional to sharp and flat. The tops of lenses are flat and capped by low angle and horizontal laminated sand. Trough cross-bedded sand (St) and medium angle planar laminated sand (Sp) are the most common sedimentary structures near the bottoms of these channels. Low angle cross-bedded sand (Sl), horizontally laminated sand (Sh), and ripple cross-laminated sand (Sr) are more common near the tops of these channels. Massive sand (Sm), massive, crudely bedded silts and muds (Fm), finely laminated to rippled silts and muds (Fl), laminated silt, sand, and clay (Fsc) are probably levee deposits, and are included in the channel association.

The second category of channel association includes .2-2 meters thick lenticular sand bodies, generally less than 10 m wide. These sand lenses are composed of fine to medium sand with sharp bases but no basal lag. These channels are commonly oriented perpendicular to main channel orientations. Planar laminated sand (Sp) is the most common sedimentary structure and is associated with lateral accretion surfaces. These types of channels are generally isolated in sheet sand and overbank fine associations. These types of channels are interpreted as splay channel deposits.

Sheet Sand Association (SS)

Sand sheets are laterally extensive and consist of very fine to fine grained silt and silty sand (Fig. 4.2). These sand sheets range from .2 to 4 meters in lateral extent. These sand sheets are associated with fluvial deposits. Basal contacts show little evidence of erosion, and are generally flat. Upper contacts vary from sharp to gradational. The most common sedimentary structure is parallel bedded, fining upwards, horizontally laminated (Sh) to low angle crossbedded silty sand (Sp). Massive silty sand (Sm) is also common, and generally associated with paleosols. Ripple cross-laminated fine to medium sand (Sr), clay drapes and
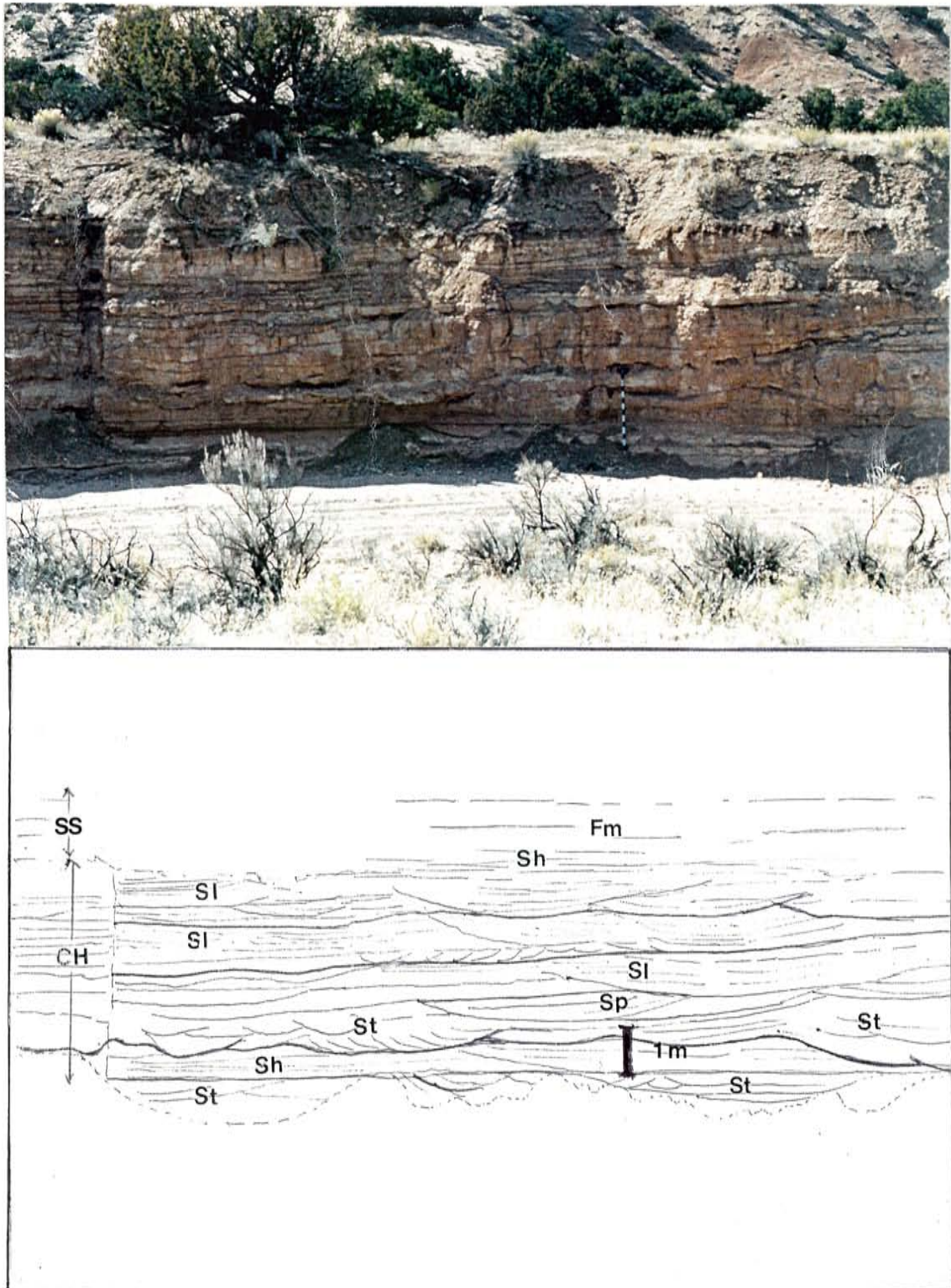
Fig. 4.1. Laterally extensive channel associations (CH) from the Chamisa Mesa Member. Outcrop faces east. The bottom figure shows bounding surfaces and associated lithofacies and facies associations.
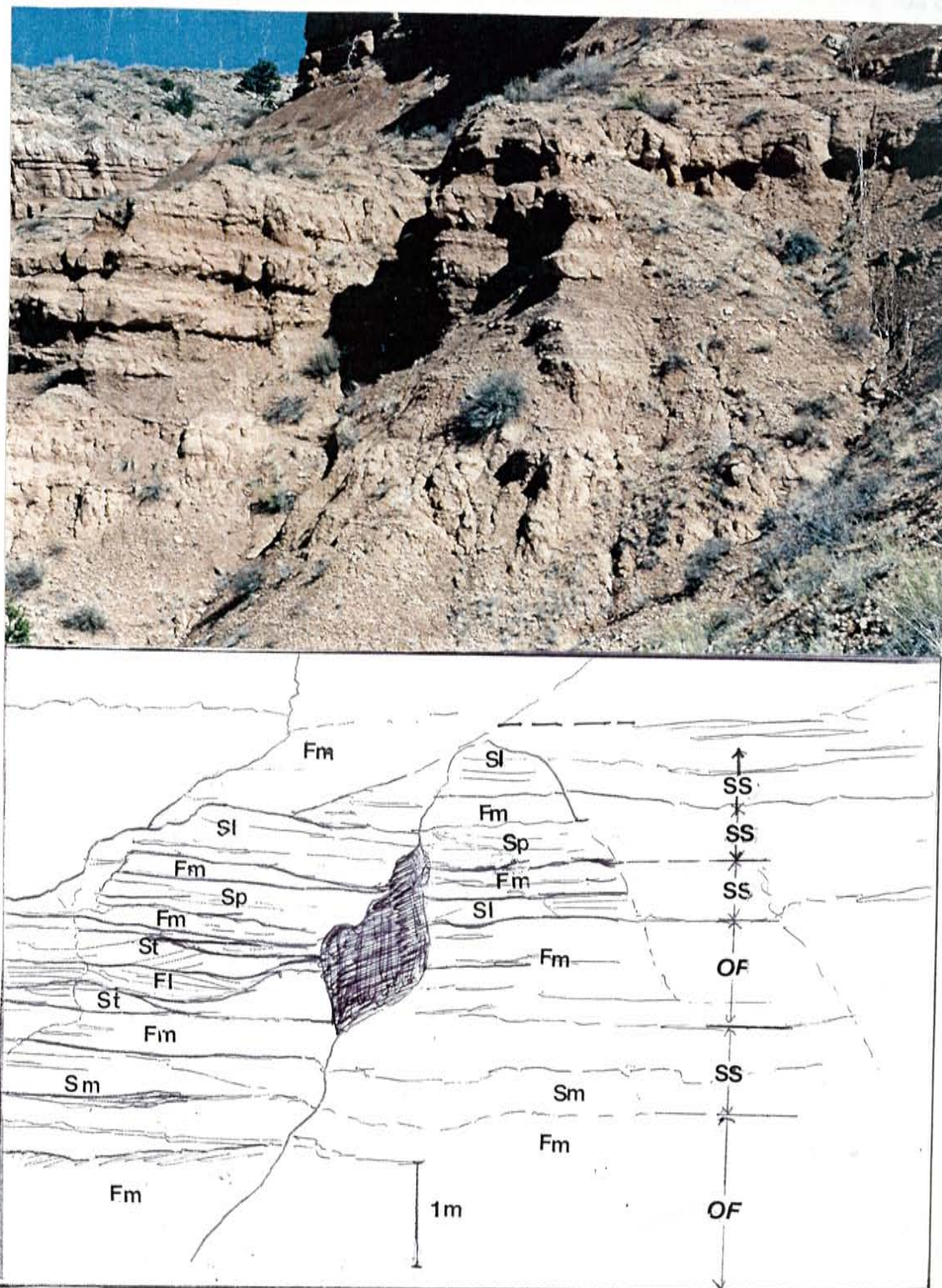
Fig. 4.2. Overbank fines (OF) and sheet sand deposits (SS) from the Canada Pillares Member. Note that the sheet sand deposits generally fine upward. The bottom figure shows bounding surfaces and associated lithofacies and facies associations.

laminated clay and silts are common at the top of this association. These sediments can be interpreted either as crevasse splay deposits, or sheet sands deposited in the distal part of an alluvial fan. When associated with channel associations they are interpreted as splay deposits. If no channels are observable along strike, then they are interpreted as alluvial fan sand sheets.

Overbank Fine Association (OF)

This association is most common in the fluvial portion of the Chamisa Mesa and Canada Pillares Members, and ranges from .2 to 6 meters thick (Fig. 4.2). It is composed primarily of dark reddish-brown finely laminated (Fsc) to massive crudely bedded clay (Fm) interbedded with grey to buff silt, silty sand and sand. Fining upwards sequences are common. Less common are finely laminated to rippled silts and muds (Fl), and silts and clays with rhizocretions and nodules (Fr).

Paleosol Association (P)

The association is divided into two sub-association classes based on primarily on primary lithologies (Davis, 1994). Paleosols developed on sand (Ps) are characterized by the lack of most sedimentary structures in the upper portion, rhizocretions, and generally weak soil zonation (Fig. 4.3). Upper contacts are commonly sharp, and lower contacts are gradational. Paleosols developed on silts and clays (Psc) are distinguished from the overbank fine association by a lack of sedimentary structures, the presence of well developed nodules, rhizocretions, blocky textures, and weak soil zonation.

Cross-stratified Eolian Dune Association (EC)

This association forms 1-3 m thick, laterally extensive (> 1 km) upper fine to lower coarse-grained tabular sand and sand bodies (Fig. 4.3). High angle (>35°) trough crossbedding (Ste) is the most common sedimentary structure. Planar laminated sand (Spe), and ripple cross-laminated sand (Sre) are present, but not common. Massive sand (Sme) is found near the tops of units, and commonly associated with rhizocretions and pedogenesis.
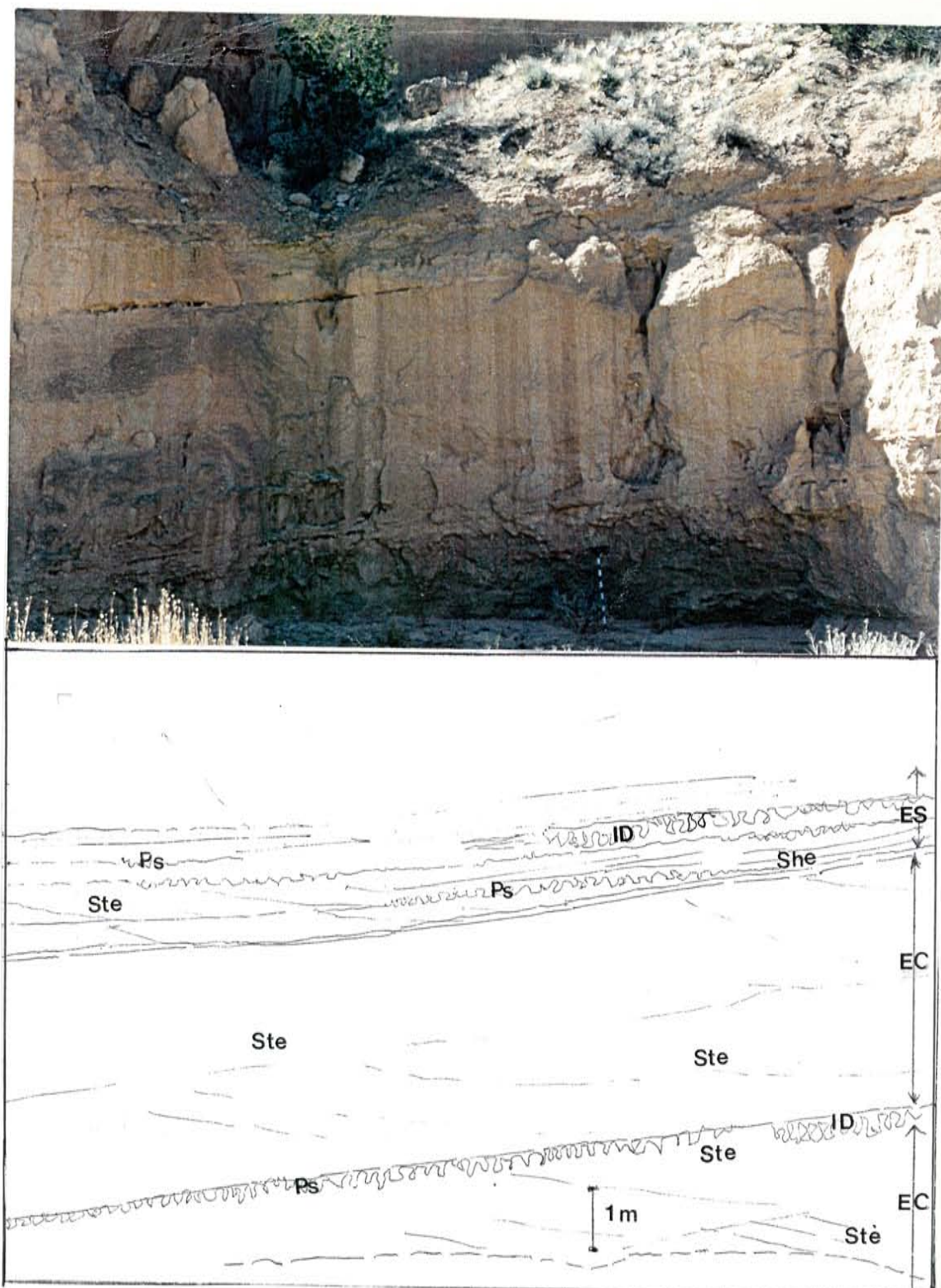
Fig. 4.3. Eolian dune (EC), and interdune (ID) associations from the Piedra Parada Member. Note the association between interdune deposits, sand sheet deposits and rhizocretions and poorly developed paleosols. The bottom figure shows bounding surfaces and associated lithofacies and facies associations.

This association is characterized by laterally extensive (> 1km), 1-2 meter thick , tabular bodies (Fig. 4.3). Grain size ranges from lower coarse to upper fine and is generally bimodal. Low angle and parallel crossbedding are the dominant sedimentary structures. Ripple cross-laminated sand (Sre) are uncommon. Rhizocretions are locally common. These deposits can be distinguished from fluvial sand sheet deposits because they are better sorted and rounded, and do not fine upwards.

Interdune Association (ID)

This facies association is characterized by thin (0.1- 0.5m thick), low angle crossbedded (Sle), or horizontal planar laminated silt, silty sand, and sand (She; Fig. 4.3). Small trough and ripple cross-laminated sand (Sre) is found locally. Rhizocretions are commonly found in interdune associations.

Playa Association(Pl)

This facies association is characterized by 0.05 to 2 m thick tabular units of greenish-grey clays. Algal tufa heads are found associated with this association in the Unnamed Member. This type of association was not analyzed in any detail for this study because it did not have a significant influence on origin of cementation in other units.

REFERENCES

Allen, J. R. L., 1986, Pedogenic calcretes in the Old Red Sandstone facies (Late Silurian-Early Carboniferous) of the Anglo-Welsh area, Southern Britain, In: Wright, V.P. (Ed.) (1986) Paleosols, their recognition and interpretation. Princeton, N.J., Princeton University Press, p. 58-86.

Atkinson, C.D., 1986, Tectonic control on alluvial sedimentation as revealed by an ancient catena of the Capella Formation (Eocene) of Northern Spain. In: Wright, V.P. (Ed.) Paleosols, their recognition and interpretation. Princeton, N.J., Princeton University Press, p. 139-179.

Chan, M. A., 1989, Erg margin of the Permian White Rim Sandstone, SE Utah. Sedimentology. v. 36, p. 235-251.

Davis, J. M., Lohmann, R. C., Phillips, F. M., Wilson, J. L., and Love, D. W., 1993, Architecture of the Sierra Ladrones Formation, central New Mexico: Depositional controls on the permeability correlation structure: Geological Society of America Bulletin, v. 105, p. 998-1007.

Kocurek, G., 1981, Significance of interdune deposits and bounding surface in aeolian dune sands. Sedimentology, v. 28, p. 753-780.

Kocurek, G., and Dott, R. H., 1981, Distinctions and used of stratification types in the interpretation of eolian sand. Journal of Sedimentary Petrology, v. 51, No. 2, p. 579-595.

Miall, A. D., 1990, Principles of Sedimentary Basin Analysis. 2nd edition, Springer-Verlag, NY, 668p..

Nadon, G. C., 1994, The genesis and recognition of anastomosed fluvial deposits: data from the St. Mary River Formation, southwestern Alberta, Canada. Journal of Sedimentary Research, v. B64, p. 451-463.

Porter, M. L., 1987, Sedimentology of an ancient erg margin: the Lower Jurassic Aztec Sandstone, southern Nevada and southern California. Sedimentology, v. 34, p. 661-680.

Retallack, G.J., 1988, Field recognition of paleosols. Geological Society of America, Special Paper 216, p. 1-20.

Retallack, G.J., 1990, Soils of the past. Unwin-Hyman, Boston.

Appendix B

Summary of Petrographic Data

Table B.1. Abundance of quartz, feldspars, and lithic fragments in the Zia Formation. Values are in volume percent .

Sample No.	Unit	Qm	Qc	Pm	Km	VRF	SRF	MRF	QFL%Q	QFL%F	QFL%L	P/F	QP/Q
72895-6	Tzu	13	0	7	3	11	2	0	36	28	36	0.68	0.02
72895-7	Tzu	13	0	9	4	3	tr.	0	44	43.	12	0.69	0.02
6595-4	Tzu	15	0	11	8	4	1	0	38	48	14	0.57	0.04
1395-1	Tzu	23	tr.	20	9	13	3	0	34	42	24	0.66	0.09
1395-2	Tzu	18	2	16	7	17	2	0	32	37	31	0.7	0.18
1395-3	Tzu	21	1	20	5	18	2	tr.	32	37	31	0.79	0.1
1395-4	Tzu	19	1	19	7	18	1	0	30	40	30	0.73	0.1
1395-5	Tzu	15	0	12	7	13	2	0	31	38	30	0.65	0.04
1395-6	Tzu	20	1	18	5	16	5	0	33	35	32.	0.78	0.14
1395-7	Tzu	20	2	20	4	11	4	0	36	39	24	0.67	0.18
1395-8	Tzu	21	1	25	5	12	3	tr.	33	45	22	0.73	0.09
1395-9	Tzu	16	tr.	19	7	18	3	1	26	39	35	0.74	0.09
1395-10	Tzu	22	0	15	2	8	3	0	44	34	22	0.67	0.01
1395-11	Tzu	19	1	15	8	12	3	0	34	40	26	0.82	0.12
122394-10	Tzu	18	tr.	19	5	12	3	0	33	42	26	0.78	0.1
122394-9	Tzu	21	tr.	20	5	11	3	0	36	42	23	0.73	0.12
122394-8	Tzu	20	tr.	22	3	16	4	0	32	38	30	0.79	0.09
122394-7	Tzu	11	tr.	9	2	3	tr.	0	44	43	12	0.83	0.05
122394-6	Tzu	20	tr.	19	5	8	2	0	38	44	17	0.73	0.06
122394-5	Tzu	12	tr.	13	2	4	2	0	38	45	17	0.67	0.14
122394-4	Tzu	15	tr.	15	2	6	2	tr.	38	42	20	0.81	0.15
122394-3	Tzu	9	tr.	8	1	4	tr.	0	41	40	19	0.63	0.06
122394-2	Tzu	6	0	7	2	4	tr.	0	31	46	23	0.70	0.05
122394-1	Tzu	13	1	14	4	11	tr.	0	32	42	26	0.75	0.11
81994-20	Tzu	14	tr.	16	3	2	1	0	39	51	10	0.75	0.08
81994-19	Tzu	16	tr.	28	5	10	1	0	32	44	23	0.80	0.09
81994-18	Tzu	9	1	18	4	21	2	tr.	18	40	42	0.84	0.23
81994-17	Tzu	3	0	4	tr.	3	4	tr.	21	32	47	0.88	0
81994-16	Tzu	0	0	0	0	0	0	0	0	0	0	0	0
81994-15	Tzu	12	tr.	15	2	7	3	tr.	32	43	25	0.82	0.1
81994-14	Tzu	15	2	16	4	18	3	0	30	34	36	0.79	0.19
81994-9	Tzu	6	tr.	7	1	5	1	0	31	39	31	0.71	0.09
81994-8	Tzu	18	tr.	20	3	13	2	0	33	41	26	0.76	0.07
81994-7	Tzu	15	tr.	16	4	15	1	0	30	37	33	0.78	0.15
81994-6	Tzu	9	0	8	2	11	1	0	29	36	36	0.62	0.15
81994-5	Tzu	12	tr.	10	2	4	1	0	42	43	15	0.58	0.02
81994-4	Tzu	13	tr.	13	3	8	3	0	34	39.	27	0.68	0.04
81994-3	Tzu	15	2	17	3	12	2	0	34	40.	27	0.75	0.12
81994-2	Tzu	6	0	7	2	2	43	0	10	15	75	0.74	0.05
81994-1	Tzu	11	tr.	13	4	3	1	0	38	50	13	0.78	0.08
8594-16	Tzu	13	tr.	6	5	6	2	0	41	34	25	0.57	0.07

Table B.1 Continued.

Sample No.	Unit	Qm	Qc	Pm	Km	VRF	SRF	MRF	QFL%Q	QFL%F	QFL%L	P/F	QP/Q
8594-15	Tzu	13	tr.	9	8	3	3	0	37	46	18	0.53	0.04
8594-14	Tzu	8	tr.	4	4	4	3	0	33	37	30	0.48	0.11
8594-13	Tzu	7	tr.	4	4	2	2	0	38	40	22	0.53	0.11
8594-12	Tzu	6	tr.	6	4	12	1	0	22	34	45	0.57	0.01
8594-11	Tzu	9	0	7	7	6	3	0	28	44	28	0.49	0.07
8394-6	Tzcp	14	1	4	5	12	2	0	40	24	36	0.46	0.17
8394-7	Tzcp	14	tr.	7	4	5	4	0	42	31	27	0.66	0.04
8594-5	Tzcp	25	tr.	10	6	9	4	0	47	30	23	0.63	0.05
8594-6	Tzcp	13	2	4	4	9	2	0	50	30	20	0.48	0.06
8594-7	Tzcp	21	tr.	6	6	10	5	0	45	25	30	0.51	0.14
8594-8	Tzcp	10	0	5	2	4	3	0	42	30	28	0.73	0.12
8594-9	Tzcp	23	1	7	6	6	3	0	51	30	19	0.54	0.03
8594-10	Tzcp	18	0	8	5	7	4	0	45	31	24	0.59	0.15
81895-1	Tzcp	2	0	tr.	tr.	tr.	0	0	53	31	16	0.5	0
81895-2	Tzcp	4	0	1	1.3	1	0	0	51	36	13	0.55	0
81895-3	Tzcp	7	tr.	3	4	2	1	0	42	39	19	0.48	0.08
8394-5	Tzc	23	3	10	10	13	4	tr.	41	32	27	0.52	0.20
8594-3	Tzc	23	1	9	5	10	3	0	48	27	25	0.63	0.14
8594-3A	Tzc	26	tr.	8	8	15	2	0	44	28	28	0.49	0.07
8594-4	Tzc	19	tr.	9	7	7	2	0	45	35	19	0.58	0.06
8594-4A	Tzc	30	1	13	10	16	2	0	43	32	25	0.55	0.08
8394-1	Tzp	18	2	9	8	20	5	tr.	34	27	39	0.52	0.21
8394-2	Tzp	13	4	11	7	15	4	0	31	34	35	0.61	0.4
8394-3	Tzp	14	3	7	6	11	3	0	38	29	33	0.52	0.21
8394-4	Tzp	15	3	8	8	24	3	0	29	26	45	0.52	0.30
8594-1	Tzp	22	7	7	5	19	7	tr.	42	19	39	0.58	0.38
8594-1A	Tzp	23	tr.	13	7	17	4	tr.	37	31	32	0.66	0.09
8594-1B	Tzp	29	tr.	7	5	14	3	tr.	51	20	29	0.58	0.07
8594-2	Tzp	23	1	11	6	15	5	tr.	40	28	32	0.64	0.13

Abbreviations and notes: Qm = monocrystalline quartz, Qc = polycrystalline quartz (not including chert), Pm = monocrystalline plagioclase, Km = monocrystalline potassium feldspars, VRF = total volcanic rock fragments, SRF = total sedimentary rock fragments, MRF = total metamorphic rock fragment, QFL%Q = total quartz, QFL%F = total feldspars, QFL%L = total lithic rock fragments (including chert), P/F = ratio of plagioclase feldspar to total feldspar, Qp/Q = ratio of polycrystalline quartz (not including chert) to total quartz, tr. = less than 1%.

Table B.2. Abundance and types of lithic fragments, phyllosilicates, opaque grains, and heavy minerals in sandstones in the Zia Formation.

Sample No.	Unit	Bi	MSC	CHL	VRF	CHT	Argil	Ss/slt	CRF	MRF	OPQ	HM	%Lv	%Ls	%Lm
72895-6	Tzu	tr.	tr.	0	11	tr.	3	0	tr.	0	7	tr.	77	23	0
72895-7	Tzu	0	tr.	0	3	tr.	0	0	tr.	tr.	3	tr.	76	23	0
6595-5	Tzu	tr.	tr.	0	4	tr.	tr.	tr.	tr.	0	1	0	77	23	0
1395-1	Tzu	tr.	0	0	13	2	0	1	tr.	0	1	0	82	18	0
1395-2	Tzu	0	0	0	17	2	0	tr.	tr.	0	tr.	0	89	11	0
1395-3	Tzu	0	0	0	19	1	0	tr.	tr.	0	1	0	88	10	1
1395-4	Tzu	1	0	0	18	1	0	0	tr.	tr.	1	0	88	10	1
1395-5	Tzu	tr.	0	tr.	13	tr.	tr.	tr.	tr.	0	tr.	0	93	7	0
1395-6	Tzu	0	0	0	16	2	tr.	2	tr.	0	2	0	88	12	0
1395-7	Tzu	tr.	0	0	11	2	tr.	tr.	tr.	0	tr.	0	76	24	0
1395-8	Tzu	0	0	0	12	1	0	tr.	1	tr.	0	0	76	24	0
1395-9	Tzu	0	0	0	18	1	0	1	0	1	tr.	0	81	17	2
1395-10	Tzu	tr.	tr.	0	8	tr.	tr.	2	0	0	4	tr.	82	12	6
1395-11	Tzu	0	tr.	0	12	2	tr.	tr.	tr.	0	1	0	74	26	0
122394-10	Tzu	tr.	tr.	tr.	12	1	0	1	tr.	0	tr.	tr.	80	20	0
122394-9	Tzu	tr.	0	0	11	3	0	0	tr.	0	tr.	tr.	80	20	0
122394-8	Tzu	tr.	0	0	16	2	0	2	1	0	tr.	tr.	77	23	0
122394-7	Tzu	tr.	0	0	3	tr.	0	0	tr.	0	0	0	79	21	0
122394-6	Tzu	1	0	0	8	tr.	tr.	1	0	0	2	1	81	19	0
122394-5	Tzu	tr.	0	0	4	1	0	0	0	0	0	tr.	81	19	0
122394-4	Tzu	tr.	0	0	6	2	0	0	0	tr.	tr.	0	76	24	0
122394-3	Tzu	tr.	0	0	4	tr.	0	0	0	0	0	0	68	28	4
122394-2	Tzu	tr.	0	0	11	tr.	0	tr.	0	0	0	0	93	7	0
122394-1	Tzu	tr.	0	0	2	1	0	0	tr.	0	tr.	0	93	7	0
81994-20	Tzu	0	0	0	10	1	0	tr.	0	tr.	1	tr.	95	5	0
81994-19	Tzu	0	0	0	21	1	0	tr.	tr.	tr.	tr.	0	64	36	0
81994-18	Tzu	1	0	0	3	tr.	0	0	1	0	0	tr.	86	9	5
81994-17	Tzu	0	0	0	11	0	0	0	0	0	0	0	90	8	1
81994-16	Tzu	0	0	0	7	1	0	1	tr.	tr.	6	tr.	72	28	0
81994-15	Tzu	0	0	0	18	1	0	2	tr.	0	tr.	0	0	0	0
81994-14	Tzu	0	0	0	5	tr.	1	0	tr.	0	0	0	71	26	3
81994-9	Tzu	tr.	tr.	0	13	tr.	tr.	0	tr.	0	1	0	85	15	0
81994-8	Tzu	tr.	tr.	tr.	15	2	tr.	0	tr.	0	2	0	79	21	0
81994-7	Tzu	tr.	0	0	11	1	0	tr.	tr.	0	1	0	91	9	0
81994-6	Tzu	tr.	0	0	4	tr.	tr.	tr.	0	0	tr.	tr.	83	17	0
81994-5	Tzu	tr.	0	0	8	tr.	1	0	tr.	0	0	0	89	11	0
81994-4	Tzu	tr.	0	0	12	0	2	0	tr.	0	0	0	80	20	0
81994-3	Tzu	tr.	0	0	2	tr.	tr.	0	42	0	0	0	76	24	0
81994-2	Tzu	tr.	0	0	3	tr.	1	0	0	0	0	0	88	12	0
81994-1	Tzu	tr.	0	0	6	tr.	0	0	1	0	2	0	5	95	0
8594-16	Tzu	0	0	0	6	tr.	0	0	1	0	2	0	68	33	0

Table B.2. Continued.

Sample No.	Unit	BI	MSC	CHL	VRF	CHT	Argil	Ss/sltn	CRF	MRF	OPQ	HM	%Lv	%Ls	%Lm
8594-15	Tzu	0	0	0	3	tr.	0	tr.	2	0	1	0	48	52	0
8594-14	Tzu	tr.	0	0	4	tr.	0	0	2	0	tr.	0	60	40	0
8594-13	Tzu	0	0	0	2	tr.	0	0	2	0	0	0	49	51	0
8594-12	Tzu	0	0	0	12	tr.	tr.	0	tr.	0	0	0	93	7	0
8594-11	Tzu	tr.	tr.	tr.	6	tr.	2	0	tr.	0	tr.	1	67	33	0
8394-6	Tzcp	tr.	tr.	0	12	2	2	tr.	1	0	2	tr.	83	17	0
8394-7	Tzcp	tr.	tr.	tr.	5	tr.	tr.	1	1	0	2	1	58	42	0
8594-5	Tzcp	tr.	0	0	9	1	tr.	tr.	2	0	3	1	71	29	0
8594-6	Tzcp	tr.	0	0	4	tr.	1	tr.	tr.	0	tr	0	70	30	0
8594-7	Tzcp	tr	0	tr.	10	1	3	tr.	tr.	0	1	tr.	65	35	0
8594-8	Tzcp	tr.	0	tr.	4	1	tr.	tr.	0	0	1	tr.	63	37	0
8594-9	Tzcp	tr.	0	tr.	6	tr.	0	2	tr.	0	tr.	0	71	29	0
8594-10	Tzcp	0	0	0	7	2	tr.	tr.	tr.	0	1	0	63	37	0
81895-1	Tzcp	0	0	0	tr.	0	0	0	tr.	0	0	0	95	5	0
81895-2	Tzcp	tr.	0	0	1	0	0	0	tr.	0	tr.	0	97	3	0
81895-3	Tzcp	0	0	0	2	tr.	0	1	tr.	0	2	0	60	40	0
8394-5	Tzc	tr.	tr.	0	13	3	0	tr.	tr.	tr.	tr.	tr.	78	22	0
8594-3	Tzc	tr.	0	0	10	2	tr.	0	tr.	0	tr.	tr.	80	20	0
8594-3A	Tzc	tr.	tr.	0	15	1	0	tr.	tr.	0	2	tr.	89	11	0
8594-4	Tzc	tr.	tr.	0	7	tr.	tr.	tr.	tr.	0	2	1	76	24	0
8594-4A	Tzc	tr.	0	0	16	2	0	tr.	tr.	0	3	tr.	88	12	0
8394-1	Tzp	0	0	0	20	3	tr.	1	tr.	tr.	tr.	tr.	80	19	1
8394-2	Tzp	tr.	0	0	15	4	tr.	tr.	tr.	0	tr.	0	77	23	0
8394-3	Tzp	tr.	0	0	11	1	tr.	tr.	2	0	tr.	tr.	77	23	0
8394-4	Tzp	0	0	0	24	3	0	tr.	0	0	tr.	tr.	88	12	0
8594-1	Tzp	tr.	0	0	19	7	0	tr.	0	tr.	tr.	tr.	73	27	0
8594-1A	Tzp	tr.	0	0	16	2	tr.	tr.	tr.	tr.	2	tr.	85	15	0
8594-1B	Tzp	tr.	0	0	14	2	tr.	tr.	tr.	tr.	5	tr.	83	16	0
8594-2	Tzp	tr.	0	0	15	2	0	2	1	0	tr.	1	76	24	0

Abbreviations and notes: BI = biotite, MSC = muscovite, CHL = chlorite, VRF = volcanic rock fragments, CHT = chert, Argil = argillaceous rock fragments, Ss/sltn = sandstone/siltstone rock fragments, CRF = carbonate rock fragments, MRF = metamorphic rock fragments, OPQ = opaque grains, HM = heavy minerals, %Lv = total volcanic rock fragments, % Ls = total sedimentary rock fragments, % Lm = total metamorphic rock fragments, tr. = less than 1%.

Table B.3. Abundance of non-framework components (matrix and cement) and porosity in Zia samples. Values are in volume percent of whole rock.

Sample No.	Unit	Clay	Zeolite	Opaque	Spar	Micrite	Micrite/ Sparite	Total Calcite
72895-6	Tzu	0	0	2	54	6	0.1	60
72895-7	Tzu	tr.	0	2	11	52	5.0	64
6595-4	Tzu	0	0	2	38	15	0	53
1395-1	Tzu	0	tr	0	23	0	0	29
1395-2	Tzu	4	tr	0	25	0	0	25
1395-3	Tzu	0	0	0	26	12	0.5	38
1395-4	Tzu	tr	0	tr	26	12	0.5	38
1395-5	Tzu	0	0	0	26	22	0.8	48
1395-6	Tzu	0	0	3	31	0	0	31
1395-7	Tzu	7	0	3	37	0	0	27
1395-8	Tzu	tr.	0	0	30	tr.	0	30
1395-9	Tzu	0	tr.	0	32	tr.	0	32
1395-10	Tzu	16	0	0	7	6	1.0	13
1395-11	Tzu	27	0	0	4	tr.	0	4
122394-10	Tzu	0	0	0	37	0	0	37
122394-9	Tzu	2	0	0	35	0	0	35
122394-8	Tzu	1	0	0	29	0	0	29
122394-7	Tzu	5	0	3	31	34	1.1	65
122394-6	Tzu	2	0	tr.	30	2	0.1	32
122394-5	Tzu	0	0	0	60	5	0.1	65
122394-4	Tzu	0	0	0	25	29	1.2	54
122394-3	Tzu	0	0	tr.	27	33	1.2	60
122394-2	Tzu	0	0	tr.	57	14	0.2	71
122394-1	Tzu	0	0	tr.	28	28	1.0	55
81994-20	Tzu	11	0	3	38	11	0.3	49
81994-19	Tzu	0	0	0	20	15	0.8	35
81994-18	Tzu	0	0	0	27	0	0	27
81994-17	Tzu	0	0	0	22	22	1.0	43
81994-16	Tzu	tr.	0	tr.	46	46	1.0	92
81994-15	Tzu	0	0	0	37	7	0.2	46
81994-14	Tzu	0	0	0	25	13	0.5	38
81994-9	Tzu	0	0	8	56	14	0.3	70
81994-8	Tzu	0	0	0	41	2	0.1	43
81994-7	Tzu	0	0	tr.	29	8	0.3	38
81994-6	Tzu	2	0	5	31	12	0.4	43
81994-5	Tzu	5	0	5	25	25	1.0	49
81994-4	Tzu	0	0	0	22	21	1.0	43
81994-3	Tzu	0	0	0	26	16	0.6	42
81994-2	Tzu	1	0	4	24	37	1.5	61
81994-1	Tzu	1	0	5	9	32	3.5	41
8594-16	Tzu	27	0	0	30	0	0	30
8594-15	Tzu	10	0	0	36	0	0	36
8594-14	Tzu	0	0	tr.	38	21	0.6	59
8594-13	Tzu	0	0	tr.	37	32	0.9	69
8594-12	Tzu	0	0	2	24	34	1.4	58

Table B.3. Continued.

Sample No.	Unit	Clay	Zeolite	Opaque	Spar	Micrite	Micrite/ Spar	Total Calcite
8594-11	Tzu	3	0	0	33	37	1.1	69
8394-6	Tzcp	0	0	0	25	29	1.2	55
8394-7	Tzcp	6	0	3	31	5	0.2	35
8594-5	Tzcp	tr.	0	5	24	5	0.2	29
8594-6	Tzcp	8	0	2	29	28	1.0	57
8594-7	Tzcp	0	0	1	34	11	0.3	45
8594-8	Tzcp	0	0	4	59	3	0.1	62
8594-9	Tzcp	10	0	0	22	16	0.7	38
8594-10	Tzcp	14	0	10	12	26	2.2	38
81895-1	Tzcp	27	0	tr.	15	54	3.5	69
81895-2	Tzcp	17	0	0	6	65	10.4	72
81895-3	Tzcp	36	0	0	9	37	4.3	46
8394-5	Tzc	0	0	5	24	5	0.2	31
8594-3	Tzc	5	0	5	17	12	0.7	29
8594-3A	Tzc	2	0	3	9	12	1.3	21
8594-4	Tzc	7	0	5	20	6	0.3	26
8594-4A	Tzc	2	tr.	0	11	0	0	11
8394-1	Tzp	0	tr.	0	22	0	0	22
8394-2	Tzp	0	0	0	34	0	0	34
8394-3	Tzp	0	0	8	44	0	0	44
8394-4	Tzp	0	0	0	30	1	0.1	31
8594-1	Tzp	0	0	tr.	25	0	0	25
8594-1A	Tzp	50	0	tr.	15	0	0	15
8594-1B	Tzp	2	0	3	17	0	0	17
8594-2	Tzp	0	1	1	25	0	0	25

Abbreviations and notes: Clay = detrital and /or mechanically infiltrated clay,   Spar texures drusy to poikilotopic. Calcite grains less than 4 μ are classified as micrite. tr = less than 1%.

Table B.4. Estimated mean grain size, sorting, and roundness for sandstones in the Zia Formation.

Sample No.	Unit	Grain Size Class	Grain Size (mm)	Sorting	Roundness
72895-6	Tzu	Fine	0.2	Low Moderate	Subrounded
72895-7	Tzu	Lower Fine	0.14	Upper Poor	Subangular
6595-4	Tzu	Lower Medium	0.26	Low Moderate	Subrounded
1395-1	Tzu	Lower Coarse	0.6	Low Well	Subrounded
1395-2	Tzu	Lower Coarse	0.6	Well	Subrounded
1395-3	Tzu	Upper Medium	0.35	Low Moderate	Subrounded
1395-4	Tzu	Upper Fine	0.24	Well	Subrounded
1395-5	Tzu	Fine	0.18	Poor	Subangular
1395-6	Tzu	Lower Coarse	0.6	Low Moderate	Rounded
1395-7	Tzu	Lower Medium	0.25	Upper Mod.	Subrounded
1395-8	Tzu	Medium	0.35	Low Well	Rounded
1395-9	Tzu	Lower Coarse	0.55	Upper Mod.	Rounded
1395-10	Tzu	Very Fine	0.08	Poor	Subrounded
1395-11	Tzu	Upper Medium/Low Coarse	0.45	Poor	Subangular
122394-10	Tzu	Upper Medium	0.34	Well	Rounded
122394-9	Tzu	Lower Medium	0.29	Low Well	Subrounded
122394-8	Tzu	Upper Medium	0.42	Moderate	Subrounded
122394-7	Tzu	Lower Very Fine	0.07	Low Mod.	Angular
122394-6	Tzu	Lower Medium	0.27	Poor	Subrounded
122394-5	Tzu	Upper Fine/Lower Medium	0.18	Poor	Subangular
122394-4	Tzu	Upper Fine/Lower Medium	0.2	Upper Poor	Subangular
122394-3	Tzu	Lower Medium	0.27	Upper Poor	Subangular
122394-2	Tzu	Upper Fine	0.2	Upper Poor	Subangular
122394-1	Tzu	Upper Fine	0.26	Low Moderate	Subrounded
81994-20	Tzu	Lower Medium	0.27	Upper Poor	Subrounded
81994-19	Tzu	Medium	0.35	Low Moderate	Subrounded
81994-18	Tzu	Upper Medium/Low Coarse	0.48	Low Moderate	Subrounded
81994-17	Tzu	Fine	0.22	Low Moderate	Subrounded
81994-16	Tzu	No clastic grains			
81994-15	Tzu	Upper Fine/Lower Medium	0.26	Moderate	Subrounded
81994-14	Tzu	Lower Medium	0.3	Low Moderate	Subrounded
81994-9	Tzu	Lower Fine	0.14	Upper Poor	Subrounded
81994-8	Tzu	Upper Fine	0.22	Moderate	Subrounded
81994-7	Tzu	Medium	0.35	Low Moderate	Subangular
81994-6	Tzu	Upper Medium	0.45	Low Moderate	Subrounded
81994-5	Tzu	Lower Fine	0.13	Very Poor	Subangular
81994-4	Tzu	Upper Medium	0.18	Low Moderate	Subrounded
81994-3	Tzu	Upper Medium	0.45	Upper Poor	Subrounded
81994-2	Tzu	Very Fine	0.1	Low Moderate	Subrounded
81994-1	Tzu	Very Fine	0.12	Low Moderate	Subrounded
8594-16	Tzu	Fine	0.16	Low Moderate	Subrounded
8594-15	Tzu	Upper Fine	0.2	Low Moderate	Subangular
8594-14	Tzu	Lower Medium	0.26	Low Moderate	Subrounded
8594-13	Tzu	Upper Fine/Lower Medium	0.2	Upper Poor	Subrounded
8594-12	Tzu	Very Fine	0.09	Moderate	Subrounded

Table B.4 Continued.

Sample No.	Unit	Grain Size Class	Grain Size (mm)	Sorting	Roundness
8594-11	Tzu	Very Fine	0.075	Upper Poor	Subrounded
8394-6	Tzcp	Lower Medium	0.3	Low Moderate	Subangular
8394-7	Tzcp	Upper Very Fine	0.12	Upper Poor	Subangular
8594-5	Tzcp	Low Medium	0.35	Poor	Subangular
8594-6	Tzcp	Very Fine	0.08	Low Moderate	Subangular
8594-7	Tzcp	Low Medium	0.3	Low Moderate	Subangular
8594-8	Tzcp	Low Very Fine	0.075	Low Moderate	Subangular
8594-9	Tzcp	Upper Very Fine	0.12	Upper Poor	Subangular
8594-10	Tzcp	Low Medium	0.35	Upper Poor	Subangular
81895-1	Tzcp	Lower Fine	0.15	Low Moderate	Subrounded
81895-2	Tzcp	Fine	0.17	Upper Poor	Subrounded
81895-3	Tzcp	Very Fine	0.12	Upper Poor	Subrounded
8394-5	Tzc	Upper Fine/Medium	0.35	Low Moderate	Rounded
8594-3	Tzc	Low Medium	0.27	Low Moderate	Subrounded
8594-3A	Tzc	Low Medium	0.3	Low Moderate	Rounded
8594-4	Tzc	Upper Fine	0.22	Poor	Subangular
8594-4A	Tzc	Fine	0.2	Low Moderate	Subrounded
8394-1	Tzp	Upper Medium/Lower Coarse	0.55	Low Moderate	Rounded
8394-2	Tzp	Upper Medium	0.48	Well	Rounded
8394-3	Tzp	Medium	0.35	Moderate Well	Subrounded
8394-4	Tzp	Upper Medium/Low Coarse	0.6	Upper Mod.	Rounded
8594-1	Tzp	Upper Medium /Low Coarse	0.9	Moderate Well	Rounded
8594-1A	Tzp	Upper Medium /Low Coarse	0.75	Moderate	Subrounded
8594-1B	Tzp	Upper Medium /Low Coarse	0.7	Moderate	Subrounded
8594-2	Tzp	Low Medium	0.35	Low Moderate	Subangular

Table B.5. Abundance of porosity types as a percentage whole rock, in sandstones in the Zia Formation.

Sample No.	Unit	Macroporosity			Microporsity			Total Micro-porosity	Total Macro-porosity	Total Porosity
		In-Frac	In-Cem	Intra	Clay	Grain	Cement			
72895-6	Tzu	0	tr.	0	0	0	0	0.00	tr.	tr.
72895-7	Tzu	0	tr.	1	0	tr.	0	tr.	1	1
6595-4	Tzu	0	tr.	tr.	0	tr.	0	tr.	tr.	tr.
1395-1	Tzu	0	6	tr.	0	tr.	0	tr.	6	6
1395-2	Tzu	0	7	tr.	0	tr.	0	tr.	7	7
1395-3	Tzu	1	tr.	1	0	tr.	0	tr.	3	3
1395-4	Tzu	0	2	2	0	tr.	tr.	tr.	4	5
1395-5	Tzu	0	tr.	tr.	0	tr.	tr.	tr.	tr.	1
1395-6	Tzu	0	2	tr.	0	tr.	tr.	tr.	3	3
1395-7	Tzu	0	0	tr.	0	tr.	0	tr.	tr.	tr.
1395-8	Tzu	0	0	0	0	0	0	0	0	0
1395-9	Tzu	0	3	0	0	0	0	0	3	3
1395-10	Tzu	0	10	2	2	tr.	2	5	12	17
1395-11	Tzu	0	10	2	tr.	tr.	0	1	12	13
122394-10	Tzu	5	0	tr.	0	0	0	0	5	5
122394-9	Tzu	0	0	tr.	tr.	tr.	0	tr.	tr.	tr.
122394-8	Tzu	0	3	0	tr.	0	0	0	3	3
122394-7	Tzu	0	0	1	0	tr.	0	tr.	1	1
122394-6	Tzu	0	5	tr.	tr.	tr.	0	tr.	5	6
122394-5	Tzu	0	6	tr.	0	tr.	0	tr.	6	6
122394-4	Tzu	0	2	1	0	tr.	tr.	1	3	4
122394-3	Tzu	0	3	2	0	tr.	1	2	5	7
122394-2	Tzu	0	4	4	0	tr.	1	2	7	9
122394-1	Tzu	0	tr.	tr.	0	tr.	tr.	tr.	1	2
81994-20	Tzu	0	tr.	0	0	0	1	1	tr.	1
81994-19	Tzu	0	14	tr.	0	0	1	1	14	15
81994-18	Tzu	0	11	tr.	0	tr.	6	6	11	17
81994-17	Tzu	0	1	32	0	3	2	5	13	37
81994-16	Tzu	0	7	0	0	0	0	0	7	7
81994-15	Tzu	0	3	tr.	0	tr.	9	9	4	13
81994-14	Tzu	0	3	1	0	tr.	0	tr.	4	4
81994-9	Tzu	0	tr.	0	0	0	0	0	tr	tr.
81994-8	Tzu	0	0	0	0	0	0	0	0	0
81994-7	Tzu	0	1	2	0	tr.	2	2	3	5
81994-6	Tzu	3	2	1	0	1	0	1	6	7
81994-5	Tzu	0	4	7	0	1	1	2	11	13
81994-4	Tzu	0	4	3	0	tr.	10	11	7	18
81994-3	Tzu	0	tr.	2	0	tr.	2	1	2	4
81994-2	Tzu	0	2	14	tr.	tr.	11	11	5	27
81994-1	Tzu	0	7	2	tr.	tr.	7	8	9	17
8594-16	Tzu	0	3	tr.	0	tr.	3	3	4	7
8594-15	Tzu	0	7	2	0	tr.	2	2	8	10
8594-14	Tzu	0	4	1	0	tr.	11	11	6	17
8594-13	Tzu	0	10	2	0	tr.	5	6	12	17
8594-12	Tzu	0	14	5	tr.	3	5	8	19	27

Table B.5. Continued.

Sample No.	Unit	Macroporosity			Microporsity			Total Micro-porosity	Total Macro-porosity	Total Porosity
		In-Frac	In-Cem	Intra	Clay	Grain	Cement			
8594-11	Tzu	0	10	2	tr.	tr.	6	6	13	19
8394-6	Tzcp	0	1	3	0	tr.	0	tr.	4	5
8394-7	Tzcp	0	11	4	0	2	0	2	16	17
8594-5	Tzcp	0	6	2	0	tr.	2	2	8	10
8594-6	Tzcp	0	1	2	0	tr.	tr.	1	3	4
8594-7	Tzcp	0	tr.	2	0	tr.	tr.	1	3	4
8594-8	Tzcp	0	tr.	4	0	1	tr.	1	5	6
8594-9	Tzcp	0	3	3	0	tr.	1	2	7	9
8594-10	Tzcp	0	2	2	tr.	tr.	tr.	1	4	5
81895-1	Tzcp	0	tr.	0	0	0	1	1	tr.	2
81895-2	Tzcp	0	tr.	1	tr.	tr.	tr.	1	1	3
81895-3	Tzcp	0	tr.	0	tr.	0	tr.	tr.	tr.	1
8394-5	Tzc	5	0	2	0	tr.	0	1	7	8
8594-3	Tzc	0	4	tr.	0	tr.	2	2	4	6
8594-3A	Tzc	0	9	2	0	tr.	0	tr.	11	11
8594-4	Tzc	0	5	2	0	tr.	4	4	7	11
8594-4A	Tzc	0	12	3	0	1	0	1	14	15
8394-1	Tzp	8	0	3	0	tr.	0	tr.	11	11
8394-2	Tzp	8	1	1	0	tr.	0	tr.	10	11
8394-3	Tzp	0	tr.	2	0	tr.	0	tr.	3	3
8394-4	Tzp	0	5	1	0	tr.	0	tr.	6	6
8594-1	Tzp	0	5	2	0	tr.	0	tr.	5	7
8594-1A	Tzp	0	17	2	tr.	2	0	2	19	20
8594-1B	Tzp	0	11	2	tr.	1	0	2	13	15
8594-2	Tzp	0	8	2	0	tr.	0	tr.	10	11

Abbreviarions and notes: In-Frac = Intergranular pore - circumgranular fracture, In-Cem = Intergranular -Intracement pore, Intra = Intragranular pore, tr. = less than 1%.

Appendix C

Paleocurrent and Orientation Data

Table C.1. Piedra Parada Member paleocurrent data, Canada Pillares type area, Canada Pillares, King Ranch. Data mostly from Gawne (1973). Data from this study indicated by *.

Dip Direction	Dip Angle		Dip Direction	Dip Angle
30	30		350	64
30	34		325	55
28	47		174	44
16	40		125	47
8	41		123	38
356	51		118	36
353	47		117	46
344	30		104	48
338	26		96	44
220	32		94	38
174	28		92	32
28	28		88	48
0	20		86	43
158	22		85	46
82	24		85	35
10	14		78	37
9	20		72	48
18	20		68	34
18	25		*64	50
196	18		*60	38
230	24		*48	52
310	16		* 32	48
110	12		*133	24
150	8		*142	18
150	6		*179	39
160	10		*170	39
113	27		*170	39
114	32		*155	36
102	24		*156	41
70	22		*155	26
162	20		*158	30
114	32		*175	43
118	26		*175	43
2.0	54		*153	31
108	55		* 1	54
105	60		*181	23
103	50		*90	10
100	59		*179	4
98	59		* 20	82
88	54		*158	50
82	52		*135	58
80	68		*130	58
38	72		*119	50
1	54		*114	60
3	55			

Statistical Data

N=88	Vector Mean = 96.5
Class Interval = 10 degrees	Conf. Angle = 15.70
Maximum Percentage = 10.2	Mean Vector Length = 0.501
Mean Percentage = 3.85	Rayleigh = 0.0

Table C.2. Piedra Parada Member orientation data, Canada Pillares type area, Canada Pillares, King Ranch.

Dip Direction	Dip Angle		Dip Direction	Dip Angle
29	3		33	0
24	3		33	0
24	3		28	1
32	2		28	1
29	3		28	1
29	3		28	1
23	2			
Statistical Data				
N=13 Class Interval = 10 degrees Maximum Percentage = 76.9 Mean Percentage = 50.0			Vector Mean = 28.3 Conf. Angle = 4.41 Mean Vector Length = 0.986 Rayleigh = 0.0	

Table C.3. Chamisa Mesa Member paleocurrent data, Canada Pillares type area, Canada Pillares, King Ranch. Data mostly from Gawne (1973). Data from this study indicated by *.

Dip Direction	Dip Angle		Dip Direction	Dip Angle
*118	8		92	48
*118	0		90	73
*114	40		86	54
*114	30		84	58
142	46		83	47
136	32		83	42
132	12		80	54
122	39		74	54
114	48		70	34
112	53		52	30
111	30		50	33
104	70		44	56
104	48		38	52
100	36		38	66
98	62		28	42
96	62		208	60
69	56		296	12
92	70		336	20
92	54		324	10
*99	11		*100	21
*101	27		*298	8
*100	21		*118	0
*113	15		*140	31
Statistical Data				
N=46 Class Interval = 10 degrees Maximum Percentage = 18.4 Mean Percentage = 5.88			Vector Mean = 88.6 Conf. Angle = 14.37 R. Magnitude = 0.725 Rayleigh = 0.0	

Table C.4. Chamisa Mesa Member orientation data, Canada Pillares type area, King Ranch.

Dip Direction	Dip Angle		Dip Direction	Dip Angle
9	5		28	1
9	5		28	1
14	5		33	0
24	3		33	0
24	3		33	0
9	5		33	0
Statistical Data				
N=12 Class Interval = 10 degrees Maximum Percentage = 36.4 Mean Percentage = 20.00			Vector Mean =19.5 Conf. Angle = 15.52 Mean Vector Length= 0.897 Rayleigh = 0.0	

Table C.5. Canada Pillares Member paleocurrent data, Canada Pillares type area, King Ranch. Data partly from Gawne (1973). Data from this study indicated by *.

Dip Direction	Dip Angle		Dip Direction	Dip Angle
*10	25		*135	18
*15	30		*125	15
*8	30		*215	10
*140	20		*220	30
*208	65		*65	20
*45	10		136	30
198	52		66	22
130	10		58	66
136	30		198	32
Statistical Data				
N=18 Class Interval = 10 degrees Maximum Percentage = 22.2 Mean Percentage = 8.33			Vector Mean = 120.3 Conf. Angle = 47.09 Mean Vector Length= 0.384 Rayleigh = 0.0703	

Table C.6. Canada Pillares Member concretion orientation data, Canada Pillares type area, King Ranch.

Dip Direction	Dip Angle		Dip Direction	Dip Angle
160	2		158	2
158	0		158	0
148	1		177	4
172	4		158	2
148	1		167	3
Statistical Data				
N=10 Class Interval = 10 degrees Maximum Percentage = 600 Mean Percentage = 33.3			Vector Mean = 161.2 Conf. Angle = 5.05 Mean Vector Length= 0.985 Rayleigh = 0.0	

Table C.7. Lower Unnamed Member, paleocurrent data from eolian facies, Canada Pillares type area, Canada Pillares, King Ranch. All data from this study.

Dip Direction	Dip Angle		Dip Direction	Dip Angle
91	24		90	4
93	39		124	2
146	43		119	2
155	43		114	2
188	9		101	23
340	17		106	23
345	17		147	38
350	18		156	38
329	18		187	11
110	13		94	44
110	3		92	30
190	33		110	13
129	2		109	8
93	34		109	3
102	33		139	7
99	3		133	8
Statistical Data				
N=32 Class Interval = 10 degrees Maximum Percentage = 25.0 Mean Percentage = 7.69			Vector Mean = 113.0 Conf. Angle = 17.04 Mean Vector Length= 0.695 Rayleigh = 0.0	

Table C.8. Lower Unnamed Member orientation data, Canada Pillares type area, Canada Pillares, King Ranch.

Dip Direction	Dip Angle		Dip Direction	Dip Angle
26	1		17	3
26	1		7	5
20	1		7	5
17	3		7	5
17	3		21	2
17	3		12	4
Statistical Data				
N=12 Class Interval = 10 degrees Maximum Percentage = 50.0 Mean Percentage = 33.33			Vector Mean = 16.8 Conf. Angle = 8.01 Mean Vector Length = 0.969 Rayleigh = 0.0	

Table C.9. Upper Unnamed Member paleocurrent data, Canada Pillares type area, Canada Pillares, King Ranch. All data from this study.

Dip Direction	Dip Angle		Dip Direction	Dip Angle
357	18		169	3
336	21		169	3
110	10		164	3
110	11		164.	3
166	43		166	3
161	14		336	21
71	28		336	21
78	57		118	21
119	15		159	2
109	7		150	7
174	2		356	23

Statistical Data

N=22
Class Interval = 10 degrees
Maximum Percentage = 31.8
Mean Percentage = 11.11

Vector Mean = 128.4
Conf. Angle = 34.75
Mean Vector Length = 0.457
Rayleigh = 0.01

Table C.10. Upper Unnamed Member orientation data, Canada Pillares type area, Canada Pillares, King Ranch.

Dip Direction	Dip Angle		Dip Direction	Dip Angle
158	2		167	4
167	4		167	4
158	2		163	3
167	4		164	3
167	4		161	3
172	4		163	3
158	2		163	3
163	3		158	2
158	2		163	3
158	2		163	3
158	2		168	4
158	2		163	3
163	3		168	4
158	2		177	5
167	4		163	3
158	2		163	3
163	3		167	4
163	3		163	3
163	3		167	4
168	4		167	4
163	3		177	5
177	5		177	5
158	2		163	3
167	4		167	4
172	4		167	4
163	3		164	3
			163	3

Statistical Data

N=54
Class Interval = 10 degrees
Maximum Percentage = 66.7
Mean Percentage = 33.33

Vector Mean = 164.1
Conf. Angle = 3.07
Mean Vector Length= 0.982
Rayleigh = 0.0

Appendix D: Definitions of Terms Used In Text

Alveolar: Originally used to describe pits or small cavities in invertebrates, or tooth sockets in vertebrates (Bates and Jackson, 1984). Use by the soil literature to describe cylindrical irregular pores, separated by a network of anastomosing micrite walls, that may or may not be filled with calcite cement (Esteban and Klappa, 1983). Pore diameters typically range from 100 to 500 microns, but can be as large as 1.5 mm. This texture is interpreted as the result of discrete channelways caused by roots in sediment (Esteban and Klappa, 1983). These textures are typically associated with rhizocretions.

Alveolar-septal: A microtexture consisting of arcuate septa up to a few hundred microns long and up to 200 microns wide, within pore spaces such as root molds (Klappa, 1980a; Wright and Tucker, 1991) or in intergranular pore spaces (Adams, 1980, 1991). Intergranular varieties form as outgrowths to coated grains. Septa typically consist of parallel-oriented needle-fiber calcite, and in some cases seem to have formed from the collapse of concentrically-coated rhizocretions (Wright and Wilson, 1987; Wright et al., 1988; Wright and Tucker, 1991).

Calcan: Micritic calcite typically occurring cutanically to subcutanically (neocalcans) to ped surfaces and conductive voids (Weider and Yaalon, 1982; Sobecki and Wilding, 1983; Drees and Wilding, 1987)

Calcrete: a near surface, terrestrial, accumulation of predominately calcium carbonate which occurs in a variety of forms from powdery to nodular to highly indurated (Wright and Tucker, 1991).

Circumgranular cracking: Irregular to globular masses separated by non-tectonic fractures and produced by alternate shrinkage and expansion (Ward, 1975; Esteban and Klappa, 1983; Wright et al., 1988). This cracking occurs around fabric grains, and is usually filled with spar cement.

Concretion: A hard, compact aggregate of mineral matter, subspherical to irregular in shape, formed by the precipitation from water solution around a nucleus (Bates and Jackson, 1984).

Crystallaria: Calcite filled cracks of variable shape, size and orientation. These cracks are due to desiccation and expansive growth followed by rapid precipitation in larger pores where evaporation and degassing would have greater effect (Wright, 1990; Wright and Tucker, 1991). If these cracks occur around crystal grains, they are called circumgranular cracking.

Crystic nodule: A nodule formed of coarse calcite crystals (crystic fabric) in a soil (Weider and Yaalon, 1982). These lack inclusion of framework grains in their initial stages and resemble calcans or crystal chambers. With increasing carbonate development, framework grains are incorporated, and larger spar crystals are precipitated (Weider and Yaalon, 1982).

Drusy: Pore filling calcite cement in which crystals coarsen towards the center of the pore.

Fenestral: Having openings or transparent areas resembling windows, usually applied to fossils (Bates and Jackson, 1984). In this study, and others (Wright, 1982), the "pane" parts of the "window" is sediment with a dense micritic microfabric, with sparry calcite veins as the "frame." This texture probably resulted from drying induced cracking of the host sediment along bedding planes (fracture borders match up). These cracks were later infilled with spar cements.

Floating Grain Microtexture: Grains appear to be "floating" in matrix. This texture can result for both grain replacements and displacements (Tandon and Friend, 1989; Wright and Peeters, 1989; Wright and Tucker, 1991). Displacive growth is common in calcrete formation and results in such features a multi-directional crystal growth (Saigal and Walton, 1988; Tandon and Friend, 1989; Wright and Peeters, 1989), linear growth (Braithwaite, 1989), and impeded growth (Maliva, 1989).

Isopachous: Calcite cement crystals of similar thickness that are oriented radially around framework grains.

Meniscus cements: Micritic calcite cements formed in-between individual framework grains or groups of grains typically associated with pedogenic environments (Warren, 1983; Wright et al., 1988; Wright and Tucker, 1991; Mora et al., 1993). Thought to result from the evaporation of vadose pore water (Warren, 1983).

Micrite: Calcite crystals < 4 microns in diameter (Folk, 1974; Folk, 1980; Drees and Wilding, 1987), or 1-8 microns (Weider and Yaalon, 1982). For this study Folk's system was used.

Micritic Envelopes: Micritic calcite cements formed around individual framework grains or groups of grains, typically associated with pedogenic environments (Warren, 1983; Wright and Tucker, 1991; Mora et al, 1993).

Microcodium: Elongate petal-shaped calcite prisms or ellipsoids, 1 mm or less in long dimension and grouped in spherical, sheet or bell-like clusters (Esteban, 1974; Esteban and Klappa, 1983). This structure is now believed to be the result of calcification of mycorrhizae, symbiotic associations between soil fungi and cortical cells of higher plant roots (Klappa, 1978).

Nodule: A small rounded mass or lump of a mineral or mineral aggregate, normally without internal structure, contrasting in composition with the rock matrix in which it is embedded (Bates and Jackson, 1984). In soil literature, called a glaebule, defined as equant to irregular in shape, and distinguished from the enclosing matrix by a greater concentration of some constituent and/or difference in fabric (Esteban and Klappa, 1983).

Phreatic: Zone of saturation (Bates and Jackson, 1984).

Poikilotopic: Cementation texture in which calcite occurs as large (1- 2 mm) optically continuous crystals encompassing framework grains, also known as "sand-calcite crystals" (Drees and Wilding, 1987)

Sparite: Calcite crystals generally greater than 10 microns (Folk, 1980), > 20 microns (Weider and Yaalon, 1982), or > 50 microns (Drees and Wilding, 1987). The term microspar is sometimes used for calcite crystals between 8 and 20 microns (Weider and Yaalon, 1982), or between 5 and 50 microns (Drees and Wilding, 1987). For this study, Folk's system was used.

Rhizocretion (Rhizolith): Organo-sedimentary structures produced by roots (Klappa, 1983, Klappa, 1991, Wright and Tucker, 1991). Five basic types of rhizoliths have been described (Esteban and Klappa, 1983; Wright and Tucker, 1991): 1) root molds and/or borings which are simply cylindrical pores left after root decay. 2) root casts which are sediment or cement-filled root molds 3) root tubules, which are cylinders around root molds 4) rhizocretions, concretionary mineral accumulations around living or decaying roots 5) root petrifactions which are mineral encrustations, impregnations or replacements of organic materials whereby anatomical root features are partly or totally preserved. These definitions are used by many authors (Cohen, 1982; Semeniuk and Meagher, 1981; Semeniuk and Searl, 1983; Wright et al., 1988; Spötl and Wright, 1992; Retallack, 1988).

Vadose: The zone of aeration (Bates and Jackson, 1984).

REFERENCES

Allen, J.R.L., 1986, Pedogenic calcretes in the Old Red Sandstone facies (Late Silurian-Early Carboniferous) of the Anglo-Welsh area, Southern Britain, In Wright, V.P. (Ed.), 1986, Paleosols, their recognition and interpretation. Princeton, N.J., Princeton University Press, p. 58-86.

Bates, R. L., and Jackson, J.A., 1984, Dictionary of geological terms. 3rd edition. Anchor books, Doubleday, New York, NY, p. 571.

Braithwaite, C.J.R., 1989, Displacive calcite and grain breakage in sandstones. Journal of Sedimentary Petrology, vol. 59, pp. 258-266.

Cohen, A.S., 1982, Paleoenvironments of root casts from the Koobi Fora Formation, Kenya. Journal of Sedimentary Petrology, v. 52, no. 2, p. 401-414.
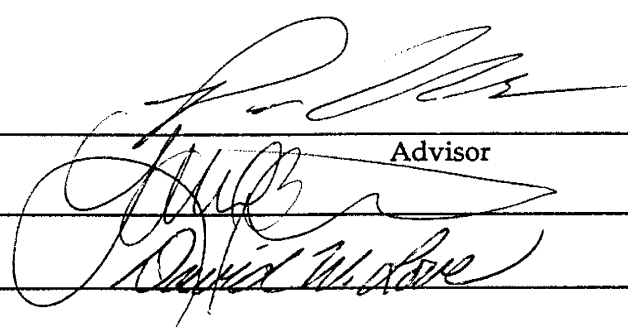
Drees, L.R., and Wilding, L.P., 1987, Micromorphic record and interpretation of carbonate forms in the Rolling plains of Texas: Geoderma, v. 40, p. 157-175.

Esteban, M, and Klappa, C.F., 1983, Subaerial exposure environment, In: Carbonate Depositional Environments (Ed. by Scholle, P.A., Bebount, D.G., and Moore, C.H.) AAPG Mem., no. 33, p. 1-54.

Folk, R.L., 1974, The natural history of crystalline calcium carbonate; effect of magnesium content and salinity: Journal of Sedimentary Petrology, v. 44, p. 40-53.

Folk, R.L., 1980, Petrology of sedimentary rocks. Hemphill Publishing Co., Austin Texas, 183p.

Gile, L.H., Peterson, F.F., and Grossman, R.B., 1966, Morphological and genetic sequences of carbonate accumulation in desert soils: Soil Science, v. 101, p. 347-360.

Goudie, A.S., 1983, Calcrete. In: Chemical sediments and geomorphology: precipitates and residua in the near-surface environment (Ed. by Goudie, A.S., and Pye, K.) Academic Press, London, p. 93-131.

Jacka, A.D., 1970, Principles of cementation and porosity - occlusion in Upper Cretaceous sandstones, Rocky Mountain Region. Twenty-Second Annual Field Conference, Wyoming Geological Association Guidebook, p. 265-285.

Jacka, A.D., 1974, Differential cementation of Pleistocene carbonate fanglomerate, Guadalupe Mountains. Journal of Sedimentary Petrology, v. 44, no. 1, p. 85-92.

Klappa, C.F., 1978, Biolithogenesis of Microcodium; elucidation. Sedimentology, v. 25, p. 489-522.

Klappa, C.F., 1979, Calcified filaments in Quaternary calcretes: organo-mineral interactions in the subaerial vadose environment. Journal of Sedimentary Petrology, v. 49, p. 955-968.

Klappa, C.F., 1980a, Brecciation textures and teepee structures in Quaternary calcrete (caliche) profiles from eastern Spain: the plant factor in their formation. Geological Journal, v. 15, pt. 2, p. 81-89.

Klappa, C.F., 1980b, Rhizoliths in terrestrial carbonates: classification, recognition, genesis and significance. Sedimentology, v. 27, 613-629.

Klappa, C.F., 1983, A process-response model for the formation of pedogenic calcretes, In: Wilson, R.C.I, ed., Residual deposits: surface related weathering processes and materials, Geol. Soc. Lond. Spec. Pub., no. 11, p. 221-233.

Machette, M.N., 1985, Calcic soils of the southwestern United States. Geological Society of America Special Paper 203, p. 1-21.

Mack, G.H., James, W.C., Monger, H.C., 1993, Classification of paleosols. Geological Society of America Bulletin, v. 105, p. 129-136.

Maliva, R.G., 1989, Displacive calcite syntaxial overgrowth in open marine limestones. Journal of Sedimentary Petrology, 59, pp. 397-403.

Milnes, A.R., 1992, Calcrete In: Weathering, soils, and paleosols (Ed. by Martini, I.P., and Chesworth, W.) Elsevier, p. 309-347.

Monger, H.C., Daugherty, L.A., and Gile, L.H.,1991, A microscopic examination of pedogenic calcite in an aridisol of southern New Mexico. in: Occurrence, characteristics, and genesis of carbonate, gypsum, and silica accumulations in soils. Soil Science Society of America, special publication 26, p. 37-59.

Retallack, G.J., 1988, Field recognition of paleosols. Geological Society of America, Special Paper 216, p. 1-20.

Semeniuk, V., and Meagher, T.D., 1981, Calcrete in Quaternary coastal dunes in southwestern Australia: a capillary-rise phenomenon associated with plants. Journal of Sedimentary Petrology, v. 51, no. 1, p. 47-68.

Semeniuk, V., and Searle, D.J., 1985, Distribution of calcrete in Holocene coastal sands in relationship to climate, Southwestern Australia. Journal of Sedimentary Petrology, v. 55, No. 1, p. 86-95.

Slate, J.L., Smith, G.A., Yang, W., and Cerling, T.E., 1996, Carbonate-paleosol genesis in the Plio-Pleistocene St. David Formation, Southeastern Arizona. Journal of Sedimentary Research, v. 36, p. 85-94.

Sobecki, T.M., and Wilding, L.P., 1983, Formation of calcic and argillic horizons in selected soils of the Texas coast prairie. Division S-5 Soil genesis, morphology, and classification. Soil Sci. Soc. Am. J., Vol 47, pp. 707-715.

Spötl, C., and Wright, V.P.,1992, Groundwater dolocretes from the Upper Triassic of the Paris Basin, France: a case study of an arid, continental diagenetic facies. Sedimentology, v. 39, p. 1119-1136.

Talma, A.S., and Netterberg, F.,1983, Stable isotope abundances in calcretes. In: Residual deposits (Ed. by R.C.I. Wilson) Geol. Soc. Lond. Spec. Pub., no 11. p. 221-233.

Tandon, S.K., and Friend, P.F.,1989, Near-surface shrinkage and carbonate replacement processes, Arran Cornstone Formation, Scotland. Sedimentology, v. 36, p. 1113-1126.

Warren, J.K.,1983, Pedogenic calcrete as it occurs in Quaternary calcareous dunes in coastal South Australia. Journal of Sedimentary Petrology, v. 53, no. 3, p. 787-796.

Weider, M., Yaalon, D.H.,1982, Micromorphological fabrics and developmental stages of carbonate nodular forms related to soil characteristics. Geoderma, v. 28, p. 203-220.

Wright, V.P.,1982, Calcrete paleosols from the lower Carboniferous Llanelly Formation, South Wales. Sedimentary Geology, 33, pp. 1-33.

Wright, V.P., and Peters, C.,1989, Origins of some early Carboniferous calcrete fabrics revealed by cathodoluminescence: implications for interpreting the sites of calcrete formation. Sedimentary Geology, v. 65, p. 345-353.

Wright, V.P., Platt, N.H., and Wimbledon, W.A., 1988, Biogenic laminar calcretes: evidence of calcified root-mat horizons in paleosols. Sedimentology, v. 35, p. 603-620.

Wright, V.P., 1990, A micromorphological classification of fossil and recent calcic and petrocalcic microstructures. In: Soil Micromorphology: a basic and applied science (Ed. Douglas, L.A.). Developments in Soil Science, 19, Elsevier, 401-407.

Wright, V.P., and Tucker, M.E., 1991, Introduction. In: Calcretes. (Ed. by Wright, V.P., and Tucker, M.E.). Int. Ass. Sediment., Reprint Series v. 2, 1-22.

This thesis is accepted on behalf of the faculty
of the Institute by the following committee:

_____
Advisor

11/22/96

Date

I release this document to the New Mexico Institute of Mining and Technology.

Student's Signature   12/13/96
                                                        Date